Mathematical Modeling and Optimization for Biological-based Treatment of Taman Timor Oxidation Pond, Johor

J-BIOTECH ENVIRONMENT SDN. BHD.

Representative / Group Members:

John R. Ockendon, Graeme Wake, Kok Lay Teo, Ryan Loxtan, Adérito Araújo, Basuki Widodo, Ali Hassan Mohamed Murid, Yeak Su Hoe, Akbar Banitalebi, Farhana Johar, Fuaada Mohd Siam, Kashif, Amir Syafiq Amir Hamzah, Siti Zulaiha Aspon, Hasniza Ramli, Noraha Markum, Noor Hazzarita Ab. Rahman, Siti Norazelah Hamdon, Nurul.

1. Introduction

A major source of water pollution comes from sewage, and it could be a serious problem when the municipal wastewater is not appropriately treated. Conventional treatment technology has both relatively high capital and operational costs. An alternative to this dilemma is to develop and apply the technologies with lower costs and better performance. Oxidation pond techniques have become very popular with small communities because of their low construction and operating cost, as well as a significant financial advantage over other recognized treatment methods (Hussein and Mohammed, 2007). Oxidation ponds are stages in a water treatment plant in which solid effluent and organic matter are degraded either in anaerobic or aerobic system. Both of anaerobic and aerobic ponds utilize indigenous microorganisms in their treatment to breakdown solid content of effluent and degrade organic matter into carbon dioxide, water, and cell biomass.

The oxidation pond that become the pilot scale study is Taman Timor Oxidation Pond, Tampoi, Johor, estimated about 1,909 square meters and has a depth about 1.5 meters, total

volume of water is 2,864.13 cubic meters or 2,864,125.13 liters (see Figures 1 and 2). To improve the efficiency of the water treatment, beneficial microorganism based product (called as mPHO) has been added to the pond to provide efficient removal and break down of solid content of effluent and pathogens, which are generally not sufficiently removed by oxidation pond. The product mPHO is made from the selected species of phototrophic bacteria (PSB). About 1,375 litres of mPHO have been applied at IWK (Indah Water Konsortium) Taman Timur, Johor, thoughout 3 months of treatments (see Figures 4 and 5). Samples were collected at two points which are CP1 (influent and application of mPHO) and CP2 (effluent) (see Figure 3). The microbial approach can help in purifying heavily polluted water especially area that exposed to sunlight. The ability of mPHO to photosynthesis and photometabolize many organic substances may help to reduce BOD (biological oxygen demand), COD (chemical oxygen demand), TSS (total suspended solids), NH3-N (ammoniacal nitrogen) and bacteria (E. Coli and Coliform) content in wastewater and increase the amount of DO (dissolved

oxygen) in the pond.

Figure 1: Location of Taman Timor Oxidation Pond in housing areas at Jalan Timur 2

Figure 2: The physical condition of Taman Timor Oxidation Pond

Figure 3: (a) shown location of sampling CP 1 (Influent), while (b) shown location of CP 2 (Effluent)

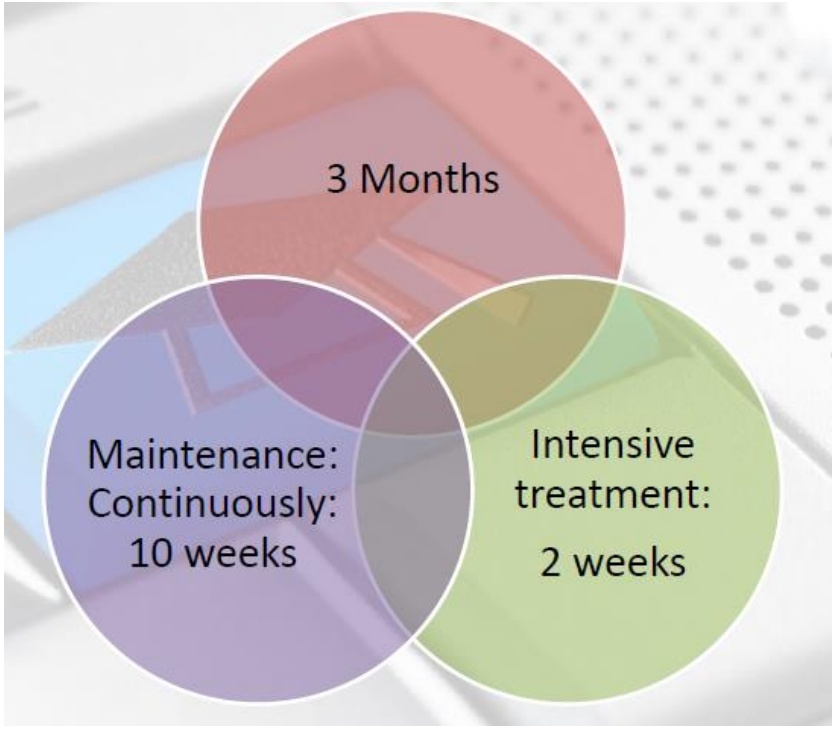

Figure 4(a): The treatment periods of Oxidation Pond

Figure 4 (b): Beneficial microorganism based product to be applied (mPHO)

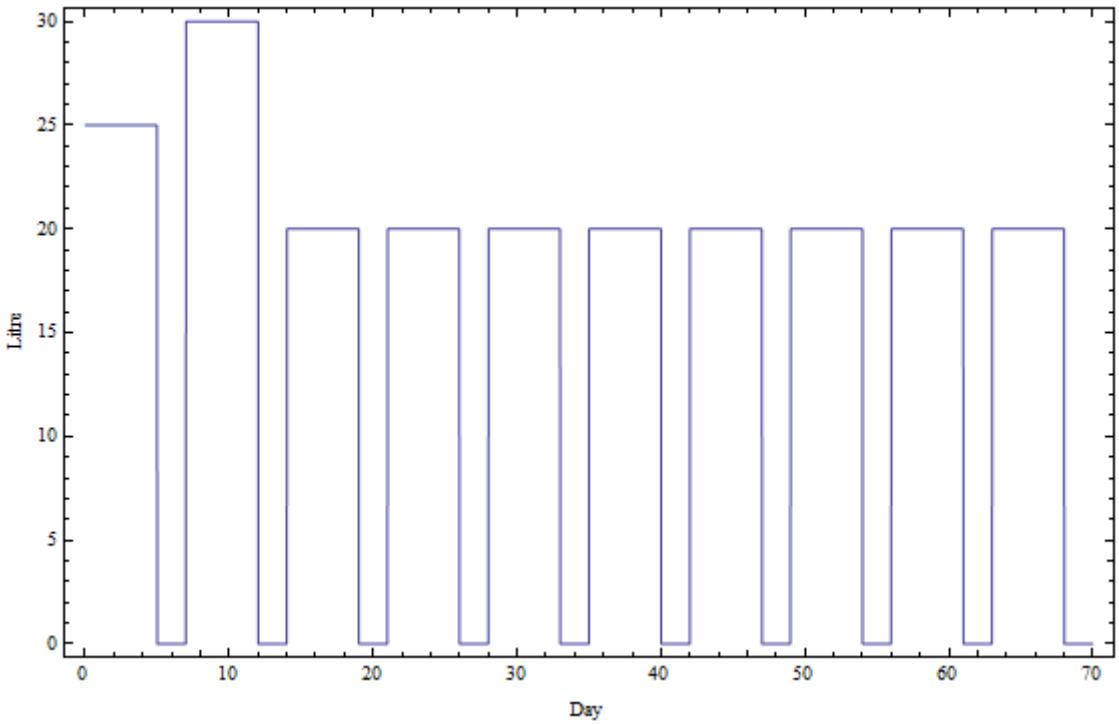

Figure 5: Treatment Schedule of mPHO Application at Taman Timor Oxidation Pond

Application / Activities			Frequency	Location
Pre- Sampling			3 times	Both Point (CP 1 & CP 2)
Treatment Approaches	**Day**	**Application / Activities**	**Quantity /Frequency**	**Location**
Intensive (Phase 1)	1	**Sampling**	**2 locations**	**Both Point (CP 1 & CP 2)**
		mPHO	25 liters	CP 1 (Influent)
	2	mPHO	25 liters	CP 1 (Influent)
	3	mPHO	25 liters	CP 1 (Influent)
	4	**Sampling**	2 locations	Both Point (CP 1 & CP 2)
		mPHO	25 liters	CP 1 (Influent)
	5	mPHO	25 liters	CP 1 (Influent)
	Break for 2 days			
	8	**Sampling**	**2 locations**	**Both Point (CP 1 & CP 2)**
		mPHO	30 liters	CP 1 (Influent)
	9	mPHO	30 liters	CP 1 (Influent)
	10	mPHO	30 liters	CP 1 (Influent)
	11	**Sampling**	2 locations	Both Point (CP 1 & CP 2)
		mPHO	30 liters	CP 1 (Influent)
	12	mPHO	30 liters	CP 1 (Influent)

Table 1: Treatment Schedule of mPHO Application at Taman Timor Oxidation Pond (Phase 1)

Treatment Approaches	Cycles (week)	Application / Activities	Quantity (Liter)	Location
Continuous (Phase 2)	1st	Application mPHO	100	CP 1 (Influent)
	2nd	**Sampling**	1	CP 1 & CP 2
		Application mPHO	100	CP 1 (Influent)
	3rd	Application mPHO	100	CP 1 (Influent)
	4th	**Sampling**	1	CP 1 & CP 2
		Application mPHO	100	CP 1 (Influent)
	5th	Application mPHO	100	CP 1 (Influent)
	6th	**Sampling**	1	CP 1 & CP 2
		Application mPHO	100	CP 1 (Influent)
	7th	**Sampling**	1	CP 1 & CP 2
		Application mPHO	100	CP 1 (Influent)
	8th	**Sampling**	1	CP 1 & CP 2
		Application mPHO	100	CP 1 (Influent)
	9th	Application mPHO	100	CP 1 (Influent)
	10th	**Sampling**	1	CP 1 & CP 2

Table 2: Treatment Schedule of mPHO Application at Taman Timor Oxidation Pond (Phase 2)

Parameter	Unit	Method	Results			
			CP 1A		CP 1B	
			Before	After	Before	After
BOD 5 days at 20˚C	mg/L	APHA 5210 B/ APHA 4500-O G	8	6.4	8.5	6.8
COD	mg/L	APHA 5220 B	30	21	37	29.6
Total Suspended Solids	mg/L	APHA 2540 D	16	12.8	<5	4
Ammonia Nitrogen	mg/L	APHA 4500-NH_3 B&C	10.8	8.64	10.2	8.16
Dissolved Oxygen	mg/L	APHA 4500-O G	8.7	10.44	7.7	9.24
Total coliform	MPN/100ml	APHA 9221 B	3.5×10^4	2.8×10^4	9.2×10^5	7.36×10^5
E. Coli	MPN/100ml	APHA 9221 G	4.7×10^3	3.76×10^3	9.2×10^4	7.39×10^4

Table 3: Justification of Treatment effectiveness of mPHO Application at Taman Timor Oxidation Pond

Table 4 to 7 shows the amount of pollutant, COD, BOD, DO and mPHO at point CP1 and CP2 after application of mPHO.

Parameter	Unit (Density)	Method	Date	Time(*t*) Day	Results	
					CP 1 (Influent)	CP 2 (Effluent)
Pollutant (Bacteria E. Coli and Coliform)	mg/L	APHA 9221 B & APHA 9221 G	29-Oct-2013	Pre-Sampling	0.1654	0.0078
			6-Nov-2013		0.1692	0.0058
			11-Nov-2013	0	0.32	0.034
			14-Nov-2013	3	0.074	0.025
			18-Nov-2013	7	0.158	0.0000198
			21-Nov-2013	10	0.076	0.0082
			3-Dec-2013	22	0.0080	0.00096
			10-Dec-2013	29	0.0038	0.000156
			16-Dec-2013	35	0.0128	0.00035
			23-Dec-2013	42	5.1	0.0176
			30-Dec-2013	49	0.199	2.32
			6-Jan-2014	56	0.16099	0.005
			13-Jan-2014	63	8.6076	0.72021
			20-Jan-2014	70	3.5026	0.412

Table 4: Measurements of Pollutant at point CP1 and CP2

Parameter	Unit (Density)	Method	Date	Time(*t*) Day	Results	
					CP 1 (Influent)	CP 2 (Effluent)
BOD & COD	mg/L	APHA 5210 B/ APHA 4500-O G & APHA 5220 B	29-Oct-2013	Pre-Sampling	103.7	48.9
			6-Nov-2013		199	106
			11-Nov-2013	0	160.8	90.3
			14-Nov-2013	3	113	59.4
			18-Nov-2013	7	148.8	89.1
			21-Nov-2013	10	165	87.3
			2-Dec-2013	22	271.8	50.1
			9-Dec-2013	29	140	103.4
			16-Dec-2013	35	206.1	102.1
			6-Jan-2014	56	130.2	95.6
			13-Jan-2014	63	226.2	150.4
			20-Jan-2014	70	602.3	204.4

Table 5: Measurements of BOD and COD at point CP1 and CP2

Parameter	Unit (Density)	Method	Date	Time(*t*) Day	Results	
					CP 1 (Influent)	CP 2 (Effluent)
mPHO (Phototrophic Bacteria)	mg/L		29-Oct-2013	Pre-Sampling	?	?
			6-Nov-2013		?	?
		APHA 9221 B & APHA 9221 G	11-Nov-2013	0	0	0
			14-Nov-2013	3	1.5×10^{-6}	3.6×10^{-7}
			18-Nov-2013	7	1.4×10^{-6}	7.4×10^{-7}
			21-Nov-2013	10	2.1×10^{-6}	3.6×10^{-7}
			2-Dec-2013	21	3.6×10^{-7}	7.4×10^{-7}
			9-Dec-2013	28	1.5×10^{-6}	2.0×10^{-6}
			16-Dec-2013	35	3.6×10^{-7}	7.4×10^{-7}
			23-Dec-2013	42	6.3×10^{-6}	2.0×10^{-6}
			30-Dec-2013	49	3.6×10^{-7}	2.9×10^{-5}
			6-Jan-2014	56	2.1×10^{-5}	7.5×10^{-7}
			13-Jan-2014	63	1.5×10^{-5}	2.0×10^{-6}
			20-Jan-2014	70	2.0×10^{-6}	7.5×10^{-7}

Table 6: Measurements of mPHO at point CP1 and CP2

Parameter	Unit Density	Method	Date	Time(t) Day	Results	
					CP 1 (Influent)	**CP 2 (Effluent)**
Dissolved Oxygen	mg/L	APHA 4500-O G	29-Oct-2013	Pre-Sampling	< 5	5.1
			6-Nov-2013		<5	<5
			11-Nov-2013	0	2.1	2.9
			14-Nov-2013	3	4.9	4.2
			18-Nov-2013	7	2.6	2.9
			21-Nov-2013	10	3.9	4.1
			2-Dec-2013	22	3.9	4.3
			9-Dec-2013	29	4.9	4.7
			16-Dec-2013	35	4.9	4.9
			6-Jan-2014	56	4.9	5.83
			13-Jan-2014	63	4.8	4.9
			20-Jan-2014	70	4.9	4.9

Table 7: Measurements of Dissolved Oxygen at point CP1 and CP2

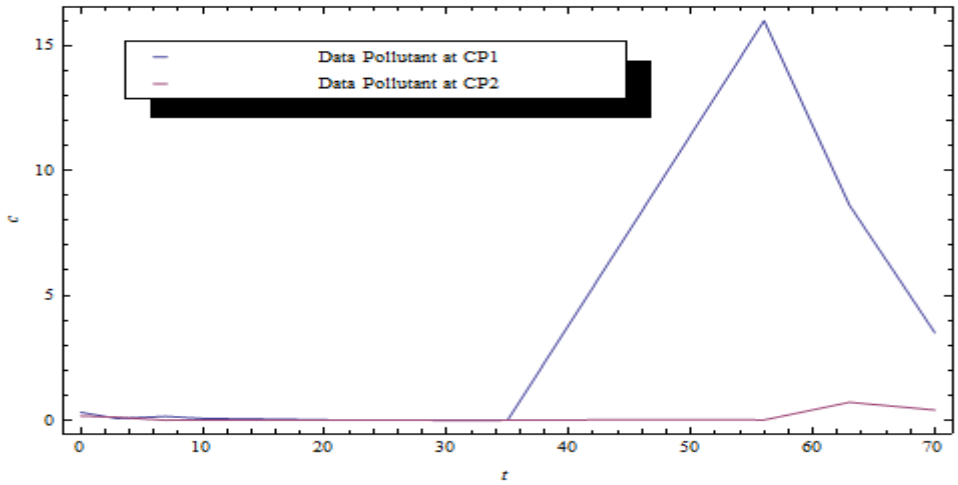

Figure 6: Graph of Pollutant at point CP1 and CP2

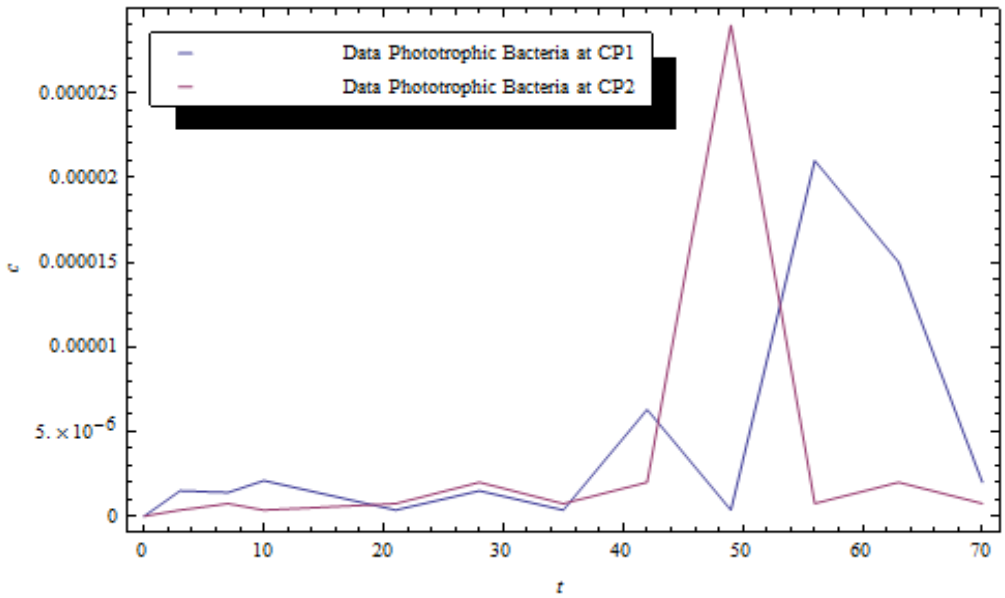

Figure 7: Graph of mPHO at point CP1 and CP2

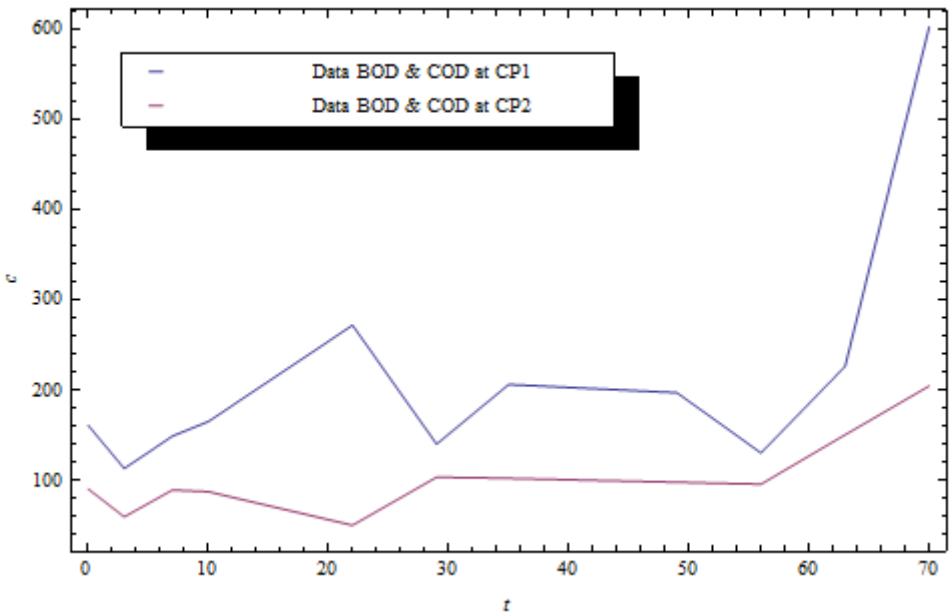

Figure 8: Graph of BOD and COD at point CP1 and CP2

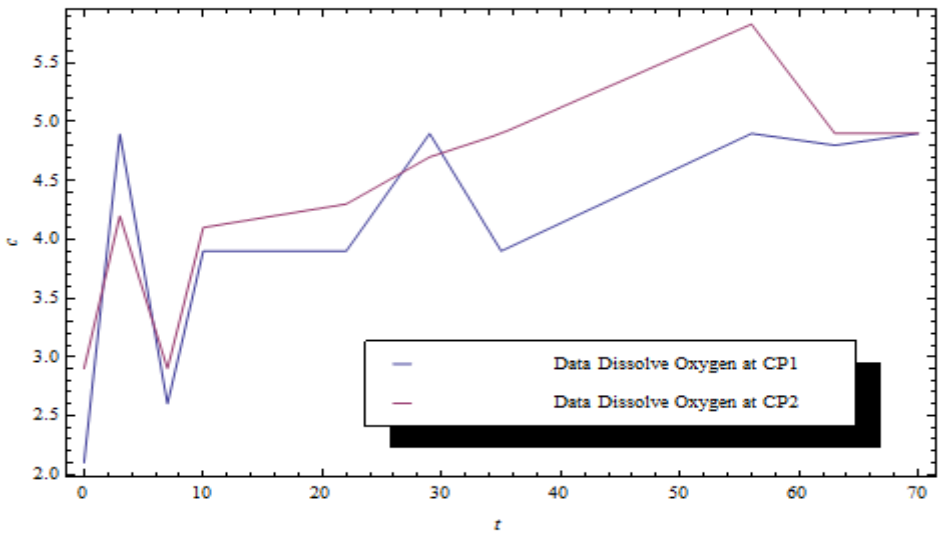

Figure 9: Graph of Dissolved Oxygen at point CP1 and CP2

However, the right amount of mPHO must be determined to ensure that sufficient dose is added, thus maintaining its efficiency and prevent excessive use. Therefore, the aim of this study is to utilize a mathematical model to determine the optimal amount of mPHO to be used in order to improve water quality of IWK oxidation pond treatment plant.

2. Mathematical Model 1: Coupled Advection Equation Model (PDE)

We model the wastewater treatment process based on the interaction that occurs between pollutant (bacteria E. Coli and Coliform), mPHO, BOD, COD and DO using the sampling data collected from the pond. We assume the pond is aerobic.

2.1 Parameters

These are all the variables and parameters used in the mathematical model:

$M(x,t)$ is the amount of phototrophic bacteria in the pond (mg/liter) where x varies along the pond from point CP1 to CP2 and t varies from initial time up to 70 days.

$P(x,t)$ is the biomass of microbes (total E. Coli and Coliform) in the pond (mg/liter).

$D(x,t)$ is the amount of both biological and chemical oxygen demand (mg/liter).

$X(x,t)$ is the amount of dissolved oxygen in the pond (mg/liter).

X_{atm} is the saturated oxygen concentration = 0.01 kg m^{-3} = $0.01 \times 10^{6} \times 10^{-3}$ mg/liter = 10 mg/liter.

α is the mass transfer of oxygen from air to water = 104.995 m^2 day^{-1}.

This is calculated as a product: re-aeration rate x A' ; the re-aeration rate is 0.055 day^{-1} and A' (the top surface area per unit length) is about 1,909 m^2.

L is the length of pond = 54 m.

W is the width of pond = 25 m.

D_1 is the depth of pond = 1.5 m.

Flow rate of water in the pond is 3.36 liter/s = 3.36 x 60 x 60 x 24 liter/ day =290, 304 liter/day.

v is the velocity of water in the pond = $\dfrac{\text{flow rate of water in the pond}}{\text{cross section area of the pond} = W \times D_1}$ =

$$\frac{290.304\,\text{m}^3/\text{day}}{1.5 \text{ x } 25 \text{ m}^2}$$

= 7.74144 m/day.

2.2 Schematic Diagram

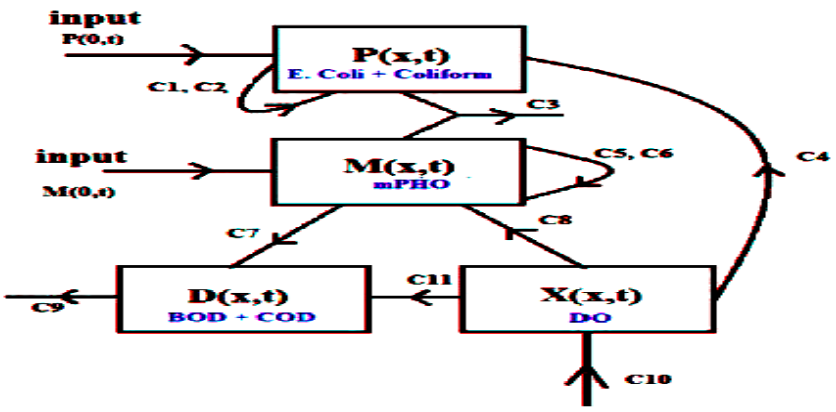

Figure 10: Schematic Diagram of the Model

2.3 Mathematical Model

Based on the schematic diagram in Figure 6, we have constructed the following mathematical model based on coupled-advection equation model (Haberman (1977), Morley (1979), and Pimpunchata *et al*. (2009)).

$$\frac{\partial P}{\partial t} + v\frac{\partial P}{\partial x} = (c_1 - c_2 P - c_3 M)P + c_4 XP$$

$$\frac{\partial M}{\partial t} + v\frac{\partial M}{\partial x} = (c_5 - c_6 M + c_8 X)M$$

$$\frac{\partial D}{\partial t} + v\frac{\partial D}{\partial x} = (c_7 M - c_9 + c_{10} X)D$$

$$\frac{\partial X}{\partial t} + v\frac{\partial X}{\partial x} = \alpha(X_{atm} - X) - c_8 XM - c_4 XP - c_{10} XD$$

$$0 \le t \le 70, \qquad 0 \le x \le 54.$$

2.4 Conditions

The initial condition and boundary condition of the mathematical model are given below.

Initial Conditions	**Boundary Conditions**
$P(0,t) = \text{data}\, mg/\ell$	$P(0,t) = \text{data}\, mg/\ell$
$M(0,t) = \text{data}\, mg/\ell$	$M(0,t) = \text{data}\, mg/\ell$
$D(0,t) = \text{data}\, mg/\ell$	$D(0,t) = \text{data}\, mg/\ell$
$X(0,t) = \text{data}\, mg/\ell$	$X(0,t) = \text{data}\, mg/\ell$
$0 \le t \le 70$	$0 \le t \le 70$

In order to obtain boundary conditions $P(0,t)$, $M(0,t)$, $D(0,t)$ and $X(0,t)$ at time t we use interpolation of data given at CP1.

2.5 Control Variable

$$M(0,t) = M_0(t) + 19.1\, c_{11}\, u(t), \qquad 0 \le t \le 70.$$

The variable u controls the value of mPHO need to be applied into the pond while c_{11} is a model parameter and $M_0(t)$ is the value of mPHO at point CP1.

2.6 Numerical Results

The first problem we need to solve is to approximate the best parameter c_1 to c_{11} of the model. For the solution of this problem we use the current schedule of the application of mPHO as shown in Figure 5.

2.6.1 Parameter Estimation

The Cost Function of parameter estimation problems is

$$\begin{aligned} f(k_1,\ldots,k_{11}) = &\sum_{i=1}^{10}\left(\left\|P(0,t_i) - P^*_{in}(t_i)\right\| + \left\|P(54,t_i) - P^*_{en}(t_i)\right\|\right) \\ &+\sum_{i=1}^{12}\left(\left\|M(0,t_i) - M^*_{in}(t_i)\right\| + \left\|M(54,t_i) - M^*_{en}(t_i)\right\|\right) \\ &+\sum_{i=1}^{10}\left(\left\|D(0,t_i) - D^*_{in}(t_i)\right\| + \left\|D(54,t_i) - D^*_{en}(t_i)\right\|\right) \\ &+\sum_{i=1}^{10}\left(\left\|X(0,t_i) - X^*_{in}(t_i)\right\| + \left\|X(54,t_i) - X^*_{en}(t_i)\right\|\right). \end{aligned}$$

This cost function has to be minimized subject to the mathematical model which describes the system of wastewater treatment and then the solution of this problem based on the current schedule in Figure 5 gives us the following parameters for the problem.

c_1 =0.47612435

c_2 =0.71919481

c_3 =2.64235329

c_4 =0.79328568

c_5 =0.14578821

c_6 =0.28664718

c_7 =0.00125591

c_8 =0.12356092

c_9 =12.0173401

c_{10}= 0.00148686

c_{11} =0.2

Using the above parameters, we simulate the mathematical model to obtain the results depicted in Figure 7 to Figure 14. Dissolved Oxygen in the pond is shown in Figure 7 and Figure 8 is the 2D graph of Dissolved Oxygen with respect to time at CP1 and CP2. As can be seen from Figure 11 and Figure 12, the amount of oxygen in the pond increase as time increases. The amount of oxygen at CP2 is always higher than at CP1.

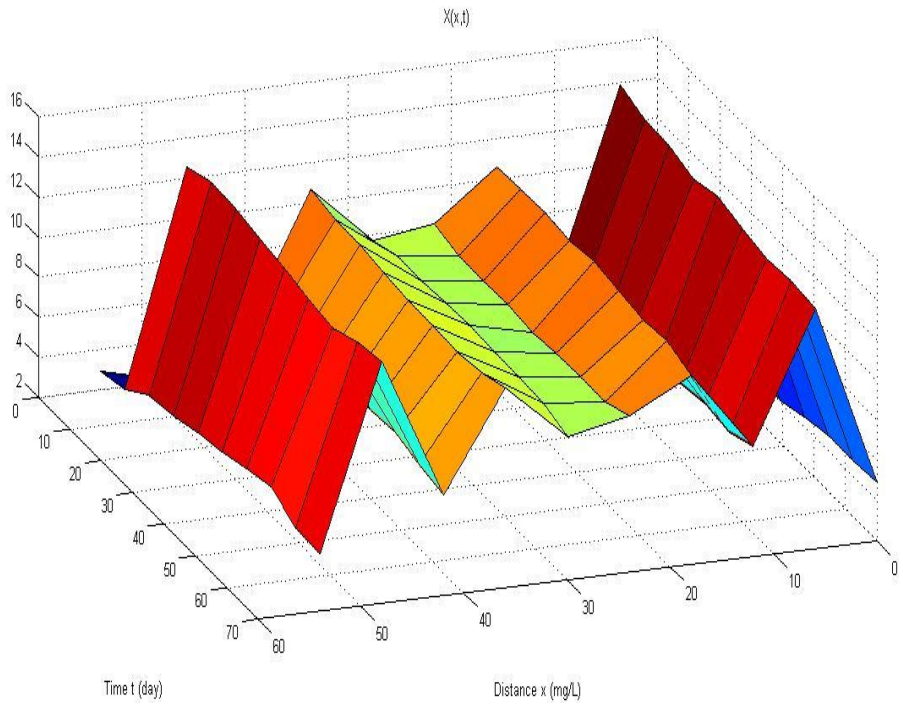

Figure 11: 3D Graph of Dissolved Oxygen in the pond

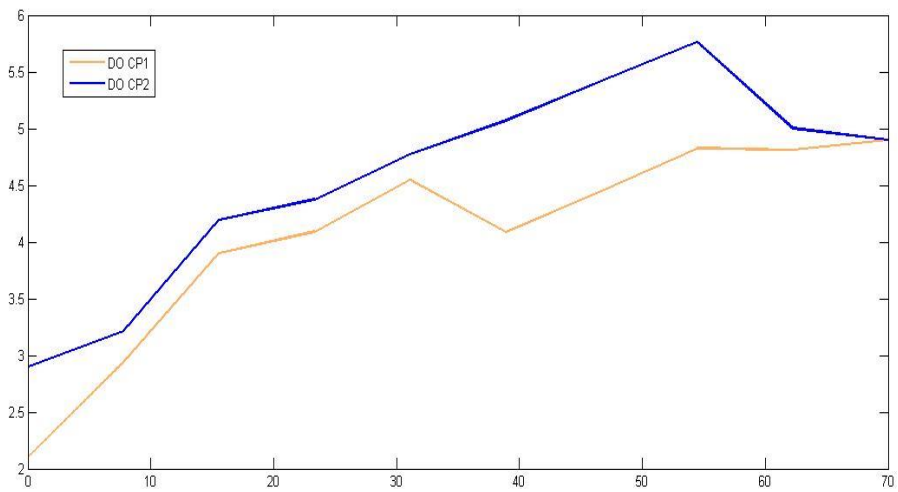

Figure 12: 2D graph of Dissolved Oxygen at CP1 and CP2 in the pond

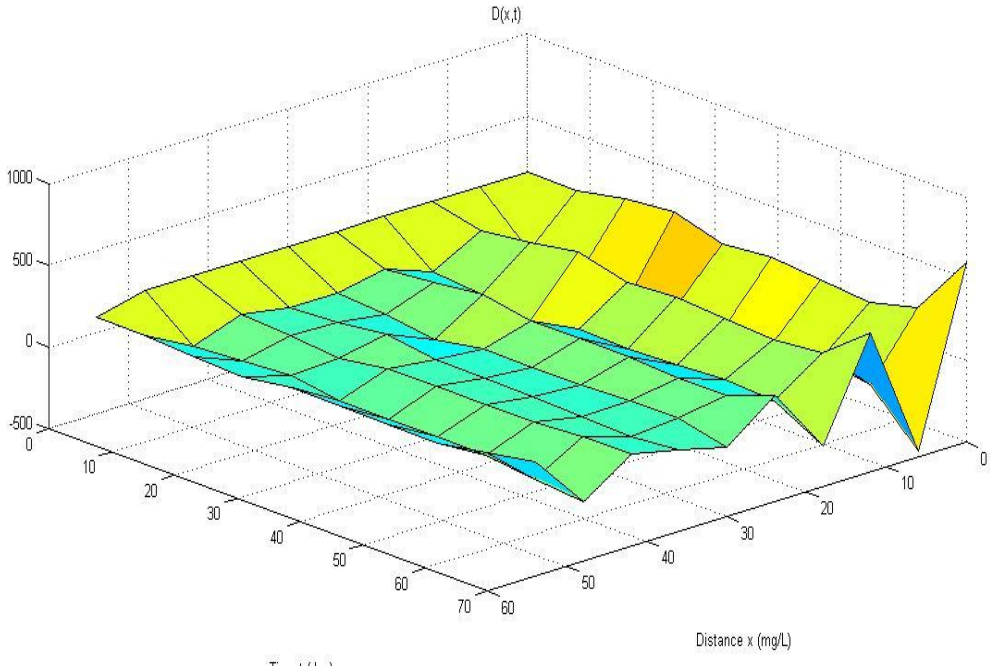

Figure 13: 3D Graph of Biological and Chemical Oxygen Demand in the pond

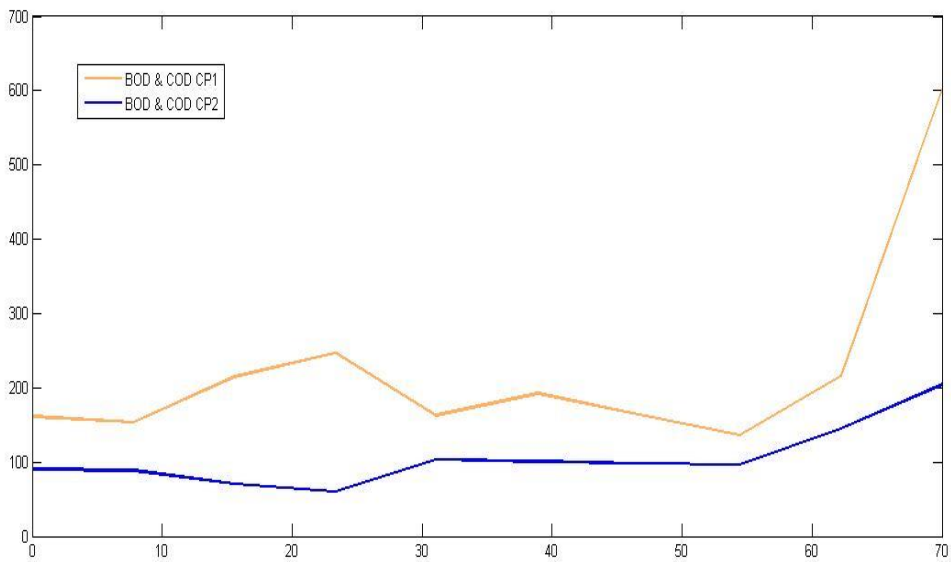

Figure 14: 2D Graph of Biological and Chemical Oxygen Demand at CP1 and CP2 in the pond

Figure 13 shows the value of chemical oxygen demand and biological oxygen demand in the pond and Figure 14 is the 2D graph of chemical oxygen demand and biological oxygen demand with respect to time at CP1 and CP2. Figure 13 shows that BOD and COD decreases with some fluctuation along with time.

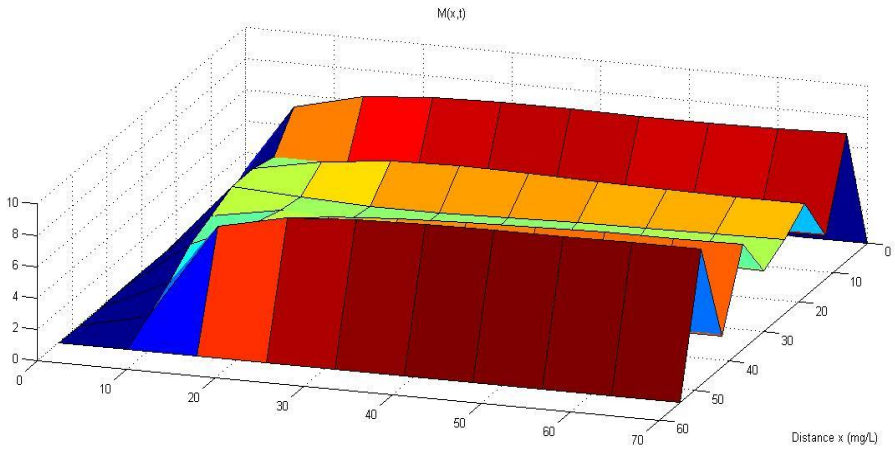

Figure 15: 3D Graph of Phototrophic Bacteria in mPHO in the pond

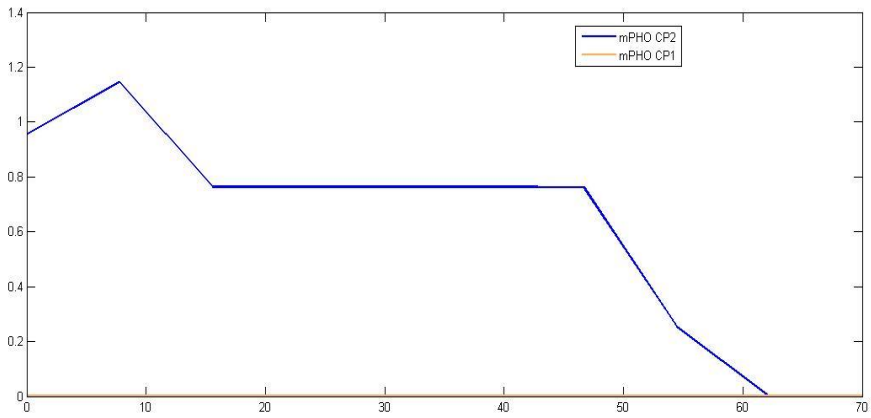

Figure 16: 2D Graph of Phototrophic Bacteria in mPHO at CP1 and CP2 in the pond

Figure 15 describes the variation of Phototrophic bacteria in mPHO in the pond in the direction from CP1 (where mPHO is applied) towards CP2 (where the wastewater is discharged) for 70 days while Figure 16 is the 2D graph of Phototrophic Bacteria in mPHO with respect to time at CP1 and CP2. Figure 15 and Figure 16 show the distribution of these bacteria in the pond respectively.

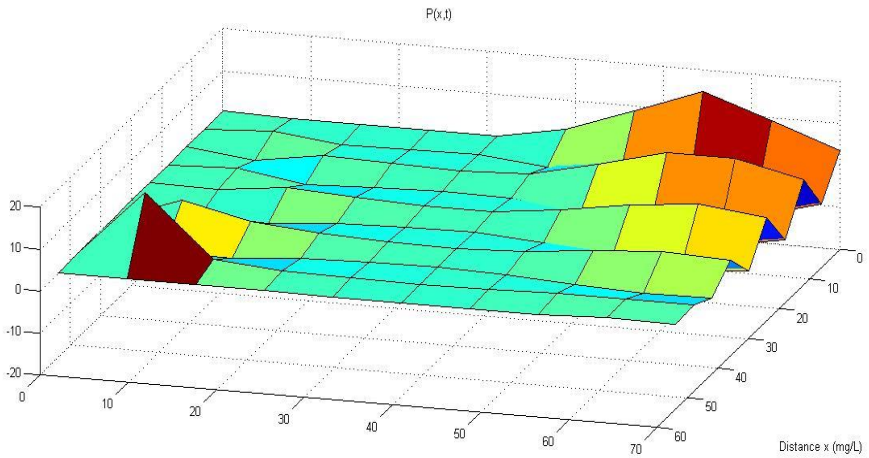

Figure 17: 3D Graph of E. Coli and Coliform in the pond

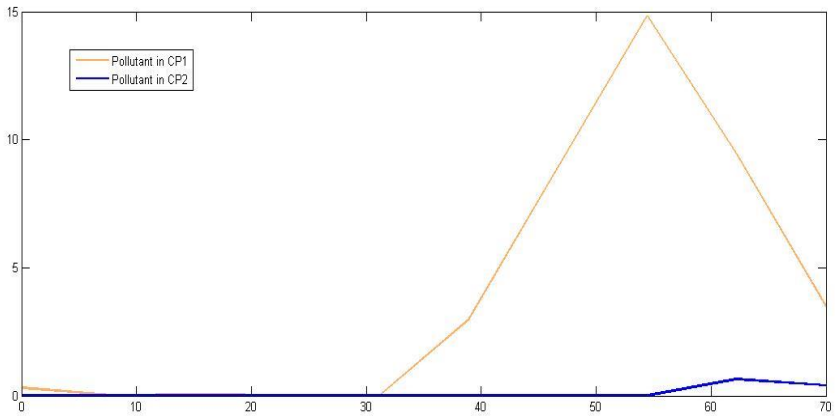

Figure 18: 2D Graph of E. Coli and Coliform at CP1 and CP2 in the pond

Figure 17 is the 3D graph of concentration of E. Coli and Coliform in the pond, and the last graph in Figure 18 which is obtained from the numerical simulation of the mathematical model describes the amount of E. Coli and Coliform at point CP1 and CP2. From Figure 17, we can see that the amount of bad microbes in the pond decreases with increasing time.

2.7 Optimal control of mPHO

Now, using the parameters obtained in the previous section an optimal control problem need to be solved to obtain the optimum schedule for the application of mPHO in the pond in such a way that it could reduce both the cost of application of mPHO itself and the environmental cost as well.

The cost function of optimal control is given by

$$\begin{aligned} min \int_1^{70} [50u(t)^2 + \int_1^{54} \omega_p P(x,t)^2 dx \\ + \int_1^{54} \omega_m M(x,t)^2 dx + \int_1^{54} \omega_D D(x,t)^2 dx \\ + \int_1^{54} \omega_x X(x,t)^2 dx] \, dt \end{aligned}$$

where ω_P, ω_M, ω_D, and ω_X are some suitable weights need to be carefully determined to balance of the environmental cost of each pollutant. In this study, we take the values of these weights all equal to 0.05.

The solution of the above problem through control parameterization method gives us the optimal value for the application of mPHO in the pond. This new schedule is shown in green against the current schedule in blue in Figure 19.

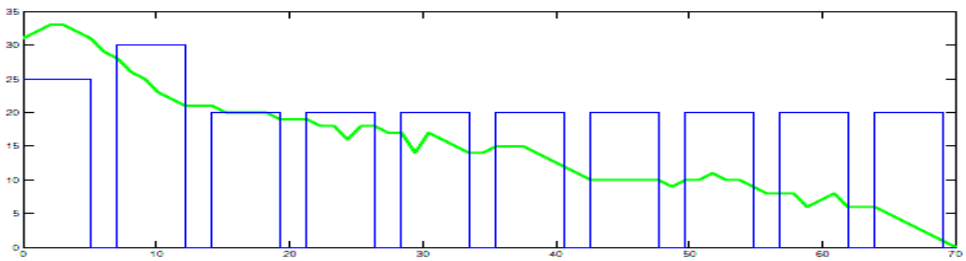

Figure 19: The new schedule for mPHO

The area under green line is 1059 which means using the current schedule in the period of 70 days we need to apply a total of 1059 liters of mPHO which cost approximately RM 52,950. However, for same period applying the current schedule leads to spend 1075 liters of mPHO which cost approximately RM 53,750 namely the new schedule helps to save 16 liters per each 70 days period. Therefore, the application of new schedule results in saving more than 83 liters of mPHO per year. The percentage of reduction of mPHO in one year is about 1.5 % which is about RM 4,171.43.

It should be noted that if we further decrease the consumption of mPHO in the schedule it doesn't help to reduce the cost. It is because if we further decrease the amount of mPHO, the environmental cost is increased.

Based on the new schedule for the application of mPHO we simulate again the mathematical model to see the effects of the schedule on the value of pollutant, BOD, COD, phototrophic bacteria and dissolved oxygen. Figure 20 to Figure 27 show the application of new schedule does not significantly change the amount of pollutant while it reduce the amount of mPHO.

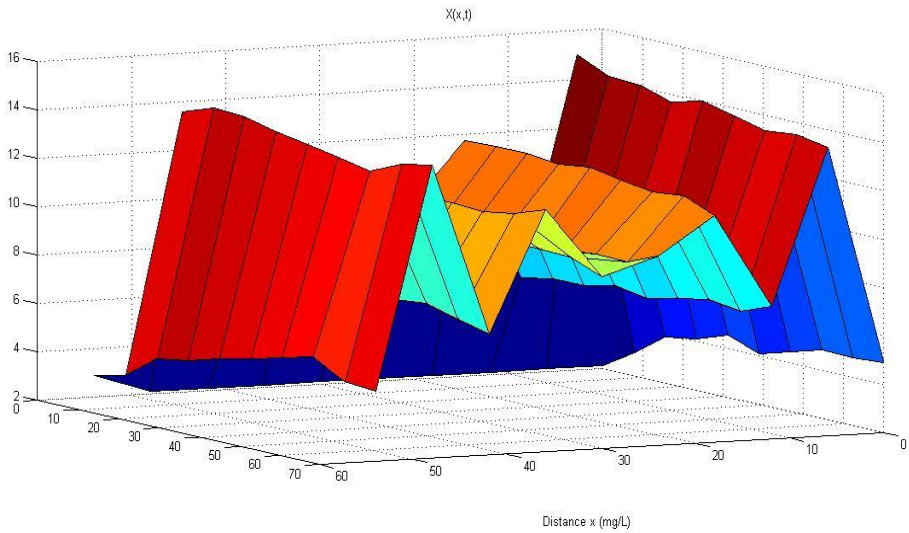

Figure 20: 3D Graph of Dissolved Oxygen in the pond

(Using new schedule)

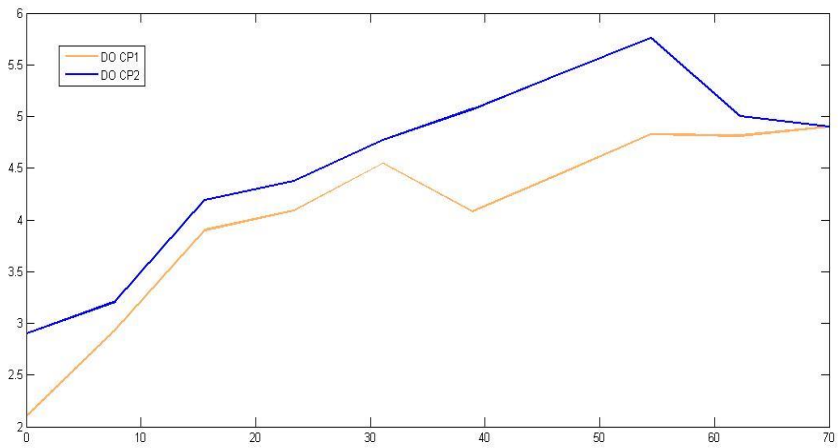

Figure 21: 2D Graph of Dissolved Oxygen at CP1 and CP2 in the pond

(Using new schedule)

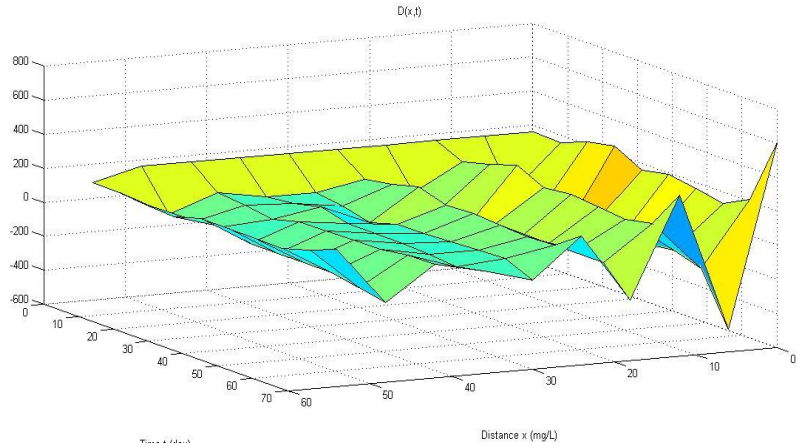

Figure 22: 3D Graph of Biological and Chemical Oxygen Demand in the pond (Using new schedule)

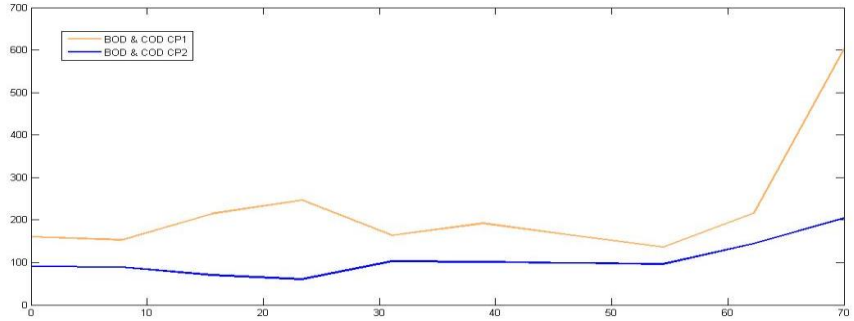

Figure 23: 3D Graph of Biological and Chemical Oxygen Demand in the pond (Using new schedule)

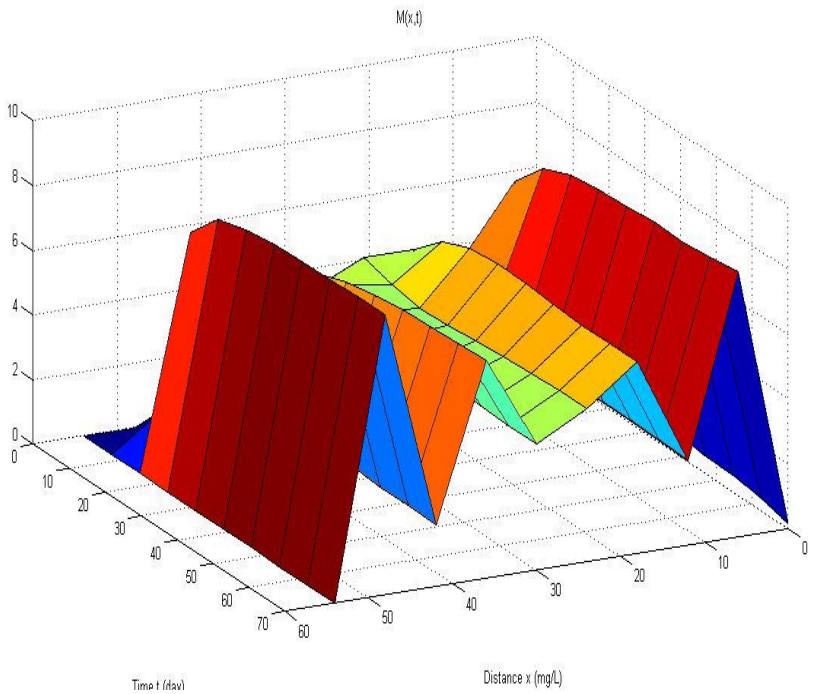

Figure 24: 3D Graph of Phototrophic bacteria in the pond

(Using new schedule)

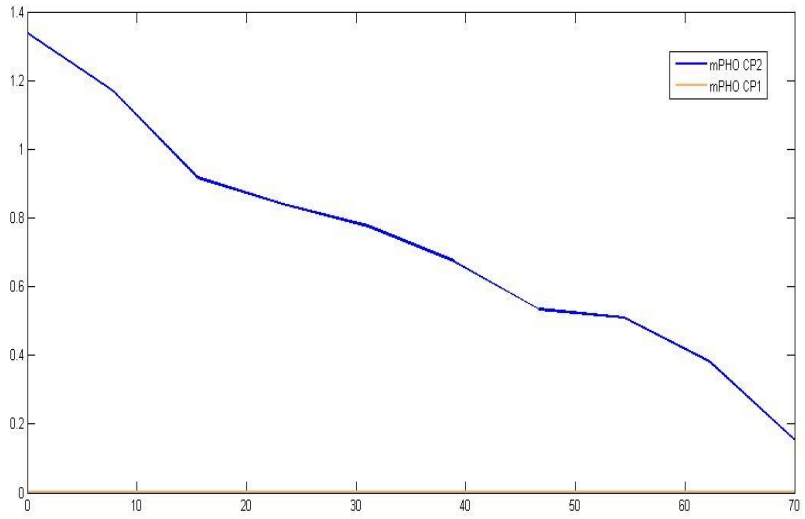

Figure 25: 2D Graph of Phototrophic bacteria at CP1 and CP2 in the pond

(Using new schedule)

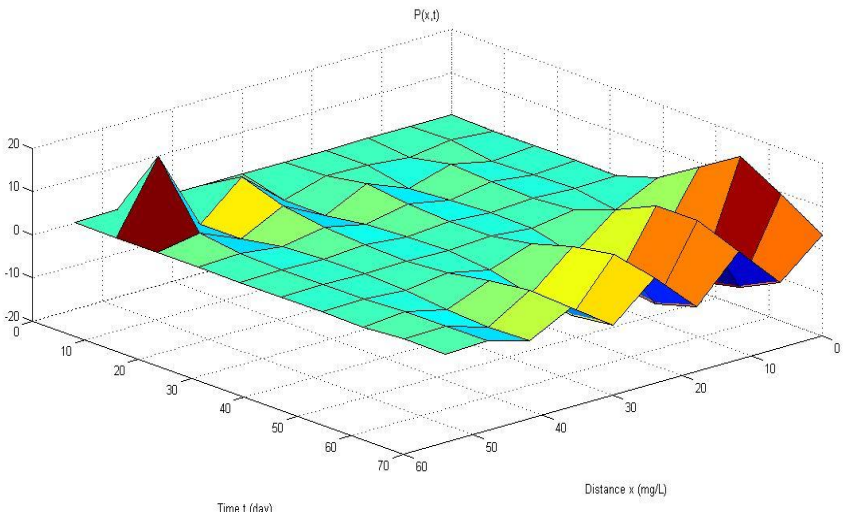

Figure 26: 3D Graph of E. Coli and Coliform in the pond

(Using new schedule)

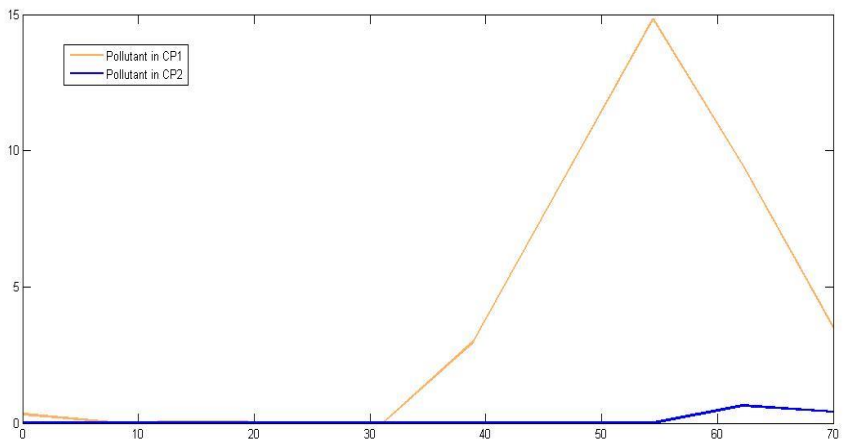

Figure 27: 2D Graph of E. Coli and Coliform at CP1 and CP2 in the pond

(Using new schedule)

3. Mathematical Model 2: Coupled Equation Model (ODE)

We model the wastewater treatment process using another model which is the first order ODE using coupled equation.

3.1 Parameters

These are all the variables and parameters used in this mathematical model 2:

$M(t)$ is the amount of phototrophic bacteria in the pond (mg/liter) where t varies from initial time up to 70 days.

$P(t)$ is the biomass of microbes (total E. Coli and Coliform) in the pond (mg/liter).

$D(t)$ is the amount of both biological and chemical oxygen demand (mg/liter).

$X(t)$ is the amount of dissolved oxygen in the pond (mg/liter).

$P_0(t)$ is the amount of microbes (total E. Coli and Coliform) at CP1 (mg/liter).

m is the amount of phototrophic bacteria in one liter of mPHO (mg/liter).

$U(t)$ is the amount of mPHO according to the schedule per liter.

$D_0(t)$ is the amount of both biological and chemical oxygen demand at CP1 (mg/liter).

$X_0(t)$ is the amount of dissolved oxygen at CP1 (mg/liter).

X_{atm} is the saturated oxygen concentration = 10 mg/liter.

3.2 Schematic Diagram

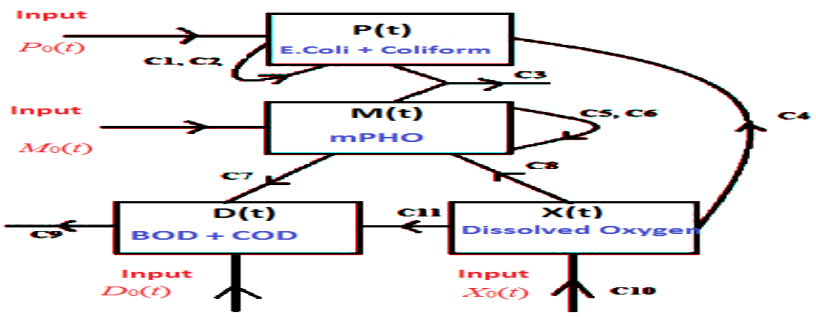

Figure 28: Schematic Diagram of the Model

3.3 Mathematical Model 2

Based on the schematic diagram in Figure 28, we have constructed the following mathematical model based on coupled equation model for ODE:

$$\frac{dP(t)}{dt} = c_1 P(t) - (c_2 P(t) + c_3 M(t))P(t) + \frac{c_4 X(t)P(t)}{X(t) + c_{11}} + \frac{v_{in} P_0(t)}{v_p}$$

$$\frac{dM(t)}{dt} = c_5 M(t) - c_6 M^2(t) + \frac{c_8 X(t)M(t)}{X(t) + c_{12}} + \frac{c_{18} v_{in} mU(t)}{v_p}$$

$$\frac{dD(t)}{dt} = -c_9 D(t) - c_7 M(t) + \frac{c_{10} X(t)D(t)}{D(t) + c_{14}} + \frac{v_{in} D_0(t)}{v_p}$$

$$\frac{dX(t)}{dt} = c_{13}(X_{atm} - X(t)) - c_{15} X(t)M(t) - c_{16} X(t)P(t) - c_{17} X(t)D(t) + \frac{v_{in} X_0(t)}{v_p}$$

$$0 \le t \le 70.$$

3.4 Conditions

In order to obtain initial conditions $P(0)$, $M(0)$, $D(0)$ and $X(0)$ we use the data given at CP2 at time $t = 0$. The initial conditions of the mathematical model 2 are given below.

Initial Conditions:

$P(0) = 0.034\ mg/\ell$, $M(0) = 0\ mg/\ell$, $D(0) = 80.3\ mg/\ell$ and $X(0) = 2.9\ mg/\ell$.

3.5 Numerical Results

The first problem we need to solve is to approximate the best parameter c_1 to c_{18} of the model. For the solution of this problem we use the current schedule of the application of mPHO as shown in Figure 5.

3.5.1 Parameter Estimation

The Cost Function of parameter estimation problems is

$$f(c_1,\ldots,c_{18}) = \sum_{i=1}^{12}\left|P(t_i)-P^*(t_i)\right| + \sum_{i=1}^{12}\left|M(t_i)-M^*(t_i)\right| + \sum_{i=1}^{10}\left|D(t_i)-D^*(t_i)\right| + \sum_{i=1}^{10}\left|X(t_i)-X^*(t_i)\right|.$$

Here $P^*(t_i)$ is the amount of pollutant measured at CP2 at time t_i, similar explanation goes for M^*, D^* and X^*.

This cost function has to be minimized subject to the mathematical model which has been describes in Section 3.3. The cost function of the system of wastewater treatment has been minimized using "FindFit" the build-in package in Mathematica software. The current schedule in Figure 5 give us the following parameters for the problem.

c_1 = 0.039028503185234

c_2= 0.303017093831469

c_3= 0.003118716709434

c_4 = 0.007630387539237

c_5 = 0.000000013437088

c_6 = 10.52449197353788

c_7 = 0.005985419375326

c_8= 0.000000006684812

c_9 = 0.173342945819984

c_{10} = 0.077546852086182

c_{11}= 0.009676848173908

c_{12}= 0.014392183433028

c_{13}= 0.003860967956404

c_{14} = 0.024991549693569

c_{15} = 0.008300150220929

c_{16} = 0.030757826871389

c_{17} = 0.001424368590934

c_{18} = 0.000000008273840

Using the above parameters, we simulate the mathematical model to obtain the results depicted in Figure 29 to Figure 32. Figure 29 is the graph of dissolved oxygen with respect to time *t*. As can be seen, the amount of oxygen in the pond increase as time increases. The amount of oxygen simulated is always higher than the amount of dissolved oxygen at CP2.

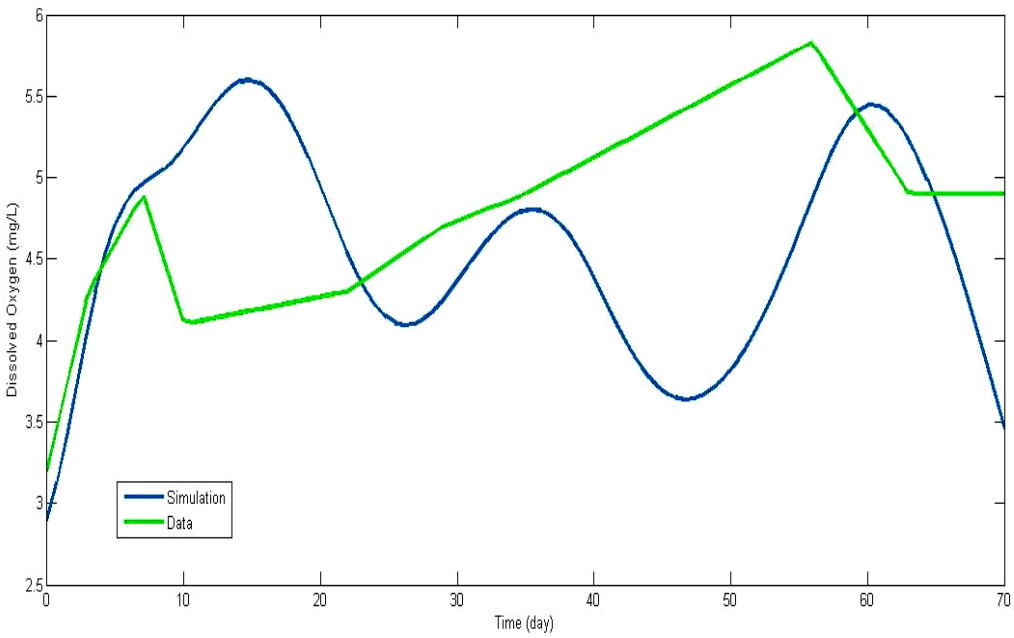

Figure 29: Graph of Dissolved Oxygen simulated and at CP2 in the pond

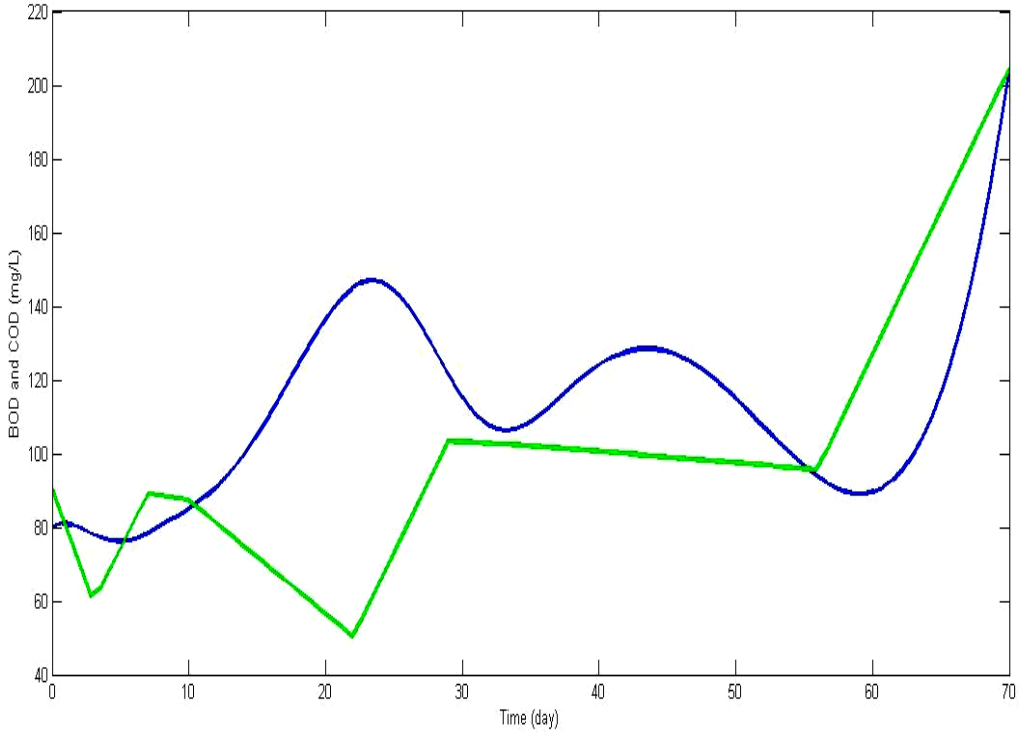

Figure 30: Graph of Biological and Chemical Oxygen Demand simulated and at CP2 in the pond

Figure 30 shows the value of chemical oxygen demand and biological oxygen demand in the pond with respect to time *t* from simulated model and at the point CP2. Figure 30 shows that the values of BOD and COD from simulated model are always lower than at the point CP2. These values also decrease with some fluctuation along with time.

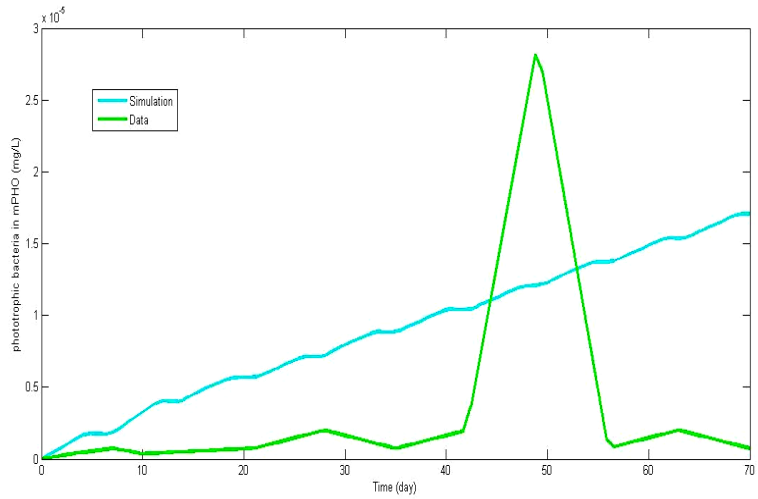

Figure 31: Graph of Phototrophic Bacteria in mPHO from simulated model and at point CP2

Figure 31 describes the variation of Phototrophic bacteria in mPHO from simulated model and at point CP2 while Figure 32 is the graph of concentration of E. Coli and Coliform in the pond also from simulated model and at point CP2.

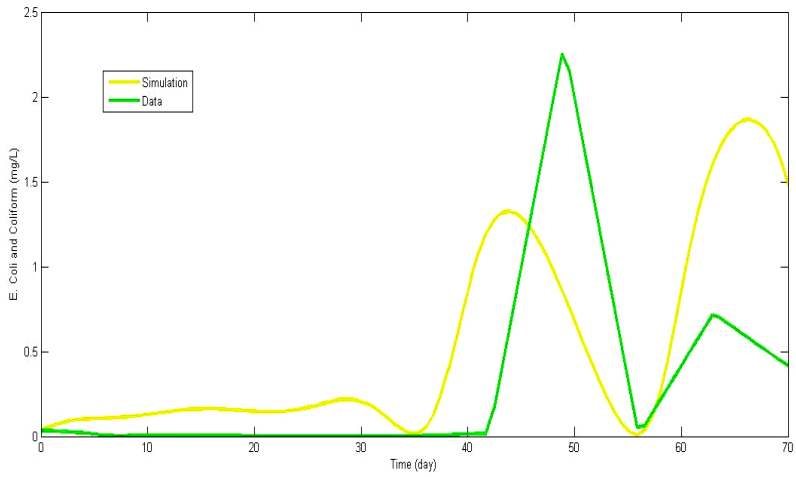

Figure 32: Graph of E. Coli and Coliform from simulated model and at CP2

From Figure 28, we can see that the amount of bad microbes in the pond decreases with increasing time.

Acknowledgement

We are very grateful to Prof. Dr. E. Soewono, Institute Teknologi Bandung, Indonesia, who contributed valuable ideas in the construction and analysis of the ODE model during his visit to UTM-CIAM (15 Jun 2014 – 26 Jun 2014).

References

Morley, D. A., (1979). *Mathematical Modelling In Water And Wastewater Treatment*. Applied Science Publishers LTD. London.

Pimpunchata, B., Winston L. Sweatmanc, Graeme C. Wake, Wannapong Triampod and Aroon Parshotame, (2009). A mathematical model for pollution in a river and its remediation by aeration. *Applied Mathematics Letters.* 22 (2009) 304-308.

Haberman, R., (1977). *Mathematical Models Mechanical Vibrations, Population Dynamics, and Traffic Flow An Introduction to Applied Mathematics.* Society for Industrial and Applied Mathematics. Prentice-Hall, Inc., Englewood Cliffs, New Jersey.

Hussein, I., Abdel-Shafy and Mohammed, A. M. Salem, (2007). Efficiency of Oxidation Ponds for Wastewater Treatment in Egypt. *NATO Science for Peace and Security Series-C: Environmental Security*. 175-184.

Chapra, S. C., (1997). *Surface Water quality Modeling*. New York, McGraw-Hill.

Appendix

J-BioTech
JOHOR BIOTECHNOLOGY & BIODIVERSITY CORPORATION

J-BIOTECH ANALYSIS LABORATORY
Block TG 1-2,UTM-MTDC Innovation Centre,
Technovation Park, 81300 Skudai,Johor Bahru
Tel no : +60(7) 520 7810 Fax : +60(7) 5207811
Email : admin@biotech.gov.my Website : www.jbiotech.gov.my

CERTIFICATE OF ANALYSIS

Date Report Release 12 November 2013
Our Reference JBAL/W/130-131/13
Company **J-BIO MICROBE INDUSTRIES SDN BHD**
Block 2, UTM-MTDC
Innovation Centre, Technovation Park
81300 Skudai, Johor Bahru, Johor
Date Sample Received 06 November 2013
Sample Description Received Two (2) samples said to be WATER
Marking A CP 1
B CP 2

Result of Analysis

PARAMETER	UNIT	METHOD	RESULTS		Std
			A	B	
Coliform	MPN/100 ml	APHA 9221 B	1.6×10^7	4.3×10^5	N/A
E. coli	MPN/100 ml	APHA 9221 F	9.2×10^5	1.5×10^5	N/A

Abbreviation :
"<" *: Less Than* *"N/A"* *: Not Available*
"ND" *: Not Detected*
FDA/BAM Method *: Standard methods of American Food and Drug Administration Bacteriological Analytical Manual Edition 8, Revision A /1998.*
APHA *: Standard Methods For The Examination of Water and Wastewater, American Public Health Association, Edition 21, 2005.*

J-BioTech

(SYTIE SYUNARTI BINTI MUHITAM @ HAZRI)
Bac.Chemical Engineering (Hons)(Biotechnology)
Microbiologist

***The above analysis based solely on the sample(s) submitted by customer.**
***This report shall not be used for advertising purposes and shall not be reproduced except in full without the written approval of J-BioTech Analysis Laboratory.**

'The Accuracy You Can Trust'

Analysis Laboratory
Johor Biotechnology And Biodiversity Corporation (JBBC)
Block TG 1-2, UTM-MTDC
Technology Centre, Technovation Park
Universiti Teknologi Malaysia, 81310 Skudai, Johor
Email : admin@jbiotech.gov.my Website : www.jbiotech.gov.my

CERTIFICATE OF ANALYSIS

Date Report Release	25 November 2013
Company	**J-Bio Microbe Iadustries Sdn Bhd** Block 2 UTM-MTDC Innovation Centre Technovation Park 81300 Skudai Johor
Date Sample Received	18 November 2013
Sample Description	Effective Microbe
Marking	mPHO

Result of Analysis

PARAMETER	UNIT	METHOD	RESULTS
			A
Phototrophic Bacteria	cfu/ml	In House	1.91×10^{7}

SITI NORAZELAH HAMDON
Microbiologist

*The above analysis based solely on the sample(s) submitted by customer.
*This report shall not be used for advertising purposes and shall not be reproduced except in full without the written approval of J-BioTech Analysis Laboratory.

The Accuracy You Can Trust

River Pollution Attenuation in Aquifers Using Bank Infiltration Technique

NATIONAL HYDRAULICS RESEARCH INSTITUTE MALAYSIA (NAHRIM)

Representative/Group Members:

Mohd Khairul Nizar Shamsuddin, Shaymaa Mustafa, Zainal Abdul Aziz, Aderito Araujo, Sharidan Shafie, Faisal Salah, Farhad Ali, Arshad Khan

Abstract

Riverbank filtration (RBF) is a natural technique for surface water treatment, based on the natural removal of pollutants from water during its transfer through the aquifer to pumping well. In this report a mathematical model is used to simulate three major processes related to RBF which are: (1) Groundwater flow and contaminants transport from river towards the pumping well (2) arrival time needed by contaminants to reach the well and (3) evolution of water chemistry due to microbial activity. While the first and second problems were solved numerically by using MODFLOW, the third problem was solved analytically. MODFLOW simulation highlighted the capture zone influenced by each pumping well. Also it was found that the contaminant needs 75 days to reach the pumping well. Furthermore, the analytical model for third problem showed that NO_3 and O_2 were consumed within 10 cm of the aquifer while SO_4 consumed within 30 cm.

1.1 Introduction

The population of Selangor has now reached around 6 million as of 2010 (Department of Statistic Malaysia, 2010). The rapid population growth in Selangor, along with unplanned urbanization and industrialization, overstrains the water supply infrastructure of the capital. In report of Malaysia Water Guide 2005, the water consumption in the state is very high. In 2003, metered domestic water consumption in Selangor was recorded at 478,995,217 cubic meters, while metered non-domestic water consumption was at 245,490,214 cubic metres. The total consumption of metered domestic and non-domestic water in Malaysia in 2003 was 1,609,574,693 cubic meters and 843,388,420 cubic meters respectively. In Selangor, domestic demand grew at an average compounded rate of 5.9% from 1960 to 2006. That year, water demand was divided between the domestic and non-domestic sectors by a ratio of 61 to 39. The projected domestic and industrial demand for peninsular Malaysia up to 2050 based on study by Economic Planning Unit, under the National Water Resources Study (Government of Malaysia, 2000), is about 4,753 million liters per day (MLD), and in 2008, it had almost tripled to 12,468 MLD and projected to reach 24,485 MLD by the year 2020. Demand projections for the Kuala Langat and Sepang districts shown the water demand is 330 MLD in 2010, but increase to 524 MLD in 2020. From the statistic of water consumption in Malaysia from 2008 until 2009 shows that there are about 12,418 water intakes in 2008, taking water directly from rivers for the water supply. The number of the water intakes and has risen to 12,583 in the year 2009 due to increased demand for water of the high demand for water, was feared that the incident would occur if the closure of water intakes are too dependent on the water surface. To meet future water requirements in the country, there has been a recommendation to build 47 new dams, besides three new inter-state water projects that include the Pahang-Selangor Inter State Raw Water Transfer. But, the infrastructure such as dams to treatment plants and distribution systems entails high investments. Operational costs

such as energy and labour cost, and cost of maintaining the dams, treatment plants, distribution network, and pumps are no less costly.

Langat River Basin is an important water supply source in the Klang Valley. There are two main dams that stored water from Langat River basin which are Langat and Semenyih Dams. Since the last 20 years, there were several occasions where water intakes and treatment plants have been closed as a result of serious river pollution. The closure of water intakes and water treatment plants has impacts on water supply and thus on economic activities for industries and other sectors. The main sources of river water pollution were discharge of domestic sewage, pollutants from agro-based industries/farming, run-offs from earthworks and land clearing and effluent discharge from manufacturing activities. According to Khairuddin and Abd Malek (2002) the sources of the Langat River pollution coming from industrial discharge (58%), domestic sewage from treatment plants (28%), construction projects (12%) and pig farming (2%). Department of Environment (DOE) of Malaysia, Ministry of Natural Resources and Environment of Malaysia, monitors the water quality of river in Malaysia based on water quality index (WQI) to evaluate the water quality status and river classification. The water quality in the basin has been deteriorating over the years, as evidenced from the water quality database compiled for 15 years. The recorded WQI ranged from 58.1 to 75, which corresponds to pollute (WQI, 0–59) and moderately polluted (WQI, 60–80). Based on the average values taken from the 2002 survey, the major pollutants in the Langat River Basin expressed as percentage of stations exhibiting quality corresponding to class 3 and above are as follows (figures in parenthesis indicate percent sampling stations): AN (94%), TSS and BOD (71%), COD (65%), and DO (53%; UPUM (2002)). Data on the contamination of the Langat River has been published by various authors: for instance, in Malaysia, Zakaria and Mahat (2006) reported the sources and concentration of polycyclic aromatic hydrocarbon (PAHs) in the river sediment in the Langat Estuary, and that this area is dominated by pyrogenic sources which means that most of the PAH compounds are coming from the atmosphere such as street dust. Farizawati et al. (2005) reported a study of Cryptosporidium and Giardia from cattle farms located near Sungai Langat and Semenyih River showed that

out of 24 samples of water taken from Sungai Semenyih, 4.2% was positive for Giardia cysts with a concentration of 1.3 cysts/l and 20.8% were positive with Cryptosporidium oocysts with a range of 0.7–2.7 oocysts/l. In Langat River, from the 43 samples taken, 23.3% were positive for Giardia cysts with a range of 1.5–9.0 cysts/l whereas 11.6% were positive with Cryptosporidium oocysts with a range of 2.5–240.0 oocysts/l. This shows that wastewater was discharged into the river signifying contamination of oocycts from the cattle farms into the river system. Liza (2010) identify the point source (PS) and non-point source (NPS) pollution using Geographical Information Systems during the base and storm flow event using the DOE data from 2004-2008 and ranked using the violation analysis which showed that E.Coli (NPS) > E.Coli (PS) > TSS (NPS) > COD (NPS) > NH_3-N (NPS) > BOD (NPS) > COD (PS) > TSS (PS) > NH_3-N(PS) > BOD (PS). It also found that the presence of E.Coli in Langat river can reach 44 times higher than limiting standard of 2000cfu/100ml. The strong concentrations of BOD and COD are related to anthropogenic pollution sources from sewage treatment plants and industrial effluents. Lee and Omar (2006), examining organochlorine insecticides from sediment and water of lake and Langat river. The results showed that endrin, chlordane and aldrin were present in all water samples with concentrations for endrin: 0.02-0.21 µg/L, chlordane: 0.05-0.16 µg/L and aldrin 0.03-0.13 µg/L. Lindane and heptachlor were rarely detected in the water samples. For sediment, lindane, endrin and heptachlor were detected in all sediment samples. Their levels in sediments were 0.28-0.53 µg/kg for lindane, 0.06-0.53 µg/kg for heptachlor and 1.06-2.06 µg/kg for endrin. The source would be from the river upstream flow through an area of oil palm plantation, where these insecticides might have been used for pest control in the past. Osman et al. (2012), identified sources of organic contaminants using chemometric techniques to classify the pollution sources in Langat river basin based on the analysis of water and sediment samples collected from 24 stations, monitored for 14 organic contaminants from polycyclic aromatic hydrocarbons (PAHs), sterols, and pesticides groups. They obtained from chemometric techniques indications that sterols (coprostanol, cholesterol, stigmasterol, β-sitosterol, and stigmastanol) are strongly correlated to domestic and urban sewage, PAHs (naphthalene, acenaphthene, pyrene, benzo[a]anthracene, and benzo[a]pyrene) from industrial and urban activities and chlorpyrifos

correlated to samples nearby agricultural sites. Othman and Gasim (2005) reported that heavy metal concentrations such as mercury (Hg), cadmium (Cd), zinc (Zn), lead (Pb), copper (Cu), nickel (Ni), iron (Fe), cobalt (Co) and manganese (Mn) in water of Semenyih river watershed were determined in the water samples. Al-Odaini et al. (2010), observed pharmaceuticals in Langat river indicate that samples collected from the remaining sampling stations along the Langat river were found to contain 15 out of the 19 targeted pharmaceuticals. However, chlorpheniramine, lovastatin, simvastatin, and amlodipine were never detectable in any samples. The frequencies of detection for each pharmaceutical in all thirty samples are depicted. Mefenamic acid, glibenclamide, and salicylic acid were present in samples from all the sampling sites, suggesting both their widespread use and their high degree of persistence in the environment. Metformin, chlorothiazide, and atenolol were detected in 83%, 80%, and 73% of the samples, respectively. On the other hand, nifedipine and loratadine have the lowest frequency of detection (6.6 %). The overall high pollution of the river has alarmed Malaysian scientists, population and authorities. In the past 20 years, judicial intervention and huge financial investment were undertaken to save the Langat river, but despite all attempts both the contamination upstream of Langat river and the contaminant load from the urbanisation itself are still rising and need the Strategic Planning and Management for the Langat River Basin (United Nations 2005). Based on the previous study by some researchers in Malaysia, surface waters are not generally safe for human consumption unless they are properly treated.

In tropical countries like Malaysia where the rainfalls continuously recharge river flow, the main source of dependable water supply is essentially river water. However, as development and economic activities spreads, the management of water resources can be very critical due to increase demand as well as environmental degradation. Pollution of rivers has made surface water unsuitable for sources of raw water for treatment and in certain cases has caused the treatment costs to rise unexpectedly. One of the alternative ways to improve dependable clean portable water supply that is being considered is through Riverbank filtration (RBF)

technology as a second source of water supply to guarantee clean and dependable watersupply solution without neglecting the polluted surface water.

Riverbank filtration (RBF) is a natural technique for surface water treatment, based on the natural removal of pollutants from water during its transfer through the aquifer to pumping well. This technology is applied in USA and several European countries. Recently, RBF technique has been applied for the first time in Malaysia in Pilot project conducted in Jenderam Hilir, located in Langat Basin, Selangor, Malaysia (Shamsuddin et al., 2013). This approach had been approved to be a very effective technology that reduces pollutants concentration and it has potential benefits for drinking water supply in Malaysia. To manage and operate RBF system efficiently, it is extremely important to evaluate the potential for contamination of drinking water wells by river pollution.

1.2 Problem Statement

To manage and protect the water supply, transport processes need to be predicted by using the RBF method. To date, the method has mostly been studied by using mathematical solutions. This research specifically simulates the groundwater flow and contaminants transport induced by pumping well and investigates the evolution of the water chemistry during bank-filtrations systems.

1.3 Methodology – Assumptions, Mathematical model, Algorithm

Numerical modelling by using MODFLOW code is developed to simulate groundwater flow and arrival time for pollutants transport induced by pumping well in the river bed sediments where water infiltrates. Shallow homogenous aquifers are assumed in this model. Under the

steady state and 1-dimensional saturated flow in infiltration zone, the governing equation of ground flow model in MODFLOW software is:

$$\frac{\partial}{\partial x} K_x \frac{\partial h}{\partial x} + \frac{\partial}{\partial y} K_y \frac{\partial h}{\partial y} + \frac{\partial}{\partial z} K_z \frac{\partial h}{\partial z} = S \frac{\partial h}{\partial t} + R \qquad (1)$$

where K_x, K_y and K_z are the hydraulic conductivity of the aquifers in x, y and z directions respectively. h is the head, S is storage coefficient, R is the source sink term. Finite Difference Method is used in solving the governing equations includes the initial and boundary conditions.

To simulate the arrival time required by contaminants to reach the well, MT3D MODFLOW package is used. A 2-dimensional governing equation that describes the fate and transport of pollutants in RT3D code is

$$R_d \frac{\partial C}{\partial t} = D_x \frac{\partial^2 C}{\partial x^2} + D_y \frac{\partial^2 C}{\partial y^2} - U_x \frac{\partial C}{\partial x} - U_y \frac{\partial C}{\partial y} - kC \qquad (2)$$

where C solute concentration, D diffusivity of mass transport, U_x and U_y are Darcy velocity in x and y directions, D_x and D_y are the diffusivity in x and y directions, k is the degradation rate and R_d is the retardation factor.

On other hand, analytical modelling is developed to simulate the evolution of water chemistry occurs during the water movement from river to the pumping well due to bacterial activity. Equation (2) is used with some modifications to include the microbial activity in the model as follow:

$$\frac{\varphi R_d}{q} \frac{\partial C}{\partial t} = D_x y \frac{\partial^2 C}{\partial x^2} - U_x y \frac{\partial C}{\partial x} - \beta C \qquad . \qquad (3)$$

With the following initial and boundary conditions:

$$C(x,0)=0 \quad \text{for} \quad x \geq 0 \quad \text{and } t=0$$

$$C(0,t)=C_0 \quad \text{for} \quad t \geq 0 \quad \text{and } x=0$$

$$C \to 0 \text{ as } \quad x \to \infty$$

where φ is the effective porosity, q is decay rate, y is degradation of dissolved organic matter and β is the growth rate of bacteria. The final solution is:

$$C(x,t)=C_0 \exp\left(\frac{q\alpha}{\varphi R_d}t\right)\exp\left(\left(\frac{yU_x-\sqrt{(yU)^2+4D_x y(\beta+\alpha)}}{2D_x y}\right)x\right). \quad (4)$$

This solution can be used to determine the concentration of pollutants via distance x at any time t.

1.4 Results and Discussion.

Results of implementation of MODFLOW

Numerical model is tested by data for a river flows through a valley which is bounded to the north and south by impermeable granitic intrusions. The river forms part of a permeable unconfined aquifer system horizontal hydraulic conductivity K_h = 5 m/day, vertical hydraulic conductivity K_v = 0.5 m/day, specific yield S = 0.05 effective porosity φ = 0.2 which overlies a confined aquifer of a variable thickness (K_h = 2 m/day, K_v = 1 m/day, specific storage S = 5 × 10 -5, φ = 0.25). A 2 m thick silty layer (K_h = 0.5 m/day, K_v = 0.05 m/day, φ = 0.25) separates the two aquifers. Three pumping wells pumping at 500m^3/day each abstract water from the confined aquifer. This data is applicable for the *National Hydraulics Research Institute Malaysia (NAHRIM)* situation. Fig 1 illustrates the data for the well DW2 in

Selangor site such as the distance between river and well, river width and type of soil in different layers in the aquifers.

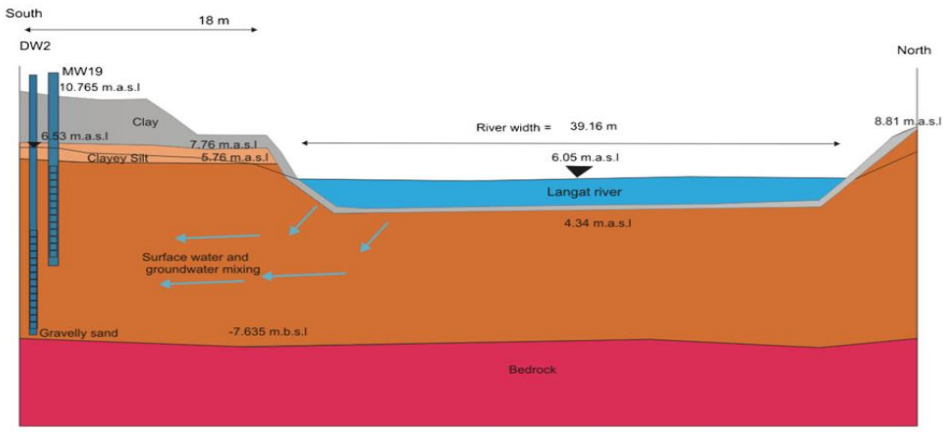

Fig (1): summarized some data for the well DW2 in the pilot project conducted in Malaysia.

By using equation (1) in MODFLOW package we can simulate the hydraulic conductivity at any location in the aquifer as shown in Fig (2). Moreover, the capture zone where the water infiltrates towards each well under the influence of pumping process is illustrated in Fig (3).

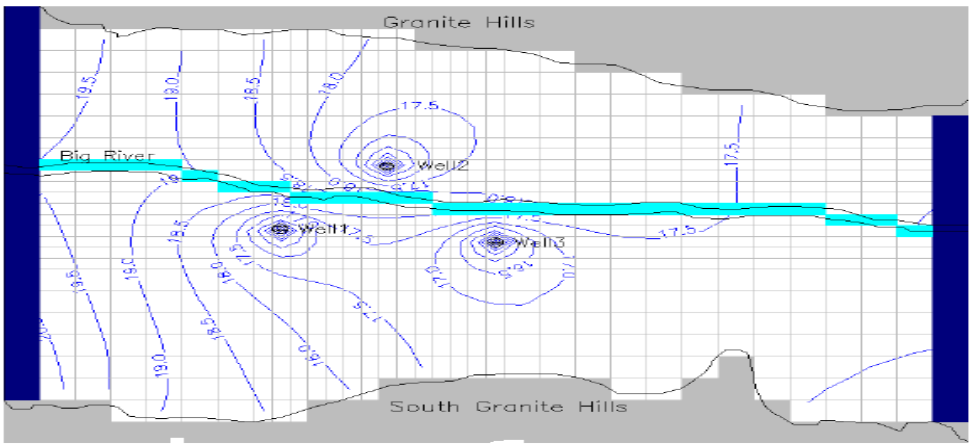

Fig (2): The hydraulic conductivity contours in aquifer surrounding the river

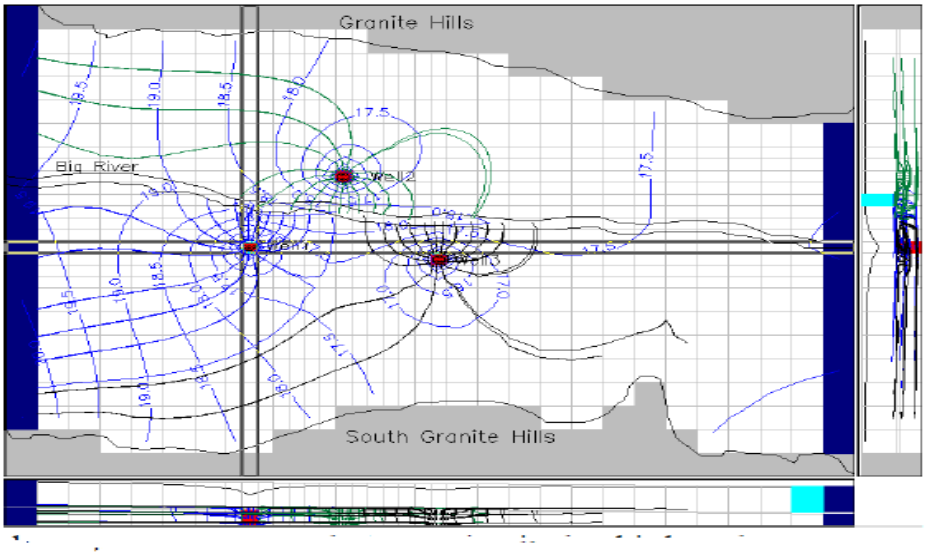

Fig (3) the capture zone of each pumping well

Also by using MT3D MODFLOW packages which depend on equation (2) we can estimate the contaminate transport and the arrival time of pollutants to reach the aquifer. It is found that contaminants in the location A1 illustrated in Fig (4) needs 75 days to reach the well 2. Furthermore, the area influenced by pollutants due to pumping process can be determined as shown in Fig (5).

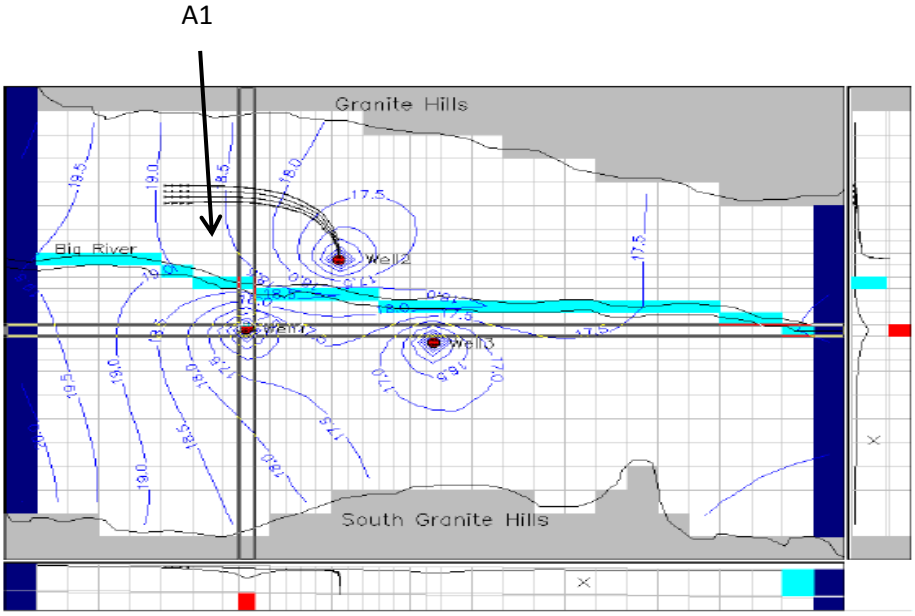

Fig (4): The transport path of pollutants from the location A1 towards the well 2

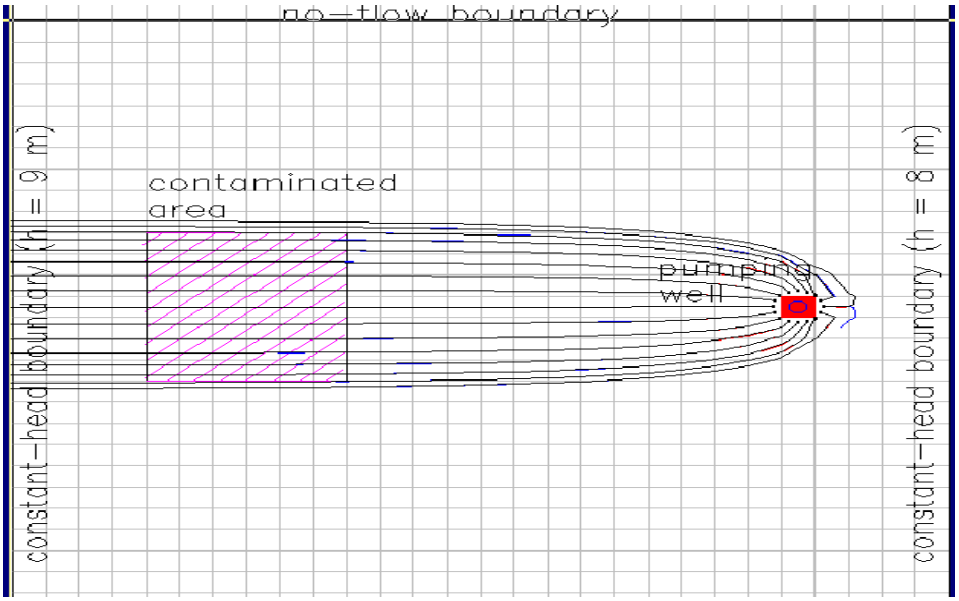

Fig (5) the contaminant area influenced by pumping well

Although MODFLOW is the most popular software used to simulate groundwater process and it can give a satisfactory result, there are some limitations for using it in RBF systems.

Limitations of MODFLOW (Brunner et al., 2010**)**

- Neglecting negative pressure gradients leads to an underestimation of the infiltration flux.
- Because rivers are assigned to only one grid cell, the infiltration flux under a river is uniform while in reality this is only true for disconnected systems.
- The size of the single grid cell of a river is assigned to influence the infiltration flux.
- The vertical discretization of the aquifer affects the infiltration flux.

Results of the Analytical model

The model (referring to equation (3) and analytical solution (4)) is tested for three different nutrients: NO_3, O_2 and SO_4. The model is compared with experimental data of Doussan et al. (1997) for NO_3, O_2 (Fig 6) and SO_4.(Fig 7), and showed that NO_3 and O_2 are consumed within 10 cm of the aquifer while SO_4 is consumed within 30 cm.

a

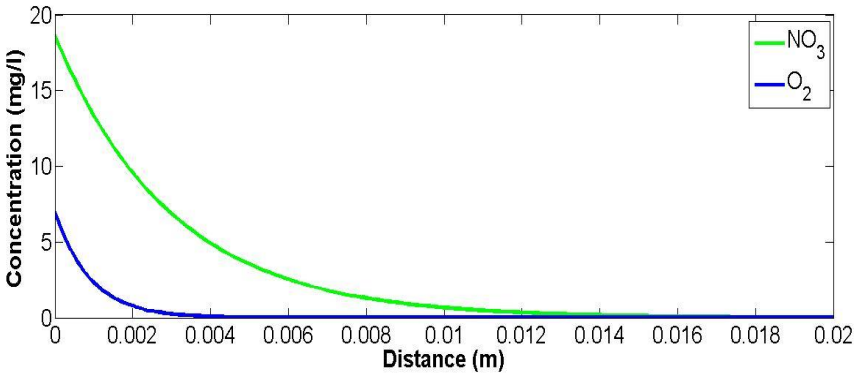

b

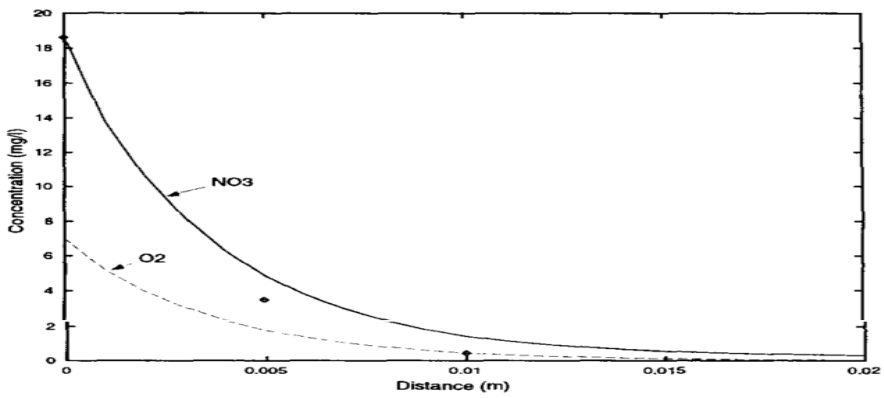

Fig (6): (a) illustrates the simulation of NO_3 and O_2 in an analytical model, (b) shows simulated lines and experimental data points for (Doussan et al., 1997)

a

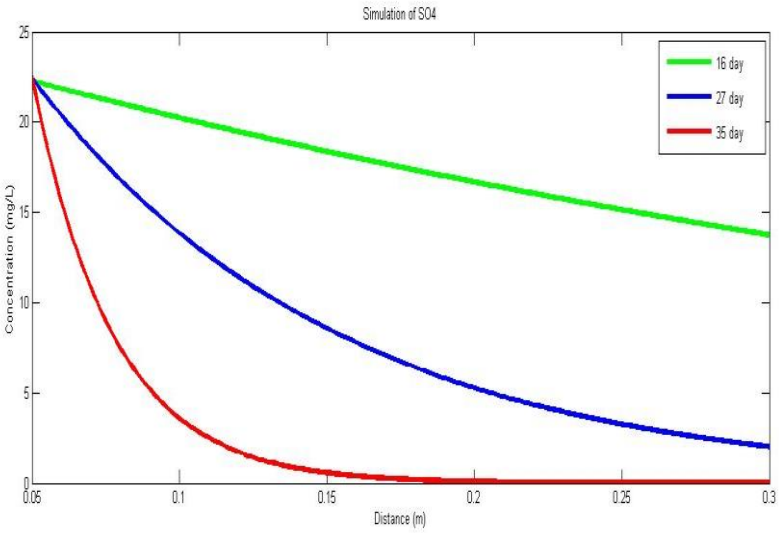

b

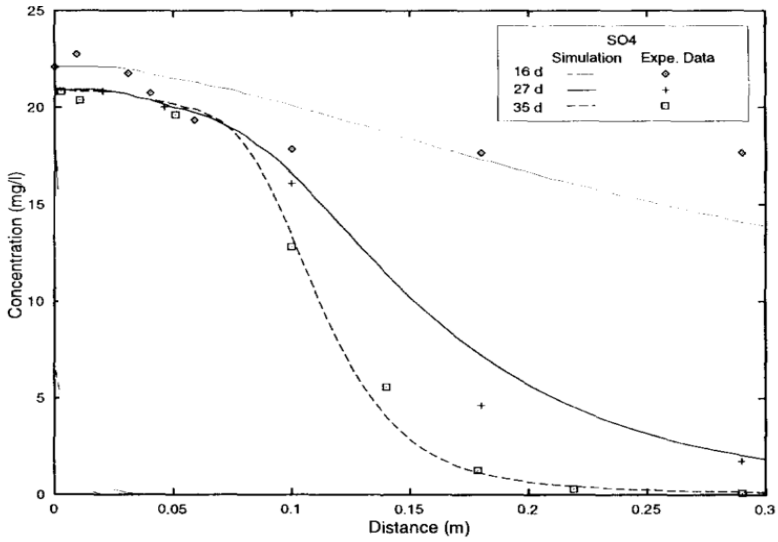

Fig (7): (a) illustrates the simulation of SO_4 after 16, 27 and 35 days, (b) shows simulated lines and experimental data points for (Doussan et al., 1997) in the same time.

1.5 Conclusion and Recommendation

Both of the numerical and analytical modelling methods are used in this report to simulate the contaminants transport and water flow in the riverbank filtration site. The numerical code MODFLOW is used to simulate water flow, hydraulic head and capture zone of each pumping well near the river. Also the particle tracking based Eulerian-Lagrangian method in MODFLOW is used to simulate the travel time taken by contaminants to reach the well. The result is calculated under the pumping rate equal 500m^3/day for each well. Although MODFLOW software is used by researchers to simulate most processes which occur in groundwater dynamics, further mathematical modelling should be developed to get more accurate results and to overcome the limitations of MODFLOW that are mentioned previously. Also, in this report, MODFLOW is only used for computing the hydraulic head and the travel time needed for contaminant to reach the pumping well. In further development of theses result, MODFLOW can be implemented to simulate:

1- The drawdown of groundwater and stream depletion rate due to pumping process.
2- The contaminant concentration in surrounding aquifer.
3- The optimum pumping rate needed so that the contaminated area lies within the capture zone of the pumping well.

On other hand the analytical model is used for evolution of water chemistry due to microbial activity. The model is compared with data collected from the literature which is applicable for the *National Hydraulics Research Institute Malaysia (NAHRIM)* situation. The model concerned only microbial activity, thus, for further development of this model, water flow process (water movement induced by pumping well) should be considered.

1.6 References

AL-ODAINI, N. A., ZAKARIA, M. P., YAZIZ, M. I. & SURIF, S. 2010. Multi-residue analytical method for human pharmaceuticals and synthetic hormones in river water and sewage effluents by solid-phase extraction and liquid chromatography-tandem mass spectrometry. *J Chromatogr A,* 1217**,** 6791-806.

BRUNNER, P., SIMMONS, C. T., COOK, P. G. & THERRIEN, R. 2010. Modeling surface water-groundwater interaction with MODFLOW: some considerations. *Ground Water,* 48**,** 174-80.

DEPARTMENT OF STATISTIC MALAYSIA 2010. Population Distribution and Basic Demographic Characteristic Report. *Department of Statistic*

DOUSSAN, C., POITEVIN, G., LEDOUX, E. & DETAY, M. 1997. River bank filtration: modelling of the changes in water chemistry with emphasis on nitrogen species. *Journal of Contaminant Hydrology,* 25**,** 129-156.

FARIZAWATI, S., LIM, Y. A., AHMAD, R. A., FATIMAH, C. T. & SITI-NOR, Y. 2005. Contribution of cattle farms towards river contamination with Giardia cysts and Cryptosporidium oocysts in Sungai Langat Basin. *Trop Biomed,* 22**,** 89-98.

GOVERNMENT OF MALAYSIA 2000. The National Water Resources Study 2000-2050.

KHAIRUDDIN, M. I. & ABD MALEK, A. 2002. Program pencegahan pencemaran dan peningkatan kualiti air sungai Langat. Proceeding Simposium Penyelidikan Lembangan Langat 2001. *In:* MAZLIN M., S. I., AHMAD FARIZ M. ABDUL HADI H. S. AND SARAH A.A.G.A. (ed.). (Eds). Lestari, UKM, Bangi.

LEE, Y. H., MOKHTAR, M., & OMAR, S. R. 2006. Organochlorine Insecticides Level Detected in Water and Sediments from the Langat River and a Lake Near to a Golf Course at Bangi, Selangor. *Sains Malaysiana.,* 35**,** 1-6.

LIZA, S. A. C. 2010. *Dissertation, Assessment of water quality characteristics during base and storm flow events on Sungai Langat Basin.* Universiti Teknologi Malaysia.

OSMAN, R., SAIM, N., JUAHIR, H. & ABDULLAH, M. P. 2012. Chemometric application in identifying sources of organic contaminants in Langat river basin. *Environ Monit Assess*, 184**,** 1001-14.

OTHMAN, M. S. & GASIM, M. B. 2005. Heavy Metals Concentrations in Water of Sungai Semenyih Watershed , Selangor. *Sains Malaysiana.*, 34**,** 49-54.

SHAMSUDDIN, M. K. N., SULAIMAN, W. N. A., SURATMAN, S., ZAKARIA, M. P. & SAMUDING, K. 2013. Conjunctive use of surface water and groundwater via the bank infiltration method. *Arabian Journal of Geosciences*.

UNITED NATIONS 2005. *Good Practices on Strategic Planning and Management of Water Resources In Asia And The Pacific*.

UPUM, U. M. C. U. 2002. Final report program Pencegahan dan Peningkatan Kualiti Air Sungai Langat.

ZAKARIA, M. P. & MAHAT, A. A. 2006. Distribution of Polycyclic Aromatic Hydrocarbon (PAHs) in sediments in the Langat Estuary. *Coastal marine science*, 30**,** 387-395.

Development of Early Warning System for Rice Blast and Brown Planthopper (BPH), Pest and Disease of Rice

MALAYSIAN AGRICULTURAL RESEARCH AND DEVELOPMENT INSTITUTE (MARDI)

Representative/Group Members:

Arifah Bahar, Norhaiza Ahmad, Shariffah Suhaila, Haliza Abdul Rahman, Fadhilah Yusof, Robiah Adnan, Syaza Eva, Graeme Wake, Ting Chee Ming, Ibrahim, Mahendran, Mohd Fitri

1.7 Introduction

Pests and diseases are major factors affecting rice production in Malaysia as well as in other rice growing countries. Brown plant hopper (BPH, Nilaparvatalugens) and rice blast disease (Pyriculariaoryzae) are considered as a major constraint in Southeast Asia. In Malaysia alone, the estimated yield loss caused by the disease was about 90 000t/ season which is valued at about RM 72 million. Although P. oryzae may infect at any parts of the aboveground parts of the plant, but infection on the panicles are the most damaging. It has been shown to significantly reduce yield, grain weight and milling quality. In the off-season 2007, total acreage affected by BPH in Muda area reached more than 4,497 ha or about 4.7% of the total planted area in the region. [1]

1.8 Problem Statement

At the moment, the defense strategies against the blast disease is still mainly based on variatal resistance with the support of chemical control. However, the issue is when is the appropriate time and situation that require chemical treatment intervention to ensure its effectiveness in controlling the disease. Usually disease incidence and severity need to be above a certain level (the threshold level) to cause significant yield loss. Therefore investigation involving predicting when the disease is likely to exceed this threshold level need to be conducted. Generally, high relative humidity and long periods of leaf wetness

under tropical climate, dew periods, plant density, fertilizer rate, optimum temperature, water stress, with the support of the presence of virulent isolates and susceptible varieties are among the main factors that contribute towards the infection, colonization and sporulation of spore on plants. The rate of BPH population build–up in the rice field is depended upon several factors including the intensity of migrant population, the susceptibility levels of the planted host varieties, the nutritional qualities of the host, the abundance of other biotic components including natural enemies and competitor organisms, and conducive physical environments as above.

The main aim of this study is to determine in advance the biological and other environmental parameters that are conducive and may trigger rice blast and BPH outbreak in the field so that the most effective preventive and control measures can be taken to prevent potential large scale outbreak to occurs. The gathered information may lead to ability to develop an effective technique to forecast rice blast and BPHoccurence in the fields. Optimization of the parameters and multiple regression analysis used to analyzed the relationships between the parameters with the in-field blast incidence and in-field generation of BPH population were known as the main constraint in developing both forecasting models. [1]

1.9 Methodology

The development of early warning system needs to take into consideration the two causes of rice blast namely, pests and diseases.Due to complexity of both problems, the scope of this reporthas been limited to pest only. However, the additional information on rice diseasesis in Appendix 1. The methodology suggested for the problem mentioned is as in the following sequence.

i- Estimation of BPH count for light trap based on tapping and sweeping
ii- Determination of light trap allocation
iii- Growth Model

1.3.1 Estimation of BPH count for light trap based on tapping and sweeping

There are three types of methods to capture BPH namely light trap, tapping and sweeping. We use inverse distance weighting method to estimate the number of BPH captured using light trap at a particular location which is in the neighbourhood of BPH captured using tapping and sweeping.The inverse distance weighting method is based on the proximity of the neighboring stations or surrounding stations to the target station.The weighted distance method is given as follows

$$W_i = \frac{d_{it}^{-p}}{\sum_{\substack{i=1 \\ i \neq t}}^{N} d_{it}^{-p}}$$

where d_{it} is the distance between the target station and the ith neighboring station. The weight decreases as the distance increases from the target station. Greater values of p assign greater influence to values closest to the target station. The value of p usually ranges from 1.0 to 6.0 and the most commonly used value for p is 2 (Xia *et al*., 1999). The formula of weighting method is given as follows:

$$X_t = \sum_{\substack{i=1 \\ i \neq t}}^{N} W_i X_i$$

where X_t is the estimated value of the missing data at the target station (light trap) t; N is the number of neighbouring (tapping and sweeping) stations; X_i is the observation at the ith neighboring station and W_i is the weight of the ith neighboring station with constraint $\sum_{i=1}^{N} W_i = 1$.

Based on the following data in Table 1, the estimated BPH count for light trap based on Tapping and Sweeping for 5 regions is as presented in Table 2.

MARDI S.Perai	16	11	8	3	2	6	4	1	0
Sawah Sempadan	25	3	3	0	5	1	0	0	0
Sg. Limau	28	0	3	1	3	3	1	6	2
Seb.Perak	19	2	2	2	2	0	0	0	0
Arau	23	5	2	4	2	4	1	0	0

Table 1: Real Data on BPH Count

Location	Estimated value at point xo:light trap	RMSE
MARDI S.Perai	16.9	0.636396
SawahSempadan	4	14.84924
Sg. Limau	3	17.67767
Seb.Perak	2	12.02082
Arau	8.9	9.970206

Table 2: Estimated Value at Light Trap Location

The estimated value of BPH count at MARDI SeberangPraistation shows the lowest RMSE (0.6364) which indicates that the method of tapping or sweeping produced almost similar result with light trap. However, other stations do not show a promising result.

The following subsection is presented under the assumption that the sampling method is done via light trap.

1.3.2 Determination of Light Trap Allocation

Light trap is one of the ways of capturing BPH. It is set up as in Figure 1. Currently, MARDI is taking samples every 3 nights. Lights are turned on that night. Insects (BPH & other natural enemies) are attracted to the light and eventually fall into the bottle trap. This is due to BPH crepuscular activity pattern (active primarily during twilight (i.e., dawn and dusk)) and phototactic behavior that influences their response to light traps as explained by MARDI Representative.

Figure 1 Visual Light-Trap taken from MARDI Pilot Study [1

The limitation of this method as discussed with MARDI representative are

i) Other insects including BPH natural enemies are also captured

ii) Difficulty in sorting insects in light trap

iii) Max count of BPH caught in 3-months=28 (too small during off-peak season)

iv) Only adult winged BPH are captured (life cycle of BPH as in Figure 2)

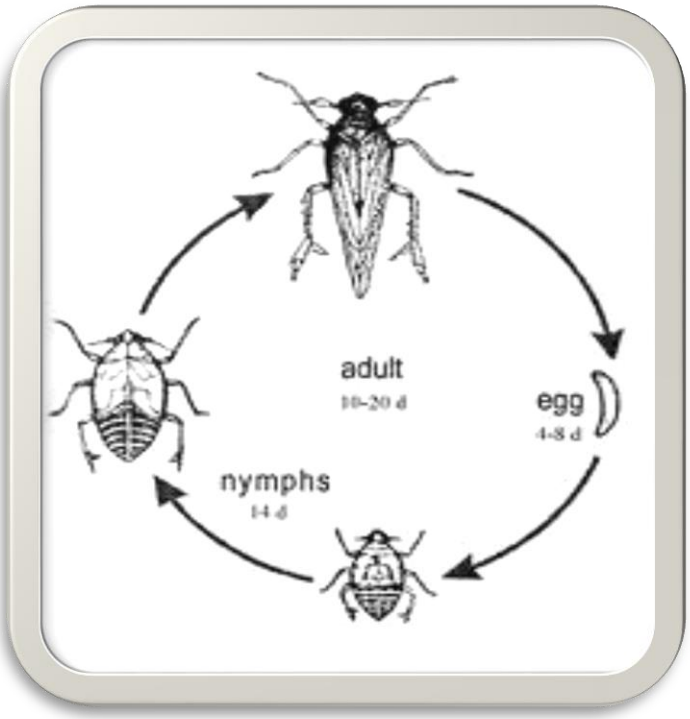

Figure 2: Lifecyle of a BPH

Based on existing light trap setting, we calculate the number of catch per trap with the following assumptions:

i) BPH flies towards the nearest trap (this is the case when the information on BPH response distance to the light intensity is not available)

ii) traps catch a number of BPH proportional to the area within the range of attraction, *r*

$$A_i^I = \pi r^2 - \sum_{j \in NN} \left(2r^2 \arctan\left(\frac{2\Omega}{d_{ij}}\right) - d_{ij}\Omega \right)$$

$$\Omega = \sqrt{r^2 - \left(\frac{d_{ij}}{2}\right)^2}$$

$$C_i^I = \frac{A_i^I}{\sum_{i=1}^{n} A_i^I}$$

r = Light intensity (to be specified).

d_{ij}= distance, between two neighboring traps,*i*th and *j*th
A_i: the area within the range of attraction for the *i*th trap minus half the area of the*j*th trap, which is the one or two next neighbours, NN.
n=total number of traps
C_i :The predicted fraction of catch for the *i*'th trap

There are two cases of setting up the light trap, the non-overlapping range of attraction (Figure 3) and the overlapping range of attraction (Figure 4).Both are taken from [2].We presented the result with non-overlapping case.

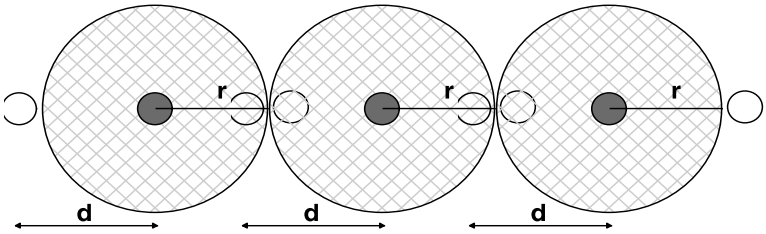

Figure 3: Range of Attraction Between Traps (no overlapping)

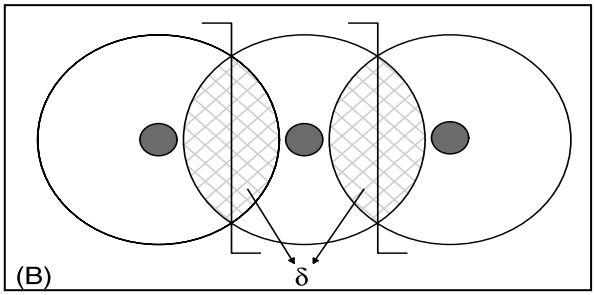

Figure 4: Range of Attraction Between Traps (with overlappingδ)

The following result shows the fraction of catch per trap per transect of 1kmfor the range of attraction, $r \in (5,300)$ meters . Figure 5 shows as range of attraction increases, percentage of catch tends to increase with a min. number of traps. For example at *r*=200-300, only need around 1-2 light traps as shown in Figure 6. At a smaller range of attraction, more light traps are needed. But the fraction of catch per trap per transect is smaller.

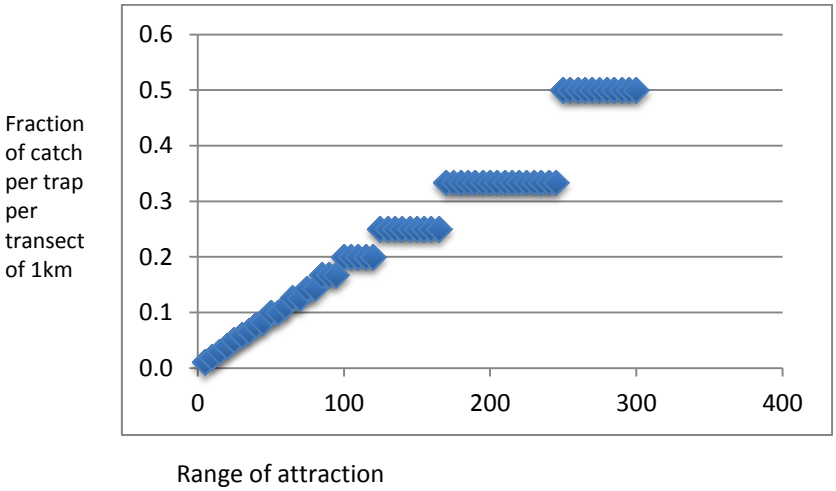

Figure 5: The relationship between Fraction of catch per trap per transect of 1km and Range of attraction

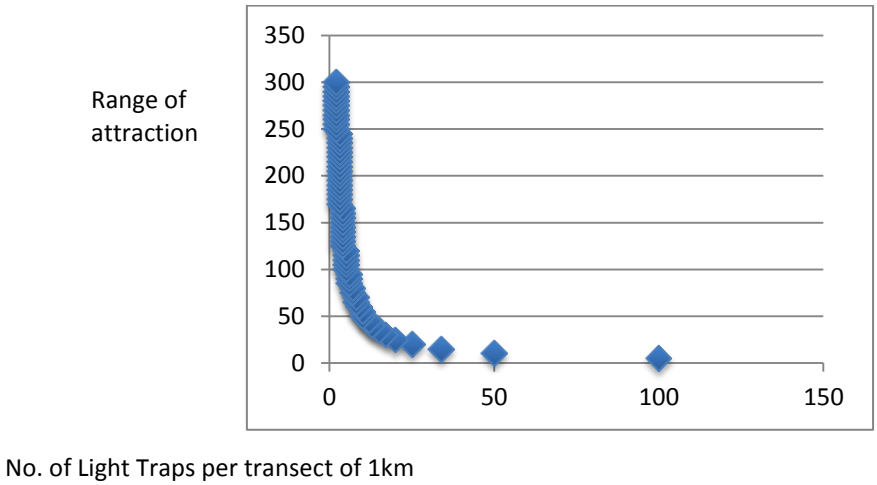

Figure 6: The relationship between Range of attraction and Number of light traps per transect of 1km

Recommendation for future study includes

i) Setting up light-traps in a transect Lines and based on wind direction
ii) Sampling nights should take into account the optimal flying conditions of BPH
iii) BPH response distance to light intensity should be investigated so that the range of attraction of BPH to the light trap can be taken into account to calculate the fraction of catch per trap using the formula

$$r^k = \sqrt{\frac{1}{I_C^k}}$$

1.9.1 Growth Model

Modelling the growth of BPH needs to consider the immigrant andemmigrant density of BPH that significantly affect the population build up in the rice field. There are two approaches to be presented namely Rice Pest Interaction Model, and BPH Prediction Model which consists of Migration Model and Growth Model.

Rice Pest Interaction Model

This generic model suggested by Wake and Syaza is developed as follows

$$\begin{aligned} \frac{dR}{dt} &= k_1 R\left(1-\frac{R}{k_2}\right) - k_3 RP \\ \frac{dP}{dt} &= rP\left(1-\frac{P}{k_0 R}\right) - \lambda P \end{aligned}$$

where:

R : the biomass of the rice (paddy) [mass area^{-1}]
P : the population of the pest [dimensionless]
k_1 : growth rate for rice [days^{-1}]
k_2 : carrying capacity for rice [mass area^{-1}]
k_3 : consumption rate of rice by the pest [days^{-1}]
k_0 : scaling constant for the carrying capacity [area mass^{-1}]
r : the growth rate for the pest [days^{-1}]
λ : predation rate for the pest (pests eaten by natural enemies e.g. insects) per capita [days^{-1}]

The steady-state points (R^*; P^*) are (0,0), (k_2,0) and

$$\left(\frac{rk_1k_2}{rk_1 - k_0k_2k_3(r-\lambda)}, \frac{k_0k_1k_2(r-\lambda)}{rk_1 - k_0k_2k_3(r-\lambda)}\right).$$

The phase plane as in Figure 7.

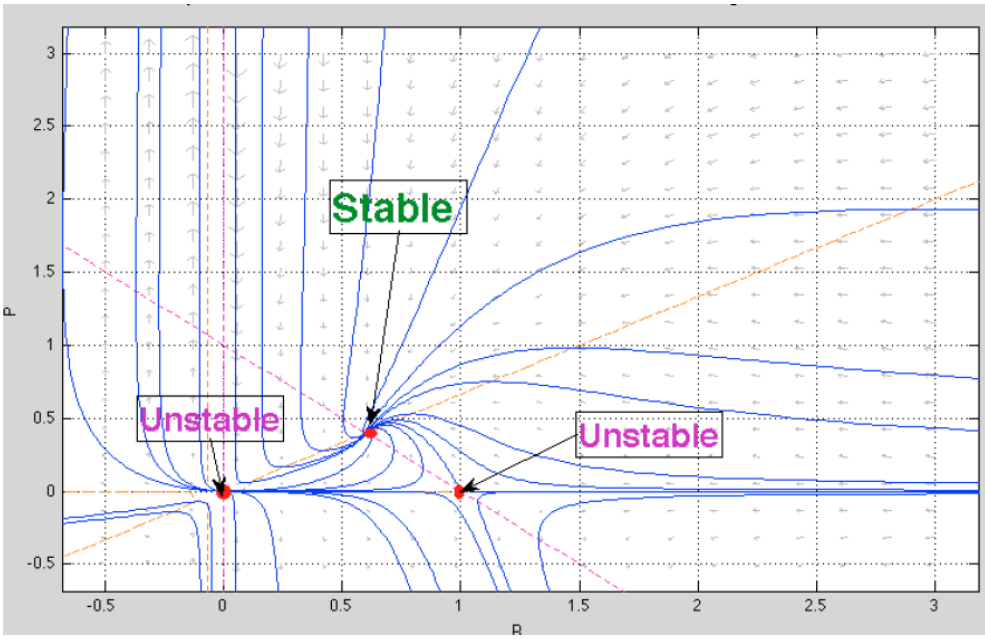

Figure 7 : The Phase Plane

Recommendations:

i- include predation rate for the pest (λ) as a function of time
ii- parameterisation using appropriate data from MARDI
iii- focus on BPH study case - the model proposed here is generic
iv- extend this model to include the nymph and adult stage of BPH

BPH Prediction Model

This prediction model as proposed by [3] consists of two sub-models namely BPH Growth Model and BPH Migration Model. In order to carry out an experiment that uses the modelto describe the density of BPH, the studied region is discretized by a grid of square cells,which is appropriate for implementing a cellular automaton inagent-based modeling. This cellular automaton considers the observed variable to be modeled as arandom process. Each cell in the

stochastic model represents asquare area of the real system. The prediction model is basedon interactions between the two sub-models, BPH migration model and BPH growth model.

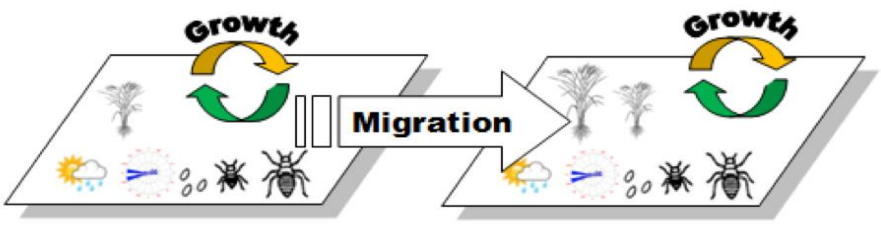

Figure 8: BPH Prediction Model shows the interaction between Growth Model and Migration Model

The migration process of BPHs in the discretized region determines the dynamical movement process in the cellular automata. It determines the outcome of the number of BPHs (out) in the future considered as one time step from a specific source cell and the rates of BPH (out) to all destinations at one time step in the future. Destination cells are determined by the semi-circle under the wind, while the radius of the circle is determined by the wind velocity and themigration time in a day. The attractiveness index and the obstruction index as given by [4] are considered as limitation.

BPH growth model

For this model, we suggest to use the model by [5] that considers deterministic model of the lifecycle of the BPH. Let T be the lifecycle of BPH, the model suggest T = 32.

$$V[t] = \begin{cases} \sum_{i \in T_1} V[i] * r_b * m, & t = 1 \\ V[t-1] * r_{en} * m, & t \in T_2 \\ V[t-1] * r_{na} * m, & t \in T_3 \\ V[t-1] * m, & otherwise \end{cases}$$

$V[t]$ gives the number of BPH at age t (i.e. ith day of BPH lifecycle).
$[i]$ denotes the number of insects at age i,
r_{en}denotes the ratio of egg number able to become the nymph,
r_{na}denotes the ratio of nymph number able to become the adult,
$r_b$denotes the ratio of eggs can be produced by an adult,
$m$denotes the ratio of natural mortality,
T_1denotes the egg giving time span,

T_2denotes the egg and time span.
T_3 denotes nymph time span.

The BPH prediction model will be integrated with Surveillance Network Model [6] that will be used to measure the trap-density inthe prediction model. Each surveillance device agent monitors thetrap-density based on the location of its cell agent. Thetrap-density is defined as equivalent to the number of adult BPHs located in a particular cell agent [5].

References

[1] MohdFitriMasarudin and Allicia Jack, Development of early warning system for brown planthopper (BPH) and rice blast, pest and disease of rice, Presentation at Mathematics in Industry Study Group MISG 2014, UTM Johor Bahru.

[2]CarstenKirkeby, KaareGræsbøll, Anders Stockmarr, Lasse E Christiansen and René Bødker,The range of attraction for light traps catching Culicoides biting midges (Diptera: Ceratopogonidae), Parasites & Vectors 2013, 6:67 doi:10.1186/1756-3305-6-67

[3]Truong Minh Thai, Truong Xuan Viet, FrédéricAmblard, Alexis Drogoul, Benoit Gaudou, Huynh Xuan Hiep, Le Ngoc Minh, Christophe Sibertin-Blanc, A framework for combining Business Intelligence & Agent-based Simulation,

[4] Truong, V.X. et al. 2013. Optimizing an Environmental SurveillanceNetwork with Gaussian Process − An optimization approach by agentbasedsimulation. *The Sixth International KES Conference on Agentsand Multi-agent Systems – Technologies and Applications (KESAMSTA 2013)* (2013), 102–111.

[5] Thai Truong Minh, Viet Truong Xuan, FrédéricAmblard,Benoit Gaudou, Christophe Sibertin-Blanc,Alexis Drogoul, Huynh Xuan Hiep& Le Ngoc Minh,An Implementation of Framework of Business Intelligencefor Agent-based Simulation, *SoICT '13 Proceedings of the Fourth Symposium on Information and Communication Technology*,(2013), 35-44.

[6]Truong, V.X. et al. 2012. Modeling a SurveillanceNetwork Based on Unit Disk Graph Technique--
Application for Monitoring the Invasion of Insects inMekong Delta Region.*PRIMA 2012: Principles andPractice of Multi-Agent Systems.*Springer.228–242.

APPENDIX 1

Logistic Regression

Logistic regression or logit regression is a type of probabilistic statistical classification model. Logistic regression measures the relationship between a categorical dependent variable and one or more independent variables, which are usually (but not necessarily) continuous, by using probability scores as the predicted values of the dependent variable.

Our goal is to estimate the regression coefficients in a model, given a sample of (X,Y) pairs. In the case of logistic regression, the X's can be numerical or categorical, buy Y's are generally coded as 0 (for those who do not have the event) or 1 (for those who have the event).

$$\pi = \frac{\exp(\beta_0 + \beta_1 x)}{1 + \exp(\beta_0 + \beta_1 x)}$$

The value of β_0 yields π when x is zero, and β_1 indicates how the probability of an occurrence changes when x changes by a single unit. Because the relation between x and π is nonlinear, β_1 does not have as straightforward an interpretation in this model as it does in ordinary linear regression.

$$L = \ln(O) = \ln\left(\frac{p}{1-p}\right) = \beta_o + \beta_1 X + \in$$

p is the proportion of successes

O is the odds of the event

L is the ln(odds of event)

X is the independent variable

$$\ln\left(\frac{p}{1-p}\right) = \beta_0 + \beta_1 x + \varepsilon$$

Based on data given: our objective is to study the relationship between incidence of disease and amount of rainfall. How these two variables are related? If the disease exists, we denote as 1 otherwise the value of 0 is assigned. So we have a binary variable as our response variable while rainfall is a continuous and numerical variable as our predictor variable.

Coefficients:

(Intercept) Rainfall

2.37394 -0.04376

Logit (y)= 2.37394 - 0.04376*Rainfall

We expect as rainfall increases, the percentage of disease will increase. However, based on the data given, the result is contradicting. We suspect maybe because of the length of data set which is so small. The plot of logit*y* vs rainfall is given as follows.

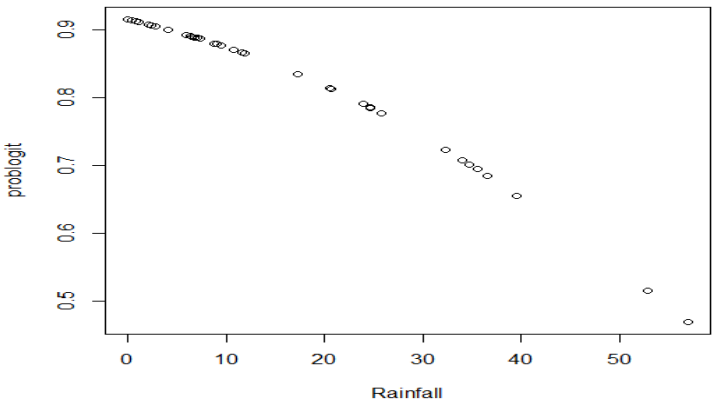

Suppose we have, positive slope.

Logit (*y*) = 2.37394+0.04376*Rainfall,

The graph is given as below which follow logistic regression

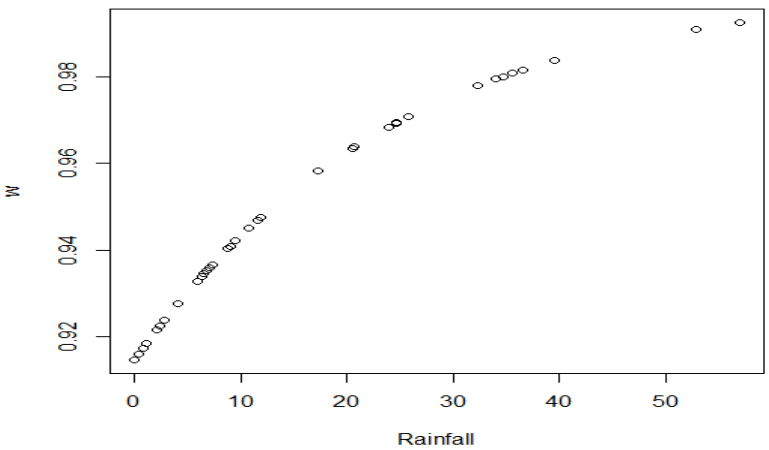

Problem remain unsolved probably due to the data limitation.

APPENDIX 2

Deterministic model

$$\frac{dS}{dt} = -R_2 S \times I$$

S-Number of plant susceptible to the disease

I-Number of plant infected by the disease

External random perturbation is considered if humidity is regarded as environmental factors effecting susceptibility

$$R_2 \to R_2 + \phi dWt$$

Stochastic Model

$$\frac{dS}{dt} = -R_2(S \times I) - \phi(S \times I)dWt$$

dWt Brownian noise

$dWt \approx \Delta W_t \square N(0, \Delta t)$

To estimate R_2 and ϕ the non-parametric method is utilized (Allen, 2007)

$$\sum_{i=1}^{N-1} f(t_i, S_i, \theta) = \frac{1}{\Delta t}\sum_{i=1}^{N-1}(S_{i+1} - S_i)$$

$$\sum_{i=1}^{N-1} g^2(t_i, S_i, \theta) = \frac{1}{\Delta t}\sum_{i=1}^{N-1}(S_{i+1} - S_i)^2$$

Stochastic model

$$R_2 = \frac{\sum_{i=1}^{N-1}(S_{i+1} - S_i)}{\Delta t \sum_{i=1}^{N-1}(SI)} \qquad \phi^2 = \frac{\sum_{i=1}^{N-1}(S_{i+1} - S_i)^2}{\Delta t \sum_{i=1}^{N-1}(SI)^2}$$

The solution of SDE is approximated by Euler numerical scheme given as the following:

$$X_{i+1}(\omega) = X_i(\omega) + f(t_i, X_i(\omega))\Delta t + g(t_i, X_i(\omega))\Delta W_i(\omega)$$

and $X_0(\omega) = X(0, \omega)$

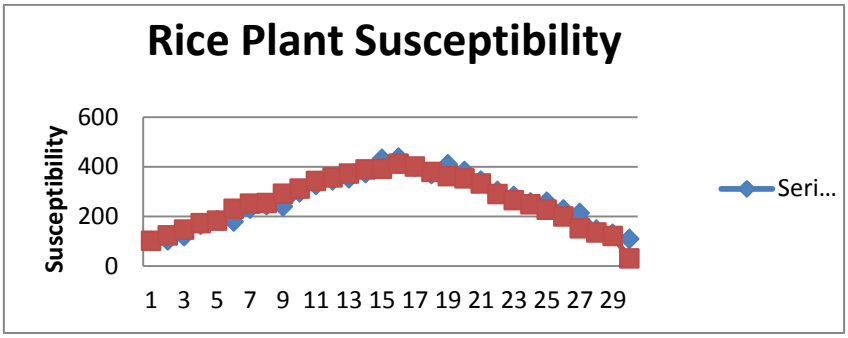

Blue line – predicted number of susceptible plant

Red Line – observed number of susceptible plant

Effects Of Stent On Blood Flow At Coronary Bifurcation

KPJ HEALTHCARE BERHAD

Representative/Group Members:
Jamal Uddin, Baba Agaaie, Esam Amir, Athirah, Airil Yasreen, Ahmad Razin, MohdAkhbar, Firdaus, Tang Aik Ying, Tan Phey Hoon, Mokhtazul Haizat, Norzieha, lyani, Zuhaila, Wan Rukaida, Tan Yan Bin, Norsarahaida, Shahrom Ujang

Abstract

The coronary artery bifurcation is a common site of atherosclerosis which is a major leading cause of heart attack. The impact of stenosis in the atherosclerotic artery is to disturb the flow pattern and produce regions with high shear rate, turbulence, and recirculation, which are key hemodynamic factors associated with plaque rupture, clot formation, and embolism. Coronary bifurcation lesionsrepresent an area of ongoing challenge in interventional cardiology. Stents are most frequently implanted in curved vessels such as the coronary arteries,but most computational studies examining blood flow patterns through stented vessels conductedto date use linear, cylindrical geometric models. It appears highly probable that restenosis occurringafter stent implantation in curved arteries also occurs as a consequence of changes in fluid dynamicsthat are established immediately after stent implantation.An investigation on the effects of stent geometry and bifurcation angle on blood flow pattern in a stented coronary artery has to be considered. The analytical and numerical methods are employed to solve the mathematical modelling of the problem. The results of the pressure and velocity at bifurcated artery show that the flow is disturbed and separation of streamlines from the vessel wall and formation of eddies may occur.

1.1 Introduction

Cardiovascular disease is used most often to describe damage caused to the heart or blood vessels by atherosclerosis (arterial disease). The development of atherosclerotic lesions strongly disturbs the blood flow at the coronary artery bifurcations. Coronary bifurcation

lesions represent an area of ongoing challenge in interventional cardiology. Contemporary studies using drug-eluting stents report a reduction in main vessel restenosis, residual stenosis and restenosis at the side branch remain an issue [1].

Nowadays stent placement becomes a common interventional procedure for treatment of coronary artery disease and its clinical outcome was better when compared to standard angioplasty. However, bifurcation lesions have always represented a major challenge for placement of stents for treatment of stenosis. Conventional bare metal stents are mostly used in clinical practice of bifurcation lesion treatments since there is no specific commercially available stent dedicated for treating bifurcations. Stent design is strongly influenced by the specific hemodynamic conditions in a given vessel. Therefore, in principal, what was previously assessed for standard stent design, should be re-assessed for stenting bifurcations[2].Stent implantation affects wall shear stress (WSS) values which might lead to in-stent restenosis, and plaque formation in pre-stent and post-stent regions. Alteration of arterial WSS may cause endothelial damage which is believed to be a major cause of plaque and thrombus formation. An investigation on the effects of stent geometry and bifurcation angle on blood flow pattern in a stented coronary artery has to be considered.[3].

1.2 Problem Statement

If the doctor insert stent in main vessel, the doctor may see the lesions at the side branch grow up to 90%. Is it a true blockage or it is just carina (angle shift)? If it is a true blockage, then the intervention is required. But, if it is just carina, how can the doctor detect this without going through another procedure (another scan, flow meter, intervention)?

1.3 Research Methodology

1.3.1 2D Analytical Model Improved Model with Stent and Stenosis

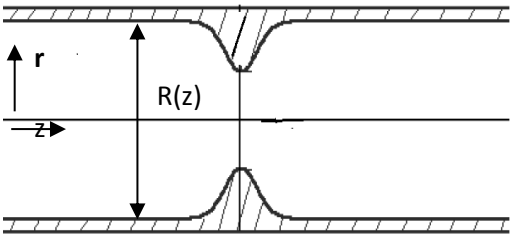

Figure 1: The profile of stenosed artery

Starting with the axial momentum equation for flow in a cylindrical tube we have,

$$\rho\left(u_r\frac{\partial u_r}{\partial r}+u_z\frac{\partial u_r}{\partial z}\right)=-\frac{\partial p}{\partial z}+\mu\frac{1}{r}\left(r\frac{\partial u_z}{\partial r}\right), \qquad (1)$$

where is the radial velocity, is the axial velocity and p is the pressure. Additionally, rho is the density and mu is the viscosity of the fluid. We now form an 'mean average' of this equation in the radial direction by integrating term by term in the radial direction. We therefore have

$$\int_0^{R(s)} r\left(u_r\frac{\partial u_r}{\partial r}\right)dr=\frac{1}{2}\frac{d}{dz}\int_0^{R(s)} ru_1^2dr, \qquad (2)$$

The second term in left hand side of (1),

$$\int\left(ru_z\frac{\partial u_z}{\partial z}\right)dr=\frac{1}{2}\frac{d}{dz}\int_0^{R(s)} ru_z^2dr, \qquad (3)$$

the terms in the right hand side,

$$\rho\frac{d}{dx}\int_0^{R(s)} ru_z^2dr=-\frac{R^2}{2}\frac{dp}{dz}+\mu R\left(\frac{\partial u_z}{\partial r}\right)_{R(s)}. \qquad (4)$$

Writing the velocity field in the form,

$$\frac{u_z}{U(z)}=1+a\eta+b\eta^2+c\eta^3+d\eta^4, \qquad (5)$$

where $\eta=\dfrac{r}{R(z)}$ and $U(z)$ is the velocity along centreline.

Applying the no-slip boundary condition to our velocity we have

$$0 = 1 + a + b + c + d, \tag{6}$$

The second boundary condition which is the symmetry condition along centreline yeilds

$$\frac{\partial u_z}{\partial r} = 0, \tag{7a}$$

From when we have $a = 0$. The boundary condition are identical to that of constant tube radius and the velocity close to Poiseuille profile therefore we require,

$$\frac{\partial^2 u_z}{\partial r^2} = \frac{-2U(z)}{R^2(z)}, \tag{7b}$$

along η. Imposition of this as constant leads to

$$b = -1 \; c = -d.$$

Finally the imposed constant along the wall of the tube will requires profile that satisfy z-component momentum equation that is:

$$0 = -\frac{dp}{dz} + \mu \frac{1}{r} \frac{\partial}{\partial r}\left(r \frac{\partial u_r}{\partial r} \right),$$

along $\eta = 1$. From (4) using algebraic relationship and manipulation the constant coefficient c, can be related to the pressure gradient as:

$$c = -\frac{\phi + 4}{7}, \tag{9}$$

where $\phi = \frac{R^2}{\mu U} \frac{dp}{dz}$. It is possible to eliminate $U(z)$ using the continity equation of integral form

$$Q = \int_0^{R(s)} 2\pi r u_r(r)\, dr, \tag{10}$$

we have

$$U(z)=\frac{210}{97\pi K^2}\left(Q+\frac{\pi R^4}{105\mu}\frac{dp}{dz}\right).$$

Approximating the nonlinear term in (4) using Poiseuille profile we.have

$$u_z=2\overline{U}\left(1-\eta^2\right),$$

Where the average velocity is related to volume rate as,

$$Q=\pi R^2\overline{U}, \tag{11}$$

$$\rho\frac{d}{dz}\int_0^{R(z)} ru_z dr=\frac{2\rho}{3}\frac{d}{dz}\left(R^2\overline{U}^2\right). \tag{12}$$

From (4) the two terms of the right hand side of can be simplified using (9) and (10) to get the pressure gradient in which U is eliminated.

$$\frac{dp}{dz}=\frac{5432}{1675}\frac{\rho Q^2}{\pi^2 R^5}\frac{dR}{dz}-\frac{8\mu Q}{\pi R^4}. \tag{13}$$

Going back to equation (5) we have

$$\frac{u_z(r,z)}{\overline{U}_0}=2\left[\frac{R_0}{R(z)}\right]^2\left(1-\eta^2\right)+\mathrm{Re}\left[\frac{R_0}{R(z)}\right]^3\frac{dR}{dz}\left[\frac{8}{225}(1-\eta^2)-\frac{4}{15}\eta^3+\frac{4}{15}\eta^4\right], \tag{14}$$

(14) is the explicit expression for $u_z(r,z)$ where the Reynolds number for tube given as

$$\mathrm{Re}_0=\frac{2\rho\overline{U}_0R_0}{\mu}.$$

1.3.2 2D Analytical Model Flow in a Bifurcated Artery

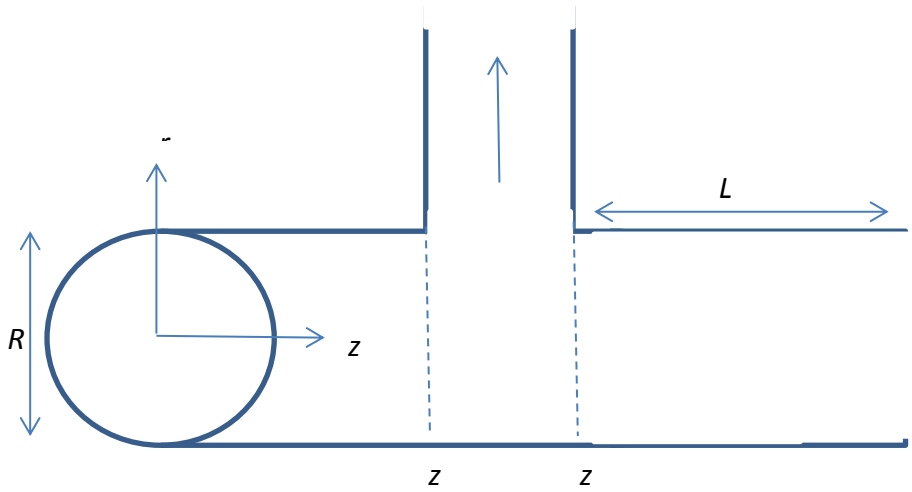

Figure 2 : Schematic of bifurcated artery

Let, $\frac{R_0}{L} = \varepsilon \ll 1$. Then use the following scales,

$$w = u_0 W, \qquad u = \varepsilon U_0 U, \qquad z = LZ, \qquad r = R_0 R.$$

So we get the governing equations

$$\frac{\partial W}{\partial Z} + \frac{\partial U}{\partial R} + \frac{U}{R} = 0, \tag{1}$$

$$\frac{\partial P}{\partial Z} = \left(\frac{\partial^2 W}{\partial R^2} + \frac{1}{R}\frac{\partial W}{\partial R} \right), \tag{2}$$

$$\frac{\partial P}{\partial R} = 0, \tag{3}$$

where the boundary conditions,

$$W = 0 \text{ and } U = f(z) \text{ on } R = 1,$$

$$U = 0 \text{ and } \frac{\partial W}{\partial R} = 0 \text{ on } R = 0.$$

We solve equations (1) and (2) with the boundary conditions given, here we get

$$W = \frac{1}{4}\frac{\partial P}{\partial Z}\left(R^2 - 1\right),$$

and

$$U(Z,R) = -\frac{1}{4}\frac{\partial^2 p}{\partial z^2}\left(\frac{R^3}{4} - \frac{R}{2}\right).$$

By letting $U(Z,1) = f(Z)$ so we can write down $U(Z,1)$ as follows,

$$f(Z) = -\frac{1}{4}\frac{\partial^2 p}{\partial z^2}\left(\frac{R^3}{4} - \frac{R}{2}\right)\Big|_{R=1}.$$

If $f(Z) = kP$ where $Z \in \left[Z_1, Z_2\right]$,

$$kp\left[H\left(z - z_1\right) - H\left(z - z_2\right)\right] = \frac{1}{16}\frac{\partial^2 p}{\partial z^2}.$$

Solving the above equation, then we get the pressure is

$$P = P_0 + ASinh(4\sqrt{k}Z).$$

Pressure at Z_1,

$$P = P_0 + ASinh(4\sqrt{k}Z_1).$$

Pressure at Z_2,

$$P = P_0 + ASinh(4\sqrt{k}Z_2).$$

Pressure difference is

$$\Delta P = ASinh(4\sqrt{k}Z_2) - ASinh(4\sqrt{k}Z_1),$$

finally,

$$U = k\Delta P \Rightarrow U = Ak\left[ASinh(4\sqrt{k}Z_2) - ASinh(4\sqrt{k}Z_1)\right].$$

1.3.3 ADINA Software

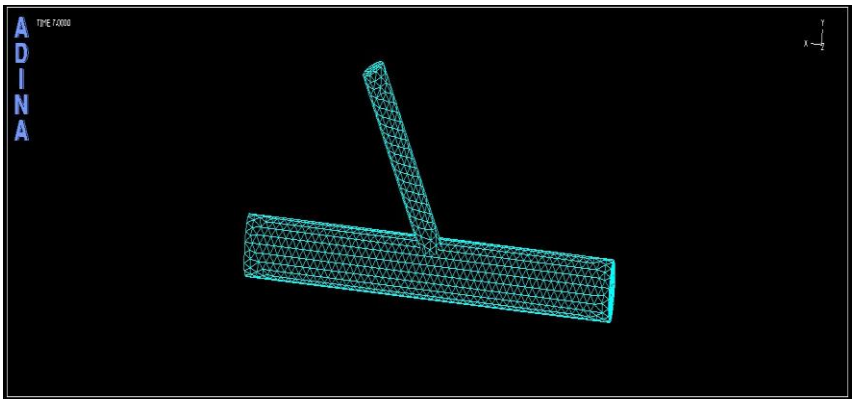

Figure 3: Geometry of a Bifurcated Artery (110111 element, Relative tolerance for Degree of Freedom 0.001, Density 1000kg/m^3, Viscosity 0.00143.)

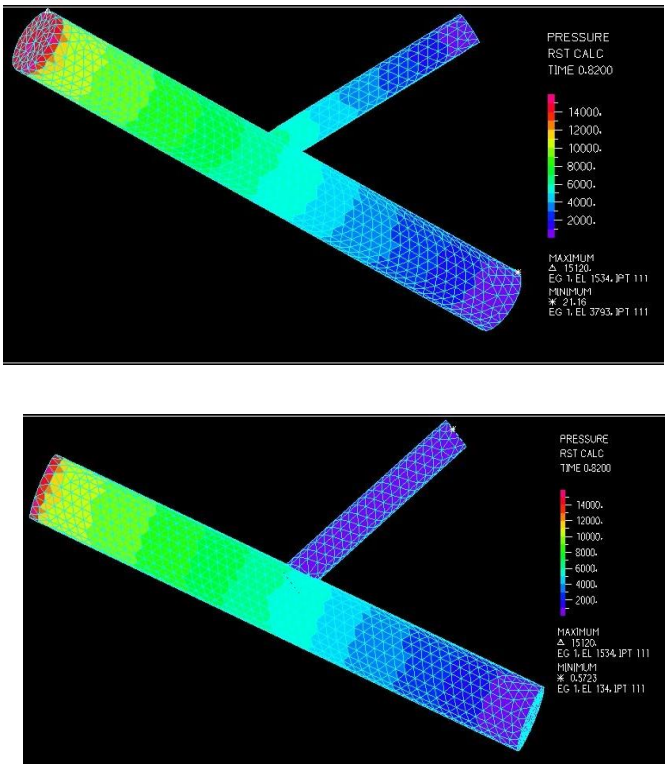

Figure 4: Pressure along the tubea)when $k = 10e-4$, b) when $k = 10e-5$ (110111 element, Relative tolerance for Degree of Freedom 0.001, Density 1000kg/m^3, Viscosity 0.00143)

1.3.4 2D Finite Difference Model Improved Model with Stent and Stenosis

From the Governing Equation,

$$\tilde{r}\frac{\partial \tilde{w}}{\partial \tilde{z}}+\frac{\partial(\tilde{u}\tilde{r})}{\partial \tilde{r}}=0,$$

$$\frac{\partial \tilde{w}}{\partial \tilde{t}}+\frac{\partial(\tilde{w}\tilde{u})}{\partial \tilde{r}}+\frac{\partial \tilde{w}^2}{\partial \tilde{z}}+\frac{(\tilde{w}\tilde{u})}{\tilde{r}}=-\frac{1}{\rho}\frac{\partial \tilde{p}}{\partial \tilde{z}}+\frac{\mu}{\rho}\left(\frac{\partial^2 \tilde{w}}{\partial \tilde{r}^2}+\frac{1}{\tilde{r}}\frac{\partial \tilde{w}}{\partial \tilde{r}}+\frac{\partial^2 \tilde{w}}{\partial \tilde{z}^2}\right),$$

$$\frac{\partial \tilde{u}}{\partial \tilde{t}}+\frac{\partial \tilde{u}^2}{\partial \tilde{r}}+\frac{\partial(\tilde{w}\tilde{u})}{\partial \tilde{z}}+\frac{\tilde{u}^2}{\tilde{r}}=-\frac{1}{\rho}\frac{\partial \tilde{p}}{\partial \tilde{r}}+\frac{\mu}{\rho}\left(\frac{\partial^2 \tilde{u}}{\partial \tilde{r}^2}+\frac{1}{\tilde{r}}\frac{\partial \tilde{u}}{\partial \tilde{r}}+\frac{\partial^2 \tilde{u}}{\partial \tilde{z}^2}-\frac{\tilde{u}}{\tilde{r}^2}\right),$$

Boundary conditions given as,

$$\tilde{w}(\tilde{r},\tilde{z},\tilde{t})=0,\quad \tilde{u}(\tilde{r},\tilde{z},\tilde{t})=\frac{\partial \tilde{R}}{\partial \tilde{t}}\ \text{ for }\ \tilde{r}=\tilde{R}(\tilde{z},\tilde{t}),$$

$$\frac{\partial \tilde{w}(\tilde{r},\tilde{z},\tilde{t})}{\partial \tilde{r}}=0,\quad \tilde{u}(\tilde{r},\tilde{z},\tilde{t})=0\ \text{ for }\ \tilde{r}=0,$$

$$\tilde{w}(\tilde{r},\tilde{z},\tilde{t})=2U_0\left(1-\frac{\tilde{r}^2}{\tilde{R}^2}\right),\quad \tilde{u}(\tilde{r},\tilde{z},\tilde{t})=0\ \text{ for }\ \tilde{z}=0.$$

$$\frac{\partial \tilde{w}(\tilde{r},\tilde{z},\tilde{t})}{\partial \tilde{z}}=0=\frac{\partial \tilde{u}(\tilde{r},\tilde{z},\tilde{t})}{\partial \tilde{z}}\ \text{ for } \tilde{z}=\tilde{L},$$

$$\tilde{w}(\tilde{r},\tilde{z},0)=0,\quad \tilde{u}(\tilde{r},\tilde{z},0)=0\ ,\ \tilde{p}(\tilde{r},\tilde{z},0)=0\ \text{ for }\ \tilde{z}>0.$$

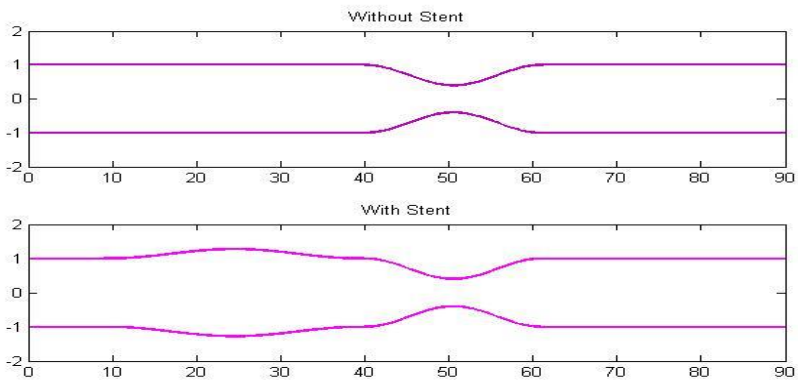

Figure 5 :Schematic Diagram of the Stenosis and Stent

$$\tilde{R}(\tilde{z},\tilde{t}) = \begin{cases} a_1(\tilde{t})\left[r_0 + \frac{\delta_1}{2}\left(1+\cos\left(\frac{\pi(\tilde{z}-S_1)}{Z_1}\right)\right)\right], & S_1 - Z_1 < z < S_1 + Z_1 \\ a_1(\tilde{t})\left[r_0 - \frac{\delta_2}{2}\left(1+\cos\left(\frac{\pi(\tilde{z}-S_2)}{Z_2}\right)\right)\right], & S_2 - Z_2 < z < S_2 + Z_2, \\ a_1(\tilde{t})[r_0], & \text{otherwise} \end{cases}$$

where $a_1(\tilde{t}) = 1 + k_R \sin(\omega_p \tilde{t} + \phi)$.

The result via finite Difference, with
$\mathrm{Re} = 300, \rho = 1050 kgm^{-3}, \delta = 0.6R_0, \mu = 0.035, R_0 = 1.$

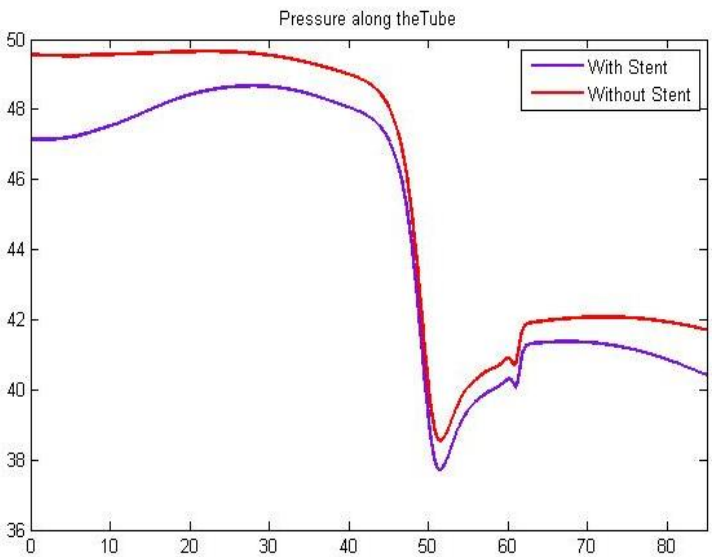

Figure 6 : Pressure along the tube with and without stent

1.3.5 2D Finite Difference Model flow in a Bifurcated Artery with Stenosis

$$\rho\left(\frac{\partial u}{\partial t} + u\frac{\partial u}{\partial r} + w\frac{\partial u}{\partial z}\right) = -\frac{\partial p}{\partial r} + \mu\left(\frac{\partial^2 u}{\partial r^2} + \frac{1}{r}\frac{\partial u}{\partial r} - \frac{u}{r^2} + \frac{\partial^2 u}{\partial z^2}\right),$$

$$\rho\left(\frac{\partial w}{\partial t}+u\frac{\partial w}{\partial r}+w\frac{\partial w}{\partial z}\right)=-\frac{\partial p}{\partial r}+\mu\left(\frac{\partial^2 w}{\partial r^2}+\frac{1}{r}\frac{\partial w}{\partial r}+\frac{\partial^2 w}{\partial z^2}\right),$$

$$\frac{\partial u}{\partial r}+\frac{u}{r}+\frac{\partial w}{\partial z}=0.$$

The boundary condition respect to the governing equation,

$$\frac{\partial w}{\partial r}=0 \text{ on } r=0, \quad 0\le z\le z_3,$$

$$w(r,z,t)=0 \quad \text{on} \quad r=R_1(z,t),$$

$$\tilde{w}(\tilde{r},\tilde{z},\tilde{t})=0 \quad \text{on} \quad r=R_2\left(z,t\right), \quad z_3\le z\le z_{\max},$$
$$w(r,z,t)=w_\circ \quad \text{at} \quad t=0.$$

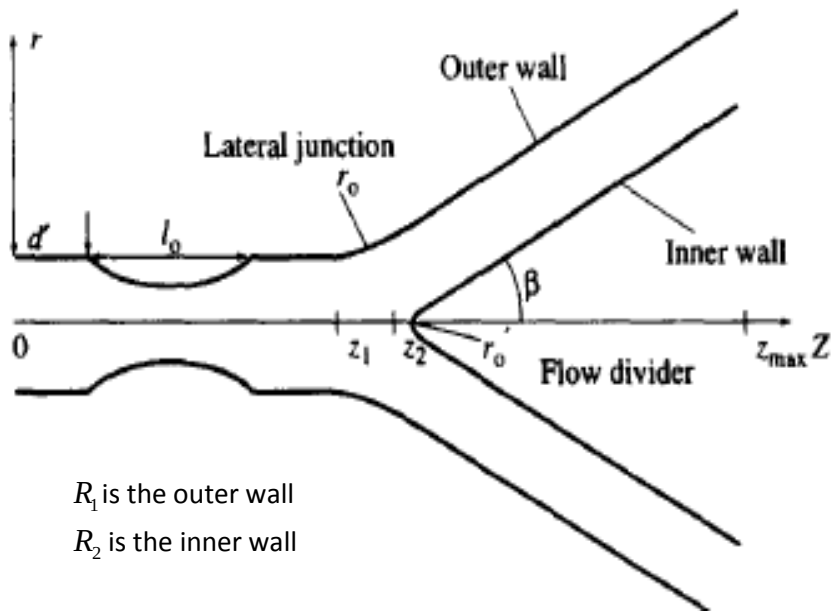

Figure 7: Model of the problem

The geometry is complicated and need to be transformed in order to immobilizing the bifurcated arterial wall in the transformed coordinate.

$$\xi = \frac{r - R_2}{R_1 - R_2} = \frac{r - R_2}{R},$$

$$R_1(z,t) = \begin{cases} a_1(t), 0 \le z \le d' \text{ and } d' + l_0 \le z \le z_1 \\ \left[a - \frac{4\tau_m}{l_0^2}(l_0(z-d') - (z-d')^2)\right] a_1(t), d' \le z \le d' + l_0 \\ \left[a + r_0 - \sqrt{r_0^2 - (z-z_1)^2}\right] a_1(t), z_1 \le z \le z_2 \\ [2r_1 sec\beta + (z - z_3)tan\beta] a_1(t), z_2 \le z \le z_{max} \end{cases}$$

$$R_2(z,t) \begin{cases} 0, 0 \le z \le z_3 \\ \left(\sqrt{r'^2_0 - (z - z_3 - z'_0)^2}\right) b_1(t), \qquad z_3 \le z \le z_3 + r'_0(1 - sin\beta) \\ [r'_0 cos\beta + z_4] b_1(t), z_3 + r'_0(1 - sin\beta) \le z \le z_{max} \end{cases}$$

Solution procedure for the problem,

Step1- Radial Coordinate Transformation
Step2-Discretization
Step3-MAC Method

The procedure needs much efforts and time but it can be solved using MAC method. The result os streamline is shown below.

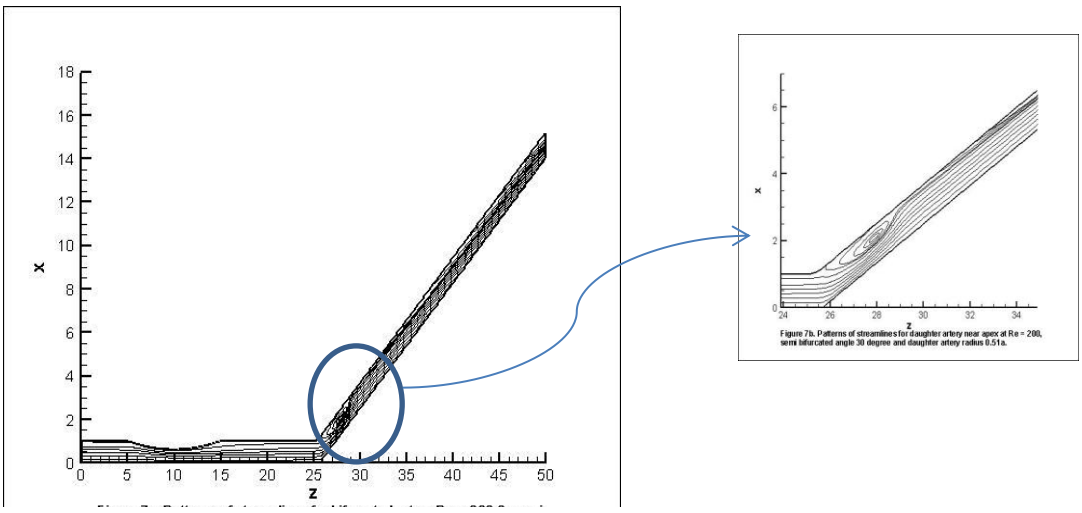

Figure 8 : The streamline pattern for Reynolds number 200.

1.3.6 Finite Element for Coronary Bifurcation Effects of Stent on Blood Flow

Mass equation,

$$\frac{\partial u}{\partial x} = 0,$$

Momentum equation,

$$\rho \frac{\partial u}{\partial t} + \rho u \frac{\partial u}{\partial x} = -\frac{\partial p}{\partial x} - \frac{\rho f u^2}{\sqrt{A}},$$

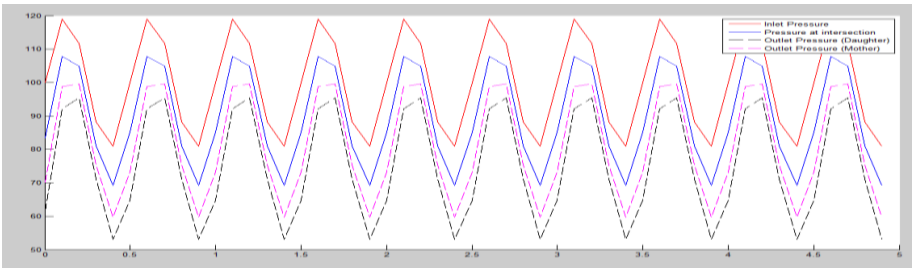

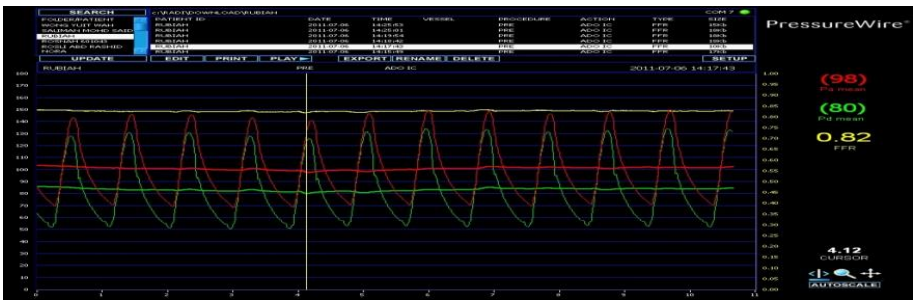

Figure 9: The pressure calculated compared to the pressure from a Pressure

Wire We assume that the velocity distribution is constant since the equation could not provide any information.

$$\frac{\partial u}{\partial x} = 0 \Rightarrow u = \text{constant},$$

$$\underbrace{\rho \frac{\partial u}{\partial t} + \frac{\partial p}{\partial x}}_{\text{Bernoulli equation}} = -\frac{\rho f u^2}{\sqrt{A}},$$

$$\vec{u}_1 = \vec{u}_2 = \vec{u}_3 = \vec{u}_4.$$

We hypothesize that the "pinching" is the reduction in the flow rate hence velocity. To prove it, we must allow the change of the velocity distribution.

** It is a "naïve" hypothesis. A better one would consider the elasticity of the artery wall as well (fluid structure interaction).

By considering

$$\frac{\partial A}{\partial t} + \frac{\partial (Au)}{\partial x} = 0.$$

Momentum equation

$$\rho \frac{\partial u}{\partial t} + \rho u \frac{\partial u}{\partial x} = -\frac{\partial p}{\partial x} - \frac{\rho f u^2}{\sqrt{A}},$$

The variation in the area, A in time mimic changes of area during the insertion of the stent. Without the proper data, we assumed it be sinusoidal in times.

$$A_1 = A_{01}\left(1 + 0.2\sin\left(\frac{2\pi t}{20}\right)\right).$$

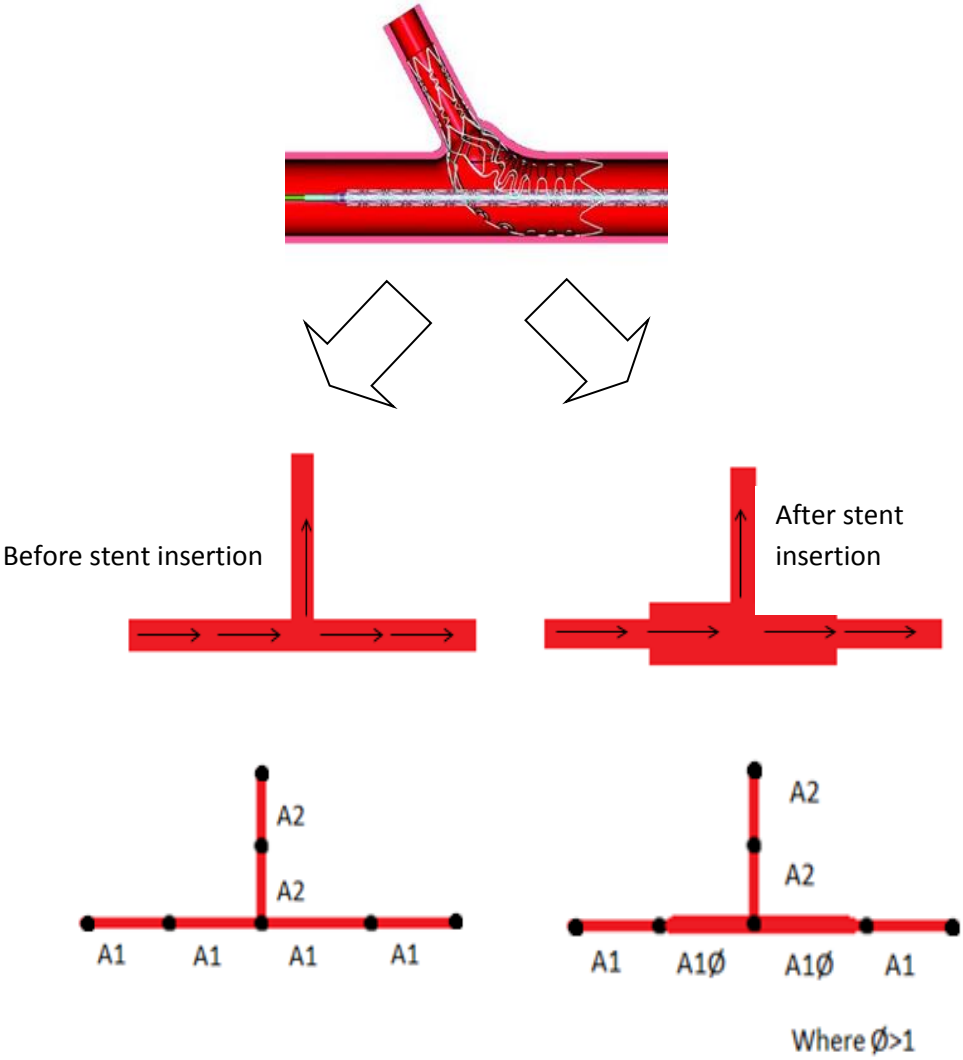

Figure 10: The Schematic Problem

Mass equation

$$\frac{\partial A}{\partial t}+\frac{\partial (Au)}{\partial x}=0.$$

Momentum equation

$$\rho\frac{\partial u}{\partial t}+\rho u\frac{\partial u}{\partial x}=-\frac{\partial p}{\partial x}-\frac{\rho f u^2}{\sqrt{A}},$$

thus,

$$\begin{bmatrix} m & 0 \\ 0 & 0 \end{bmatrix}\begin{Bmatrix} \dot{u} \\ \dot{p} \end{Bmatrix}+\begin{bmatrix} kN+k & c_2 \\ c_1 & 0 \end{bmatrix}\begin{Bmatrix} u \\ p \end{Bmatrix}=\begin{bmatrix} 0 \\ f \end{bmatrix},$$

where

$$m=\int_0^L \rho N_i N_j dx,$$

$$F=\frac{0.02\pi\cos\left(\frac{\pi t}{10}\right)}{1+0.2\sin\left(\frac{\pi t}{10}\right)}\int_0^L L_j dx,$$

$$kN=\int_0^L N_i N_j u dN_j dx,$$

$$k=\int_0^L \frac{\rho f}{\sqrt{A}} N_j N_k U_k N_i dx,$$

$$c_1=\int_0^L L_i dN_j dx,$$

$$c_2=\int_0^L N_i dL_j dx.$$

Hints on the “pinching” phenomena,

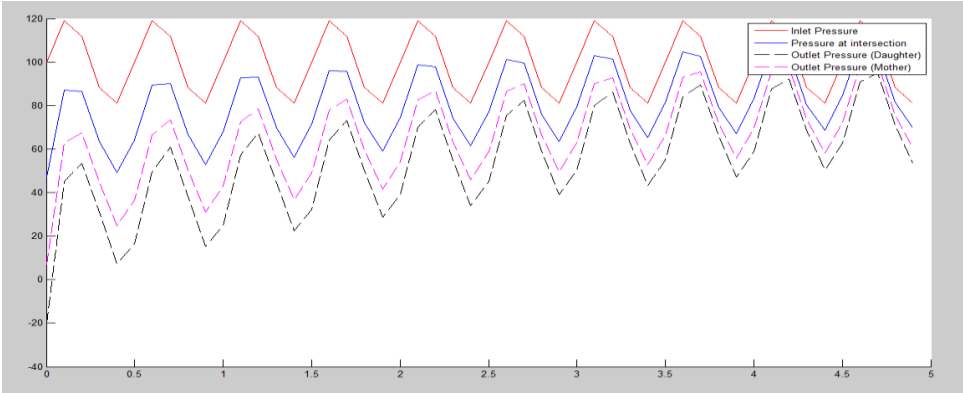

Figure 11: Pressure diference in time

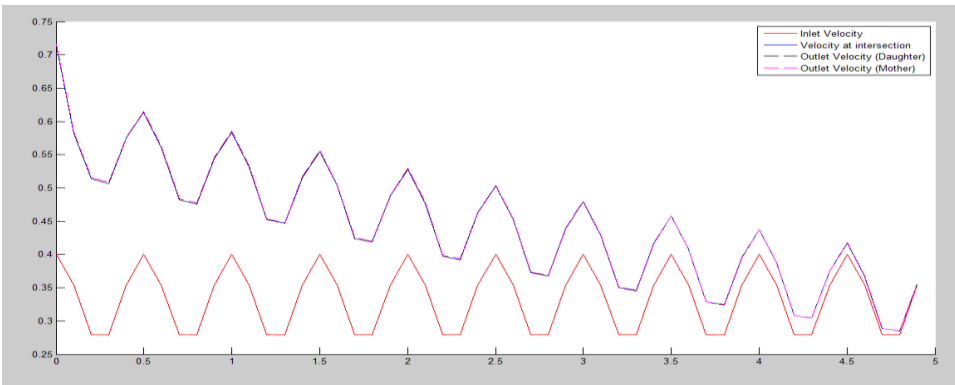

Figure 12: Velocity difference in time

Pinching" is the typical phenomena at which the area is enlarged, pressure increase and velocity hence flow rate reduces. For the time being reduction in the flow rate is associated with the reduction in the dimension of the daughter perceived as pinching. For some peculiarities,

Area change time function

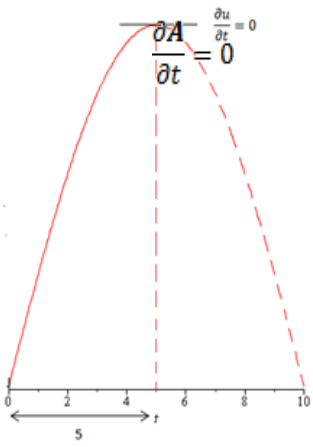

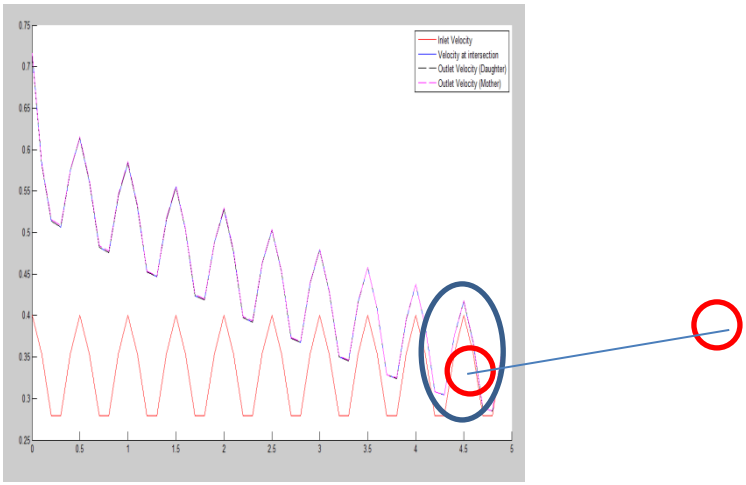
Inlet Velocity
Velocity at intersection
Outlet Velocity (Daughter)
Outlet Velocity (Mother)

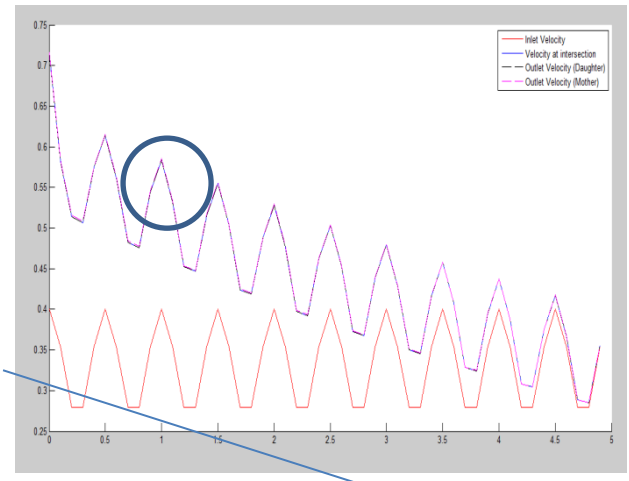
Inlet Velocity
Velocity at intersection
Outlet Velocity (Daughter)
Outlet Velocity (Mother)

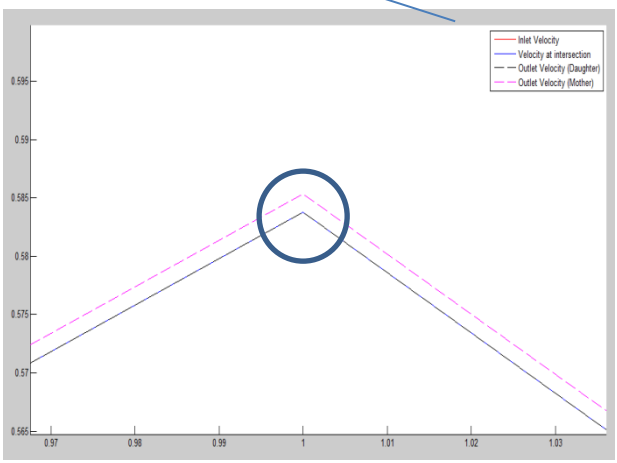
Inlet Velocity
Velocity at intersection
Outlet Velocity (Daughter)
Outlet Velocity (Mother)

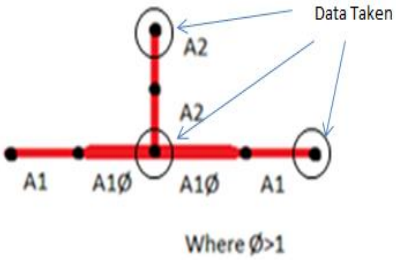
Data Taken
A2
A2
A1
A1Ø
A1Ø
A1
Where Ø>1

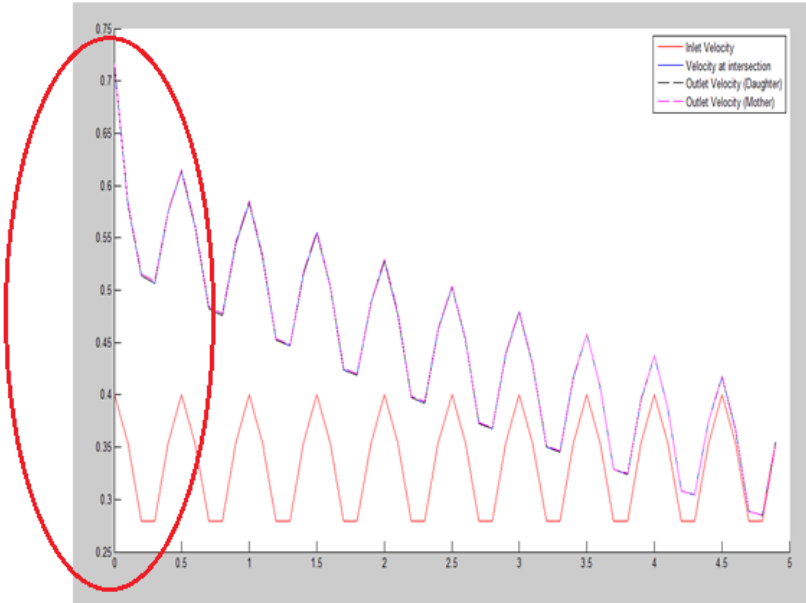

Figure 13: The velocity

At time, t=0, the velocity should be the same at inlet and outlet. This peculiarity is due to the chosen area time function.

$$A_1 = A_{01}\left(1+0.2\sin\left(\frac{2\pi t}{20}\right)\right),\ \frac{\partial A}{\partial t}\Big|_{t=0} = 0.02\pi A_0 \neq 0,\ \frac{\partial A}{\partial t} + \frac{\partial(Au)}{\partial x} = 0.$$

1.4 Conclusion and Recommendation

The results of the pressure and velocity at bifurcated artery presented in the previous sections show that the flow is likely to be disturbedand separation of streamlines from the vessel wall andformation of eddies may occur.It is important to elucidate thepossible connection between blood flow and the localizedgenesis and development of atherosclerosis and thrombosis.The importance of stent in the bifurcated artery will be study further.

There are some limitations in this study that should beaddressed. Firstly, were assumed to have a rigid wall ratherthan elastic wall; therefore, the simulation does not fullyreflect the realistic physiological situation as the coronarywall moves during cardiac cycles. Secondly, the assumptionof a Newtonian blood model becomes important especiallyin low flow and low wall shear stress regions. Nevertheless,a previous study has shown that the assumption of aNewtonian model is reasonable in this configuration.Thirdly, the realistic plaques position may be affected by leftcoronary side branches that have not been evaluated in thisstudy. Thus, future studies will use coronary models with amore realistic idealized geometry, extended to evaluate theeffect of side branches. For future works, the study should consider Fluid Structure Interaction (FSI) and concentrate on the best full Navier-Stokes 2D and 3D with the powerful method especially Finite Element Method.

1.5 Reference

[1] Victor H.T. Chen & Samin K. Sharma, **SIS 2006 Yearbook** Chapter 3 *BIFURCATION STENTING*, http://www.sis.org/yearbook_2006.php.

[2] Marjan Molavi Zarandi, Rosaire Mongrain, Olivier F. Bertrand and Ali Bonakdar,Non-Newtonian Effects on Blood Flow Dynamics in Stented Coronary Artery Bifurcations, ASME 2010 3rd Joint US-European Fluids Engineering Summer Meeting: Volume 1, Symposia – Parts A, B, and C, Montreal, Quebec, Canada, August 1–5, 2010

[3] JOHN F. LADISA JR., DOUGLAS A. HETTRICK,LARS E. OLSON,ISMAIL GULER, ERIC R. GROSS,1 TOBIAS T. KRESS,1 JUDY R. KERSTEN,DAVID C. WARLTIER, AND PAUL S. PAGEL, Stent implantation alters coronary artery hemodynamics and wall shear stress during maximal vasodilation, *J ApplPhysiol*93: 1939–1946, 2002.

Green Propulsion Regenerative Electromagnetic Suspension System (Gpress)

PERUSAHAAN OTOMOBIL NASIONAL SDN. BHD. (PROTON)

Reprentative/Group Members:

K. K. Viswanathan, Shamsuddin Ahmad, Normah Maan, Lim Yeou Jiann, Nor Hafizah Ahmad Kailani, Nurul Farahain Mohammad, Nurul Izyan Mat Daud, Anuar Alias

Abstract

A vehicle suspension system is defined as a mechanical system of springs or shock absorbers connecting the wheels and axels to the chassis of a wheeled vehicle. The car suspension system will improve the comfort of the car subject to different road profiles. The main objective of this study is to formulate a mathematical model on electromagnetic car suspension system which gives more comfortable for travellers. In this study, the model is solved using control theory to analyse the system and presented results and discussed.

1.10 Introduction

Automotive industry is one of the major revenue in Malaysia. Suspension systems provide a dual purpose which is contributing to the car's handling and braking, and keeping vehicle occupants comfortable and reasonably well isolated from road noise, bumps, and vibrations. The current vehicles are using a passive suspension system that incorporates with hydraulic damper and mechanical spring. The conventional system is not assuring can improve the vehicle handling and passenger safety especially when the transportation research board had reported that 51 % of the serious car accidents are caused by rollover. . The perfect automotive suspension system can absorb road shocks rapidly and could return to its normal position slowly while maintaining optimal tire to road contact [1-3]. However, this is difficult to realize by passive suspension system, where a soft spring allows for too much movement

and a hard spring causes passenger discomfort due to road irregularities. Hence, the new approach is increasingly developed to influence the dynamic performance of the vehicle. A new method and product has been introducing to the automotive industry to overcome this problem.

Basically in order to model and investigate the dynamic behavior of the suspension system, a full car model is preferred [4]. However roll and pitch behavior can also be modelled as an equivalent force disturbance acting on the body mass. Hence, this paper is concentrated on a quarter car model. Conventionally the passive suspension is installed on the current vehicle. The quarter car model for this passive suspension system that consists of one-fourth of the body mass, suspension components and one wheel are represented. Meanwhile, the quarter car model for active suspension system, where the linear permanent magnet actuator is installed in parallel with the spring.

Based on an article on cars in the Indian and Global Car Industry, car suspension is a device that forms a linkage of springs that bond between the vehicle and its wheels. The spring are developed in a variety of shapes, types, sizes, and capacities. Some of the common types of spring used in the suspension system are the leaf springs, coil springs, and the torsion bars.The key function of the car suspension is to deliver a smooth ride and maintain an excellent control. It does this by maintaining the tyre position at an optimum angle that eventually maximizes traction control, steering control, braking, and even acceleration.

When acceleration transforms into force or when vehicle runs down on a bumpy road, the vertical energy travels through the frame of the vehicle. This forceful energy is trapped by the car suspension system that reduces the tyre friction, eventually preventing the car from jumping of the road. In absence of suspension springs, the car comes bounding back with a greater force, resulting in a dangerous and uncomfortable ride.

To have best results from the car suspension system, it is important to adjust the position by doing wheel alignment. The four basic alignment adjustment are toe in/out,

camber, caster, and ride height. Toe in/out is the direction in which the tyres point, camber is the angle of the tyre with the road surface, caster is the axis line of the steering wheel, and ride height is the height of the cars chassis. All these adjustment points should be properly aligned in order to have maximum performance of the car suspension.

The purpose of a suspension system is to support the vehicle body and increase ride comfort. The ride comfort is improved by means of the reduction of the body acceleration caused by the car body when road disturbance from smooth road and real road roughness. Although car suspensioncome in a variety of configurations, the basic elements are springs and shock absorbers. Spring provide a simple mechanical disconnect between the shocking forces sustained by the vehicles wheels and axles and the body of the car with the passengers inside. The majority of modern cars employ classic coil springs that are affixed vertically or at a vertical angle between the axle and the cars frame. In some cases torsion bars or metal leaf spring are used. They serve the same purpose as coil spring.

Suspension systems serve a dual purpose which is contributing to the cars road holding/handling and braking for good active safety and driving pleasure, and keeping vehicle occupants comfortable and reasonably well isolated from road noise, bumps, vibrations, and others. These goals are generally at odds, so the turning of suspensions involves finding the right compromise. It is important for the suspension to keep the road wheel in contact with the road surface as much as possible, because all the forces acting on the vehicle do so through the contact patches of the tires. The suspension also protect the vehicles itself and any cargo or luggage from damage and wear. The design of front and rear suspension of a car may be different.

Kevin Schappell, United States stated that "Suspension", when discussing cars, refers to the use of front and rear springs to suspend a vehicles "sprung" weight. The springs used on today’s cars and trucks are constructed in a variety of types, shapes, sizes, rates, and capacities. Types include leaf springs, coil springs, air springs, and torsion bars. These are

used in sets of four for each vehicle, or they may be paired off in various combinations and are attached by several different mounting techniques. In engineering term, the suspension system can be categorized into passive, semi-active and active suspension system according to external power input to the system and/or a control bandwidth.

1.11 Problem Statement

Basically in order to model and investigate the dynamic behavior of the suspension system, a full car model is preferred. However roll and pitch behavior can also be modeled as an equivalent force disturbance acting on the body mass. Hence, this paper is concentrated on a quarter car model as shown in Figure 1. Conventionally the passive suspension is installed on the current vehicle. It is shown in the Figure 1 (a) where the quarter car model for this passive suspension system that consists of one-fourth of the body mass, suspension components and one wheel are represented. Meanwhile, the quarter car model for active suspension system, where the linear permanent magnet actuator is installed in parallel with the spring, Figure 1 (b)

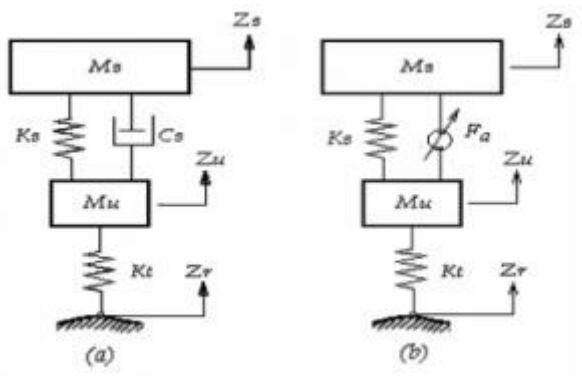

Figure 1. Passive and active quarter car model

The assumptions of a quarter car modeling are as follows: the tyre is modeled as a linear spring without damping, there is no rotational motion in car body, the behavior of spring and damper are linear, the tyre is always in contact with the road surface, and effect of friction is neglected so that the residual structural damping is not considered into vehicle modeling.

A 9-slot, 10-pole quasi-Halbach magnetized tubular machine with modular winding, Figure 2, has been developed for active suspension. Each pole of the magnetic armature comprises of one radially and one axially magnetized ring magnet. The salient feature of the quasi-Halbach magnetization is that the axially magnetized magnets essentially provide a return path for the radial air-gap flux, and hence, the flux in the inner bore is relatively small. As a result, the use of a very thin ferromagnetic tube or even a nonmagnetic tube on which to mount the magnets will not significantly compromise the thrust force capability. This is conducive to reducing un-sprung mass and hence enhancing the dynamic capability of active suspension.

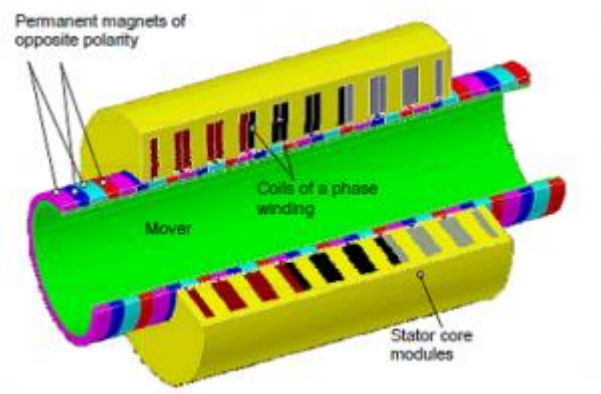

Figure 2: Schematic of 9-slot, 10-active pole tubular PM machine with quasi-Halbach magnetization

Based on the topology from the above design, Figure 2, a new design is proposed. The detail design is described in Figure 3 below. Based on the design, the mathematical derivation for optimization expressions of current i, electromagnetic force, and magnetic field $B$are required.

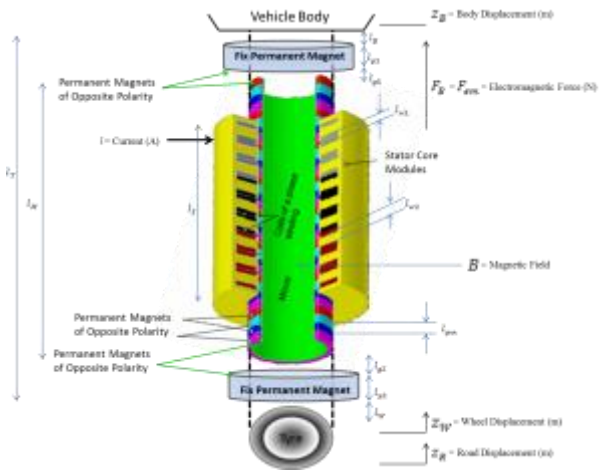

Figure 3: New design of GPRESS

1.12 Methodology – Assumptions, Mathematical model, algorithm

Problem Formulation

A mechanical damper to be imitated by using electromagnetic damper. To derive a mathematical model describing the motion, we apply newton's second law of motion in a vertical direction. Assuming both the car body and the wheels are moving vertically upwards with the spring and damper (dashpot) both extended, so we get a mathematical formulation which is to be a differential equation in displacement function which may be linear or nonlinear and consists of terms in magnetic field and electric current. Figure 4 shows the diagram on magnetic suspension system.

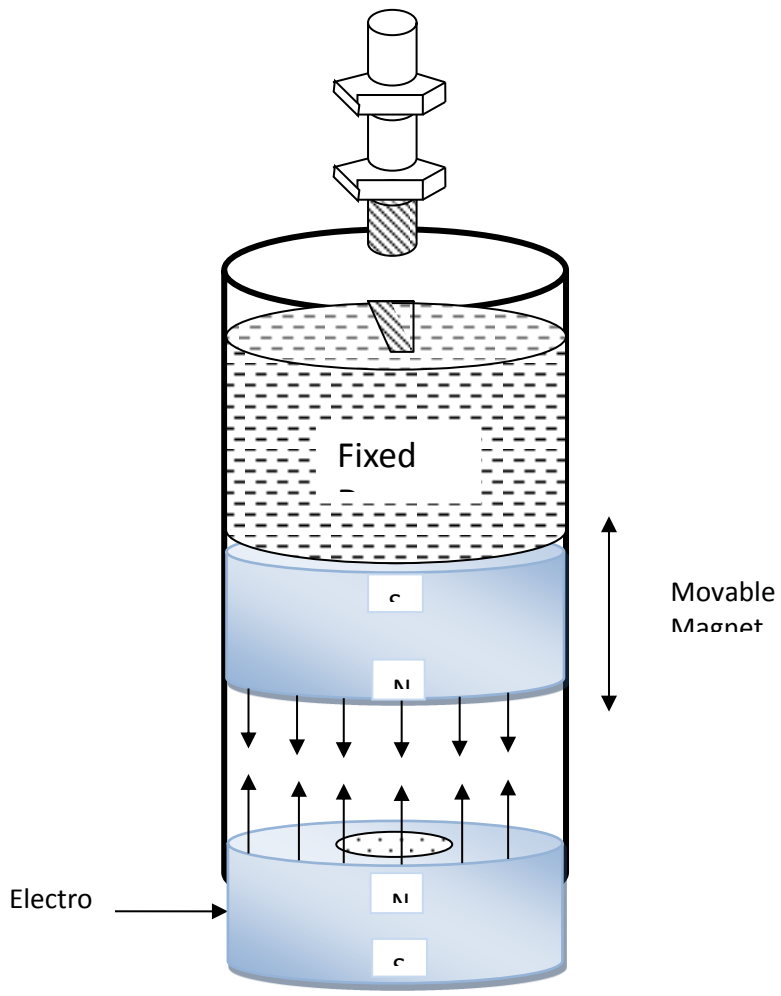

Fig. 4: Simple diagram of suspension

The equation of motion is

$$m\frac{d^2x}{dt^2} = \frac{M_0 I^2}{(x-X)^2} - \frac{M_0 I_0^{\,2}}{X_0^{\,2}} \qquad (1)$$

Repulsive force is $F = \dfrac{M_0 I^2}{(x-X)^2} = \dfrac{M_0 I^2}{Z^2}$,

where $Z = x - X$.

and

$$M_0 = \beta N^2$$

where N is the number of coil turns and β is a constant dependent upon actuator geometry and size. Then

$$\frac{\partial F}{\partial I} = 2\frac{M_0 I}{Z^2} \text{ and } \frac{\partial F}{\partial Z} = -\frac{2M_0 I^2}{Z^3}$$

By Taylor expansion about point (I_0, Z_0), we have

$$F(I,Z) \approx F(I_0,Z_0) + \left.\frac{\partial F}{\partial I}\right|_{(I_0,Z_0)}(I - I_0) + \left.\frac{\partial F}{\partial Z}\right|_{(I_0,Z_0)}(Z - Z_0)$$

$$= F(I_0, X_0) + \frac{2M_0 I_0}{(x(0) - X_0)^2}(I - I_0) - \frac{2M_0 I_0^{\ 2}}{(x(0) - X_0)^3}(x - X - x(0) + X_0)$$

$$= \frac{M_0 I_0^{\ 2}}{(x(0) - X_0)^2} + \frac{2M_0 I_0}{(x(0) - X_0)^2}(I - I_0) - \frac{2M_0 I_0^{\ 2}}{(x(0) - X_0)^3}(x - x(0) - (X - X_0))$$

$$= \frac{M_0 I_0^{\ 2}}{X_0^{\ 2}} + \frac{2M_0 I_0}{X_0^{\ 2}}(I - I_0) + \frac{2M_0 I_0^{\ 2}}{X_0^{\ 3}}(x - (X - X_0)) \qquad (2)$$

From (1) and (2) we have

$$m\frac{d^2x}{dt^2} = \frac{2M_0 I_0}{X_0^{\ 2}}(I - I_0) + 2\frac{M_0 I_0}{X_0^{\ 3}}(x - (X - X_0))$$

or

$$m\frac{d^2x}{dt^2} = \frac{2M_0 I_0}{X_0^{\ 2}} J(t) + 2\frac{M_0 I_0}{X_0^{\ 3}}(x - y(t)) \qquad (3)$$

where

$$J(t) = I - I_0 \text{ and } y(t) = X - X_0$$

Method of Solution

The equation (3) can be solved using control system.

Set $k1 = \frac{2M_0 I_0}{mX_0^2}, \quad k2 = \frac{2M_0 I_0}{mX_0^3}.$

Then Equation (1) become

$$x''(\mathrm{t}) = k1J(\mathrm{t}) + \mathrm{k}\,2(\mathrm{x(t)} - \mathrm{y(t)}). \tag{4}$$

And $\mathrm{x(t)} - \mathrm{y(t)}$ is measurable. Let

$$x_1 = x$$
$$x_2 = x_1'$$

and Equation (2) is transformed into a system as

$$\frac{d}{dt}\begin{bmatrix} x_1 \\ x_2 \end{bmatrix} = k1\begin{bmatrix} 0 \\ J(\mathrm{t}) \end{bmatrix} + k2\begin{bmatrix} 0 \\ x_1(\mathrm{t}) \end{bmatrix} - k2\begin{bmatrix} 0 \\ \mathrm{y(t)} \end{bmatrix} + \begin{bmatrix} x_2 \\ 0 \end{bmatrix}.$$

We need the system to satisfy this condition

$$\mathrm{k1J(t) = k\,2(x_1(t) - y(t)) + u(t)} \tag{5}$$

Such that $u(\mathrm{t})$ can be control where $|x(\mathrm{t})| \le \varepsilon, \forall t \in [0, \mathrm{T}]$.

Substitutes (4) into the system we have

$$\frac{d}{dt}\begin{bmatrix} x_1 \\ x_2 \end{bmatrix} = \begin{bmatrix} 0 & 1 \\ 0 & 0 \end{bmatrix}\begin{bmatrix} x_1 \\ x_2 \end{bmatrix} + \begin{bmatrix} 0 \\ 1 \end{bmatrix} u(t) \tag{6}$$

$$\dot{\mathrm{X}} = A\mathrm{X} + Bu(t)$$

Then we set $u(\mathrm{t}) = \mathrm{DX}$, where $D = \begin{bmatrix} d_1 & d_2 \end{bmatrix}$. Therefore the system (6) can be written as

$$\dot{\mathrm{X}} = (A + BD)\mathrm{X}. \tag{7}$$

Choose D such that there exist eigenvalues of the system (7) in second quadrant complex plane. So, we can choose

$$d_2 = -n,$$

$$d_1 < \frac{-n^2}{4},$$

where $d_2 > d_1$.

1.13 Result and Discussion

The results are presented in the figures solving the equation (7) for different values of n. Figure 5 shows the oscillation of the body vertically 0 < t < 10.The value of n = 2 is fixed from this graph the value of x decreases rapidly until t=0.5 and there is a slow variation upto t = 2.5 and constant afterwordst > 2.5. Similary, Figure 6shows the oscillation of the body vertically 0 < t< 10.The value of n = 3 is fixed from this graph the value of x decreases rapidly until t = 0.4 and there is a slow variation upto t = 1 and constant afterwordst >1. Figure 7 shows the oscillation of the body vertically 0 < t< 10.The value of n = 4 is fixed from this graph the value of x decreases rapidly until t = 0.2 and there is a slow variation upto t = 0.6 and constant afterwordst >0.6.Figure 8 shows the oscillation of the body vertically 0 < t< 10.The value of n = 5 is fixed from this graph the value of x decreases rapidly until t = 0.1 and there is a slow variation upto t = 0.9 and constant afterwordst >0.9.

From these results it can be seen that the car ride may be comfortable since the car body vertical acceleration does not exceed our prediction of the car suspension travel limit and passengers comfort measure.

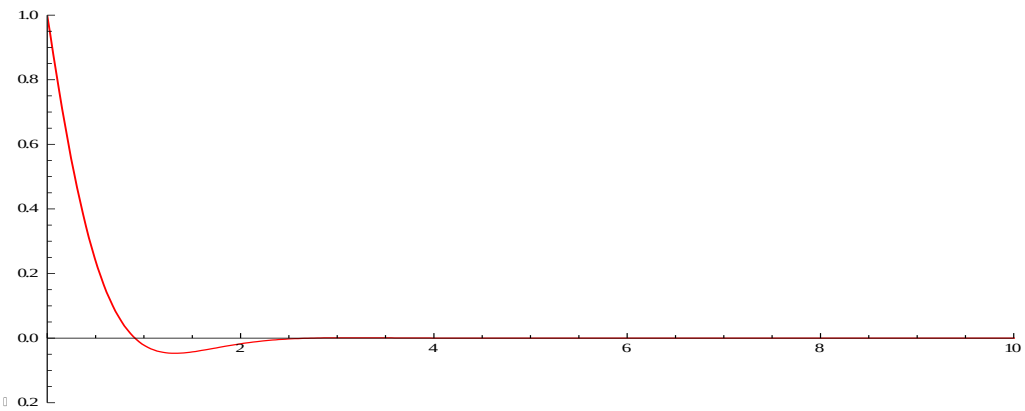

Figure 5. Variation of displacement with time t for n=2

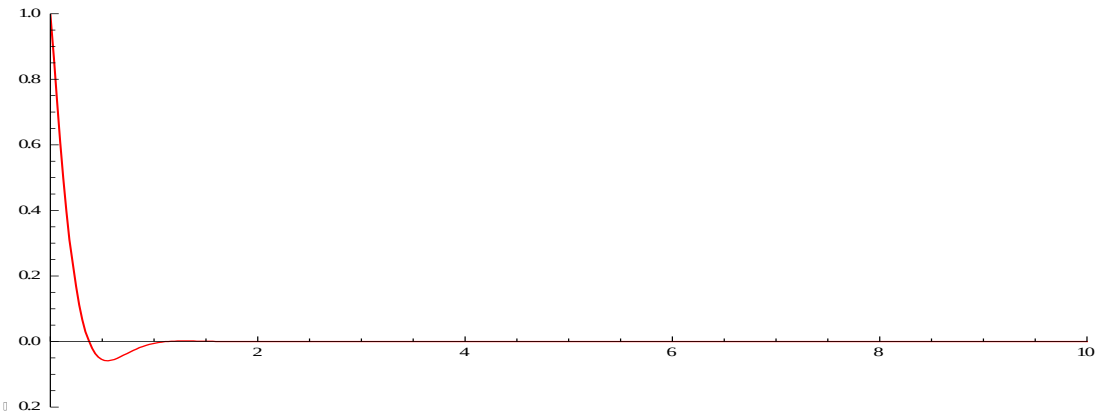

Figure 6. Variation of displacement with time t for n=3

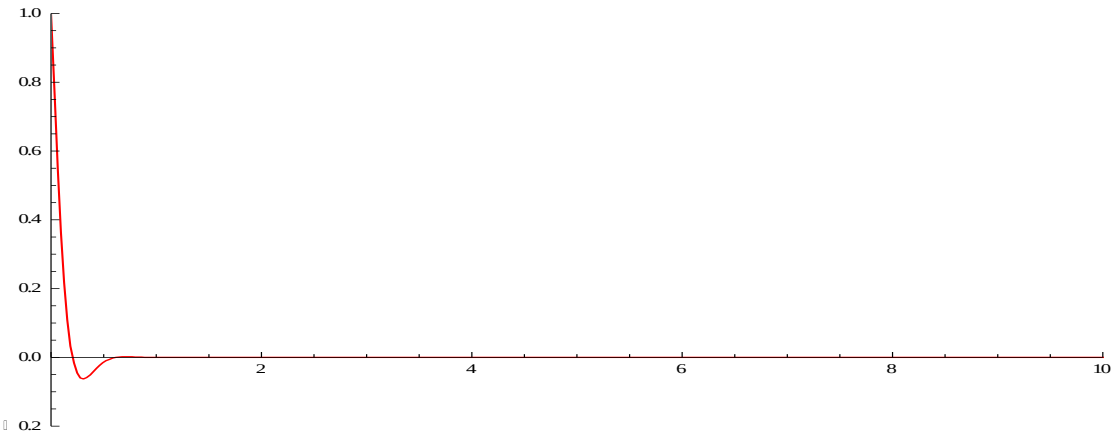

Figure 7. Variation of displacement with time t for n=4

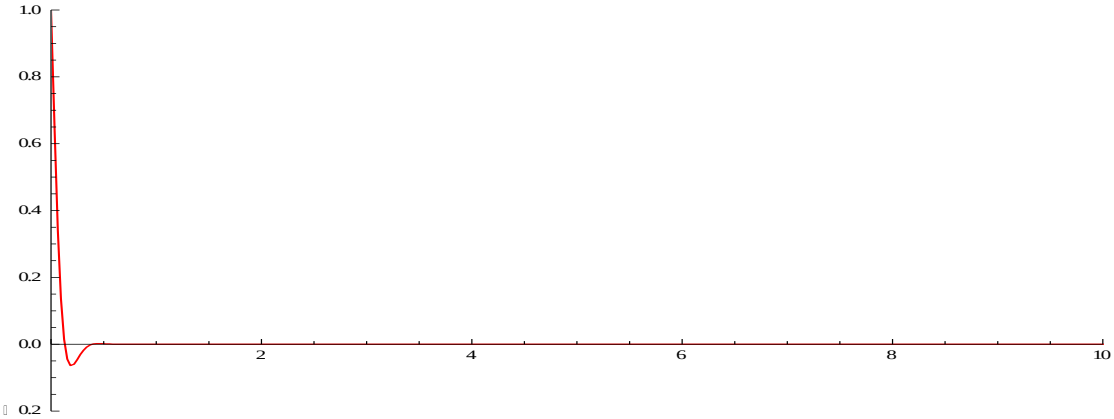

Figure 8. Variation of displacement with time t for n=5

1.14 Conclusion and Recommendation

An approach of the electromagnetic suspension system has been presented. The simplified mathematical model has been developed.
The GPRESS has the ability to give much smoother ride than any luxury sedan, and less roll and pitch than any sports car.

We need to refine the model and include other parameters to get better results.

1.15 References

[1] Clark, R. E., et al. "Design optimization of moving-magnet actuators for reciprocating electro-mechanical systems." Magnetics, IEEE Transactions on 31.6 (1995): 3746-3748.

[2] Trumper, David L., Won-Jong Kim, and Mark E. Williams. "Design and analysis framework for linear permanent-magnet machines." Industry Applications, IEEE Transactions on 32.2 (1996): 371-379.

[3] Z. Q. Zhu and D. Howe, “Magnet design considerations for electrical machines equipped with surface mounted permanents,” in Proc.13 th Int. Workshop Rate-earth Permanent Magnets Applicat.,(1994) , pp.151 – 160.

[4] Kruczek, Ales, and Antonin Stribrsky. "H∞ Control of Automotive Active Suspension with Linear Motor."Proceedings of the 3rd IFAC Symposium on Mechatronic Systems. 2004.

Optimal Water and Energy Consumption for Industry Water Networks

PROCESS SYSTEM ENGINEERING CENTER (PROSPECT)

Representative/Group Members:

Sharifah Rafidah Wan Alwi, Lim Jeng Shiun, Kok Lay Teo, Ryan Loxton, Shaharuddin Salleh, Zaitul Marlizawati Zainuddin, Syarifah Zyurina Nordin, Nur Arina Bazilah Aziz, Rasvini Rajendran, Ahmad Zharif Salami Mohd.Taha, Hossien

Abstract

Freshwater and world energy demands will considerably increase mainly due to the industrial growth. As industrial consumers use about 60% of the total energy used and as Malaysia progresses to become an industrialised nation, attention should be focused on the optimum use of the water and energy. Process industries for example oil refinery plant, pulp and paper mill use large amount of water and energy in their process. Enforcement of environmental regulations on industrial effluent and cost, have favoured that the discharged water from the process being re-used. However, the disadvantages include higher operating costs due to treatment of water until it is suitable for reuse. The end-of-pipe treatment method has been commonly applied in industry. The approach however typically requires relatively higher capital investment apart from increased chemical and operating costs. Water systems integration has later emerged as a viable and cleaner production option, and a cost-effective alternative. Majority of water operations also need water at a fixed temperature. Huge amounts of energy are also used in order to cool and/or heat water to reach operating temperatures by means of cold and heat utilities. There is thus a critical need in reducing both the consumption of water and energy.

By having a proper water and heat integration, it is envisaged that the industry is able to reduce its utility cost on water and energy. Thus the main objective is to model and solve the optimization problem involving complex water and heat integration to minimize the discharge of waste water and consumption of fresh water and energy in single contaminants based operation.In order to handle the complex problem, mathematical programming with

linear and non-linear formulation was employed and the model was solved by using optimization software namely GAMS.

1.16 Introduction

There is a real industrial challenge for ensuring good production levels while polluting and consuming natural resources as less as possible. In particular, industrial development is always linked to the use of high volumes of freshwater. The terrestrial freshwater reserves have been known to be finite and widely affected by human activities for several decades. According to a recent environmental outlook (OECD, 2008), the number of people living in areas of severe water stress will increase from 1 billion to over 3.9 billion by 2030.

As energy costs continue to rise, industrial plants need effective ways to reduce the amount of energy they consume. Conserving water helps to ensure that this important resource will be available for many generations to come. Conserving water also saves energy such as the energy needed to treat and transport the water. It is obvious that any attempt to provide a more efficient and effective water and energy management system that can reduce existing cost would lead to an increase in the national revenue as a whole. Using less water and energy is an investment in a sustainable future. In addition, the environmental impact induced by the process industry is linked both to the high volumes involved and to the diversity of toxic products generated along the process chain. Therefore, minimizing the discharge of the wastewater of a process industry will reduce the impact of contaminants on the environment.
Hence, it becomes urgent to propose feasible solutions which can be easily implemented in the industrial world, while respecting reasonable costs that do not weaken productivity. By developing cleaner and more economic water networks, the freshwater consumption as well as discharge of waste water can be reduced by far.

1.17 Problem Statement

Water and energy are central elements in process industry; consequently, all efforts made to reduce them contribute to environmental advances. The environmental impact induced by the process industry is linked both to the high volumes involved and to the diversity of toxic products generated along the process chain. As energy costs continue to rise and water becomes scarce resources, industrial plants need effective ways to reduce the amount of energy and water they consume. It is obvious that any attempt to provide a

more efficient and effective water and energy management system that can reduceexisting cost would lead to an increase in the national revenue as a whole. Therefore, there is a need to define an optimized water and energy network thus reducing the wastewater treatment cost, fresh water cost and also energy cost.

Given a set of water processes with various contaminants amount, temperature, flow constraints; and a set of operations, each requiring a specific water composition at a fixed temperature; the main aim of this project is to find the optimal design of water and heat exchangers network that involves complex water and heat integration in order to minimize the fresh water and energy consumption as well as discharge of waste water in single contaminant based operation considering the resource recovery, reduction, outsourcing and regeneration with the used of models in multi-criteria decision making (MCDM) and mathematical programming.

1.18 Methodology – Assumptions, mathematical model, algorithm

The main aim is to construct the mathematical model of the problem under consideration.

a) mathematical model for water and direct heat integration,

Figure 1 shows the water network superstructure of the direct heat transfer.Superstructure is essential to illustrate out all the possible flow configurations for one optimization study and gain insight for the possible ways to solve the complex problem (Handani*et al*., 2010).

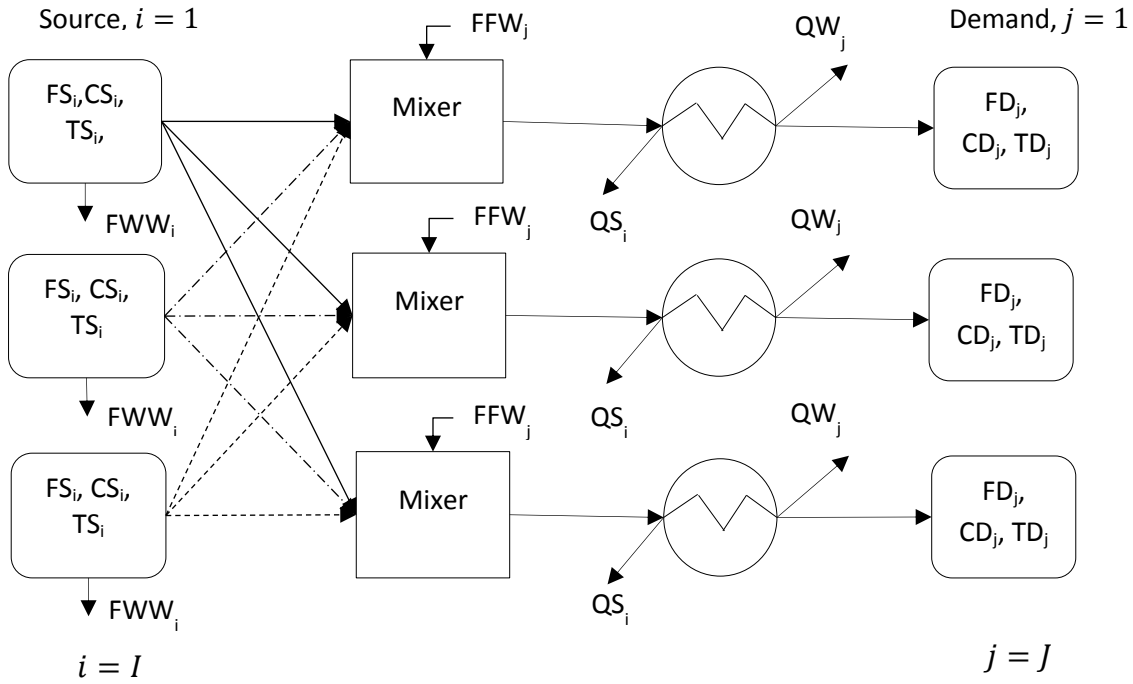

Figure 1: General water network superstructure for direct heat transfer

Assumptions made in modelling the problem are:

1) There are no flow rate losses or gains, and hence, no changes in water flow rates in the water operations(steady state).
2) The system only allows for direct heat transfer. Non-isothermal mixing (different temperature) is assumed for mixing between sources.
3) Continuous system which means that the water system is assumed to be operating continuously.
4) Steady state of heat transfer is assumed.
5) There is no contaminants concentration constraint for the discharged wastewater.
6) All contaminants concentrations for each demand and source are fixed to their maximum values.
7) Fresh water is free from contaminants.
8) Targeted temperature must be fulfilled through supplying or withdrawing the heat via hot and cold utilities.
9) Each source will have a constant temperature.

10) A single source of fresh water at fixed temperature 20°C is assumed.

Given a set of global water operations with multiple contaminants level and various temperatures, the mathematical model is developed so that simultaneous fresh water and energy consumption minimisation can be achieved.

Let

i = index of sources

j = index of demand

Parameter

FS_i = flow rate of water at source i

FD_j = flow rate of water at demand j

TS_i = Temperature of water from source i

TD_j = Targeted temperature of water at demand j

CD_j = contaminant concentration of demand j

CS_i = contaminant concentration of source i

CFW = contaminant concentration of fresh water

H_p = Heat capacity of water

TFW = Temperature of fresh water

Variable

FFW_j = flow rate of fresh water into demand j

FWW_i = flow rate of waste water from source i

F_{ij} = flow rate of water from source i to demand j

QW_j = Amount of energy withdrawn per hour

QS_j = Amount of energy supplied per hour

The objective functionsare to minimize both fresh water and energy consumption.

Fresh water minimization objective function:

$$min \sum_{j} FFW_j$$

Energy minimization objective function:

$$min \sum_{j} (QW_j + QS_j)$$

subject to the following constraints

Source splitting balance:
For each source, water will be split into stream from source i to demand j and waste water. It is represented as equation below:

$$FWW_i + \sum_{j} F_{ij} = FS_i$$

Flow rateof waste water discharge from source i+ total flow rateof water transferred from source $i$to demand j = flow rate of water at source i.

Demand mixing balance:
For each demand j, the water will be mixed in the mixerand eventually transferred into demand j. Since there is no other substance other than heat that is supplied or withdrawn after the mixer, hence, mass balance on mixer can be made to represent demand balance. At the mixing point, fresh water is supplied in order to obtain the required contaminant balance. Hence, fresh water load needs to be considered in the demand balance equation. This is shown in the equation below:

$$FFW_j + \sum_{i} F_{ij} = FD_j$$

Flow rate of fresh water use for demand j + total flow rateof water transferred from source $i$to demand j =flow rateof water needed atdemand$j$.

Demand contaminant balance:
The contaminant mass from source i and fresh water cannot exceed a fixed amount of contaminant concentration at demand j

$$FFW_j CFW + \sum_i F_{i,j} CS_i \leq FD_j CD_j$$

Contaminant concentration of the fresh water $+$total contaminant concentration of water from source$i$ $=$contaminant concentration of demand j.

Energy balance on demand:
Since there is a fixed targeted temperature atdemand j, a certain amount of energywill need to be supplied or withdrawn through utility to fulfil this requirement.

$$FFW_j H_P TFW + \sum_i \left(F_{ij} H_p TS_i\right) - FD_j H_P TD_j = QW_j - QS_j$$

Amount ofenergy needed for the fresh water for demand j + total energy needed for the water transferred from source $i$to demand j – amount of energy at demand j $=$ amount of energy withdrawn for demand$j$/ amount of energy supplied for demand j. Only one energy amount variable will be positive in this case, either Qw_j / Qs_j.

Non-negativity Constraint:

$$FFW_j \geq 0 \text{ , } FWW_i \geq 0, F_{ij} \geq 0, QW_j \geq 0, QS_j \geq 0$$

b) Further reduction in cost is seen possible if we can reduce the number of mixer. Hence, the second model is developed with the objective of minimizing the number of mixers. The assumption that each demand has its own mixer is omitted and the mixers are treated as independent entities.

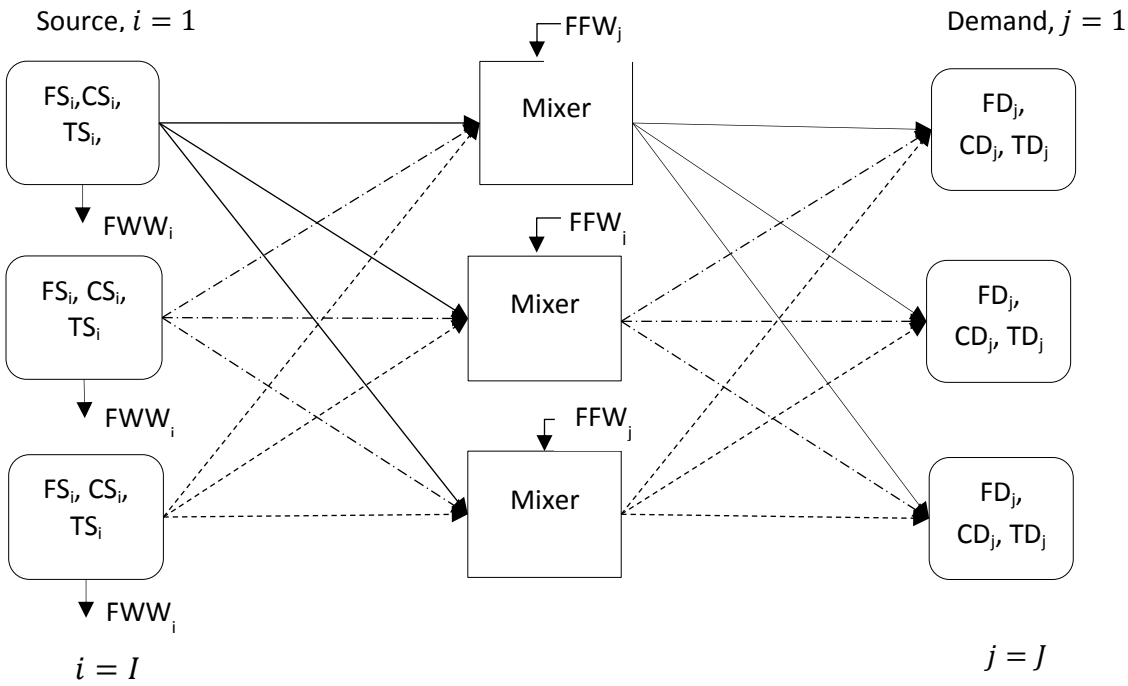

Figure 3: General water network superstructure for direct heat transfer with varying mixers.

Let

i = index of sources
j = index of demand
k = index of mixer

Parameter

FS_i = flow rate of water at source i
FD_j = flow rate of water at demand j
TS_i = Temperature of water from source i
TD_j = Targeted temperature of water at demand j
TM_k = Targeted temperature of water at mixer k
CD_j = contaminant concentration at demand j
CS_i = contaminant concentration at source i

CFW = contaminant concentration of fresh water
H_p = Heat capacity of water
TFW = Temperature of fresh water

Variable
Y_k = mixer k
FFW_k = flow rate of fresh water into mixer k
FWW_i = flow rate of waste water from source i
F_{ik} = flow rate of water from source$i$ to mixer$k$
F_{kj} = flow rate of water from mixer $k$to demand$j$
FM_k = flow rate of water that go through mixer k

The objective functions for this second model are:

Fresh water consumption minimization;

$$min \sum_k FFW_k$$

Number of mixer minimization;

$$min \sum_k Y_k$$

subject to the following constraints,

Source Splitting Point Balance:

$$FS_i = \sum_k F_{ik} + FWW_i$$

Flow rate of waste water discharge from source i+ total flow rateof water transferred from source $i$tomixer k = flow rate of water at source i.

Mixer Mixing Point Balance:

$$FFW_k + \sum_i F_{ik} = FM_k$$

Flow rate of fresh water use for mixer k + total flow rate of water transferred from source $i$to mixer k = flow rate of water that go throughmixer k.

Mixer Point Balance:

$$FM_k = \sum_j F_{kj}$$

Flow rate of water that go through mixer k = total flow rateof water transferred through mixer k to demand j.

Demand Mixing Point Balance:

$$\sum_k F_{kj} = FD_j$$

Total flow rateof water transferred through mixer k to demand j = flow rateof water needed at demand j

Mixer Selection:
If there is a flow of water throughmixer k todemand j, then Y_k will be 1.

$$F_{kj} \leq 100000Y_k$$

MixerContaminant Balance:

$$FFW_k CFW + \sum_i F_{ik} CS_i = FM_k C_k$$

Contaminant concentration of the fresh water $+$total contaminant concentration of water from source i $=$contaminant concentration of mixer k.

Demand and Mixer Contaminant Balance:

$$\sum F_{kj}\, C_k \leq FD_j CD_j$$

Total contaminant concentration of water from mixer k to demand $\leq$contaminant concentration at demand j.

Total waste water generated:

$$FWW = \sum_i FWW_i$$

Amount of waste water $=$ total waste water discharge from source i.

Binary Constraint:

$$Y_k \in \{0,1\}$$

Non-negativity Constraint:

$$FFW_k \geq 0,\, FWW_i \geq 0,\, F_{ik} \geq 0,\, F_{kj} \geq 0,\, FM_k \geq 0$$

1.19 Result and Discussion

For the model of water and direct heat integration, a case study with four demands and four sources is considered (Savulescu*et al.*, 2005). The data is presented in Table 1 and Table 2.

Table 1: Extracted demand data for the case study

Demand j	FD_j **(t/h)**	CD_j **(ppm)**	TD_j **(°C)**
1	20	0	40
2	100	50	100
3	40	50	75
4	10	400	50

Table 2: Extracted source data for the case study

Source i	FS_i **(t/h)**	CS_i **(ppm)**	TS_i **(°C)**
1	20	100	40
2	100	100	100
3	40	800	75
4	10	800	50

The model for water and direct heat integrationwas coded into GAMS software, and the result obtained isgiven in Table 3.

Table 3: Result for water and direct heat integration model

Variable	Solution
FFW(t/h)	90
FWW(t/h)	90
QW(kw/h)	0
QS(kw/h)	21000

Detail result that gives the allocation of water fromsource $i$to demand $j$is illustrated in Figure 5.

As for Model 2, it still needs some modifications since the energy consumption objective and constraint are not considered yet in the model.

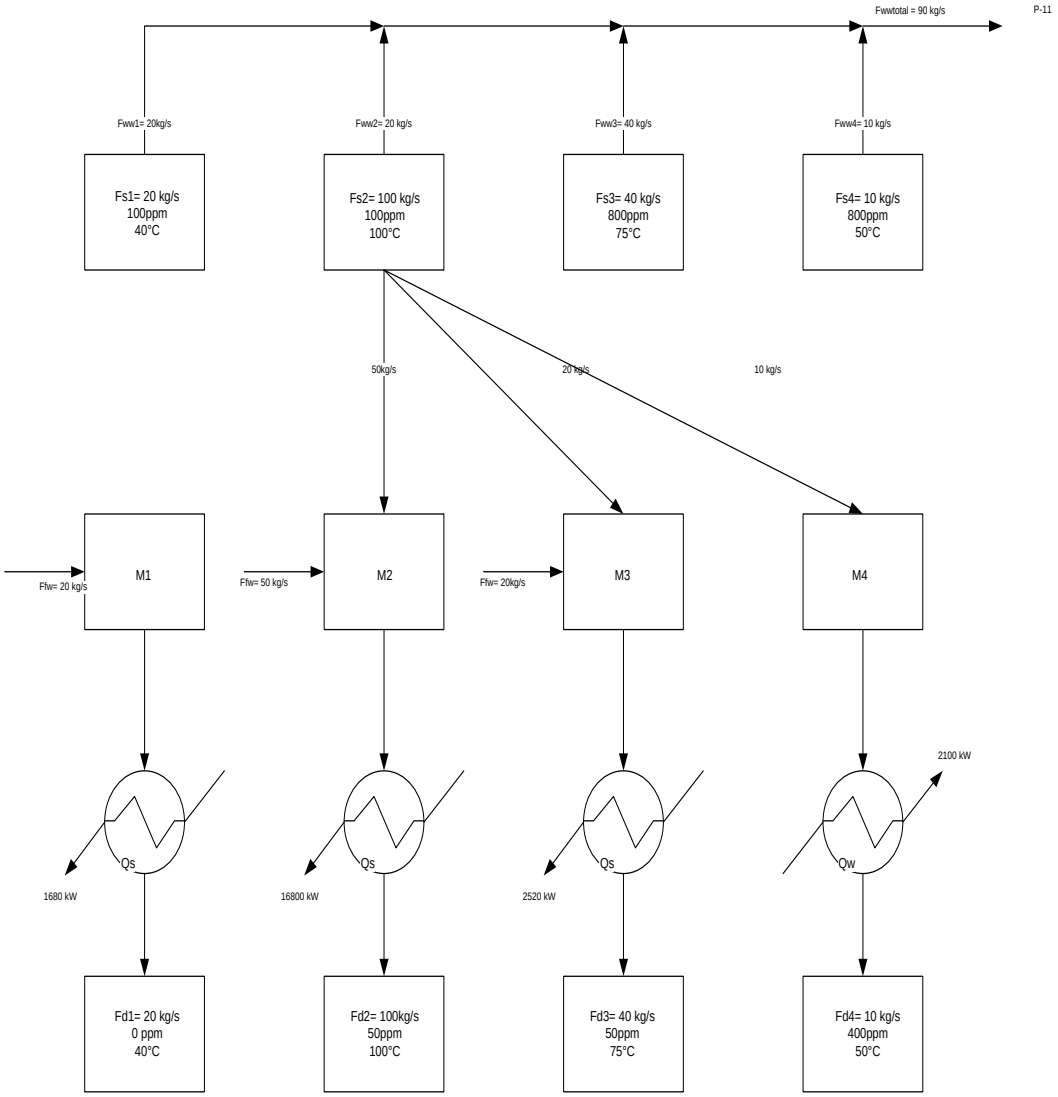

Figure 5: Water and energy superstructure that achieves minimum fresh water and energy consumption for the case study. (Direct heat transfer)

1.20 Conclusion and Recommendation

During the MISG, only basic model is able to be developed since the problem was presented to us only on the first day of the study group. Therefore, no preliminary study could be done on the problem.

Currently, work is still going on in improving Model 2 and also in developing a new model of simultaneous water, direct and indirect heat integration.

1.21 References

Organisation for economic co-operation and development, OECD Environmental Outlook to 2030, Paris, 2008.

Savulescu L.E., Kim J.K., Smith R., Studies on Simultaneous Energy and Water Minimization- Part 1: Systems with No Water Re-use. *Chemical Engineering Science*.2005, 60 (12), pp 3279-3290.

Handani Z.B., Wan Alwi S.R.,Hashim H., and Manan Z. A.,Holistic Approach for Design of Minimum Water Networks Using the MixedInteger Linear Programming (MILP) Technique. *Industrial & Engineering Chemistry Research.*2010, 49(12), pp 5742–5751.